

Post-transcriptional regulation of the central apoptotic pathway by microRNAs and RNA-binding proteins during *C. elegans* development

DISSERTATION ZUR ERLANGUNG DES DOKTORGRADES DER NATURWISSENSCHAFTEN
DOCTOR RERUM NATURALIUM (DR. RER. NAT.) AN DER FAKULTÄT FÜR BIOLOGIE DER
LUDWIG-MAXIMILIANS-UNIVERSITÄT MÜNCHEN



Ryan Sherrard

13.11.2018

1. Gutachter: Prof. Dr. Barbara Conradt

2. Gutachter: Prof. Dr. Wolfgang Enard

Tag der Abgabe: 13.11.2018

Tag der mündlichen Prüfung: 21.02.2019

Eidesstattliche Versicherung

Ich versichere hiermit an Eides statt, dass die vorgelegte Dissertation von mir selbständig und ohne unerlaubte Hilfe angefertigt ist.

Ryan Sherrard (München, den 13.11.2018)

Erklärung

Hiermit erkläre ich, dass die Dissertation nicht ganz oder in wesentlichen Teilen einer anderen Prüfungskommission vorgelegt worden ist. Ich habe mich nicht anderweitig einer Doktorprüfung ohne Erfolg unterzogen.

Ryan Sherrard (München, den 13.11.2018)

Publications Originating from this Work

Sherrard R, Luehr S, Holzkamp H, McJunkin K, Memar N & Conradt B (2017). miRNAs cooperate in apoptosis regulation during *C. elegans* development. *Genes Dev* 31, 209–222.

Acknowledgements

I remember knocking on Barbara's door back in 2013 and asking if I could stay in the lab for a PhD. That short meeting took my life down a path of cell death and RNA biology, starting with Coursera and ending with this thesis. Thank you, Barbara, for giving me the opportunity to grow as a scientist and for mentoring me over these past years. And Eric, thank you for the wise advice and great conversations...and the intense kicker matches. And thanks to you both for the continued support and interest in my curling endeavours.

To each and every member of the lab: I am grateful to have worked alongside you, but more than that, I am lucky to have gotten to know you all personally. I got my start thanks to Heinke, Stéphane, and Nadin, and I stayed because of the great atmosphere that you all created. I wish all of you the very best, and hope we continue to stay in touch.

To my extended family here in Germany: Sebs, Sandra, Saroj, Manju, Nadja, Chris, Fabian, Fabio, Joel, Laura, Dave, Louise, Sylvie, Helena, Addie, Niels, Tom, Christina, David, Athena, Oliver, and Vanessa—I could not ask for a better group of friends. You have made my years in Munich the best of my life.

To the IMPRS-LS coordination team of Ingrid, Maxi, and Hans-Joerg, and to our very own Mo: you are simply wonderful people. I appreciate all that you have done for me and for others, and I can only hope to work with people as kind as you in the future.

To my Thesis Advisory Committee, Luisa and Frank: thank you for your valuable input and direction during crucial times. And to the members of my Defense Committee, thank you for your time and feedback as my studies come to an end.

To the many cafés and biergartens in the beautiful city of Munich: thank you for keeping me well caffeinated and seeing me through the highs and lows.

And finally, to my family—Mom, Dad, and Andrea: when my three-month trip to Germany turned into an entire decade, and when my Master's degree turned into a fully fledged PhD, I could always count on your unwavering support. We might be separated by nine time zones and over 8000 km, but that never mattered. Thank you for your words of wisdom (and countless FaceTime calls) over all these years.

CONTENTS

CONTENTS

Eidesstattliche Versicherung	ii
Erklärung	ii
Publications Originating from this Work	iii
Acknowledgements	iv
Abstract	1
1 Introduction	5
1.1 Programmed cell death	6
1.1.1 Apoptosis	6
1.1.2 Programmed cell death during development in <i>C. elegans</i>	8
1.1.3 The central pathway of apoptosis	9
1.1.4 Regulation of <i>egl-1</i> and the apoptotic fate	13
1.2 Post-transcriptional regulation of gene expression	17
1.2.1 Mechanisms of post-transcriptional regulation	17
1.2.2 Post-transcriptional regulation via the 3'UTR	19
1.2.3 Post-transcriptional regulation of the cell death pathway	20
1.3 Post-transcriptional regulation by miRNAs	21
1.3.1 Biogenesis and function of miRNAs	21
1.3.2 miRNA-mediated regulation of programmed cell death	23
1.3.3 miR-35- and miR-58-family miRNAs	24
1.4 Post-transcriptional regulation by RNA-binding proteins	28
1.4.1 Function of RBPs	28
1.4.2 PUF family of RBPs	29
1.4.3 PUF proteins in <i>C. elegans</i>	31
1.4.4 Interaction between miRNA- and PUF-mediated post-transcriptional regulation	32
1.5 Aim of this study	35
2 Materials and Methods	37
2.1 Strains and general maintenance of <i>C. elegans</i>	38
2.2 Cloning and single-copy integration of <i>egl-1</i> 3'UTR reporters: miRNA binding-site variants	39

2.3	Cloning and single-copy integration of <i>egl-1</i> 3'UTR reporters: FBE variants	41
2.4	Cloning and single-copy integration of <i>egl-1</i> translational reporter	41
2.5	4D microscopy and lineage analysis of embryonic cell death	42
2.6	RNAi knockdown of <i>fbf</i> by injection of dsRNA	43
2.7	smRNA FISH	43
2.8	Quantification of mRNA copy number from smRNA FISH images	48
3	Results	51
	Preface	52
3.1	miRNA-mediated regulation of programmed cell death	53
3.1.1	Abnormally large cell corpses are present in <i>mir-35</i> -family mutants	53
3.1.2	Loss of <i>mir-58</i> -family miRNAs enhances the large-cell-corpse phenotype in <i>mir-35</i> -family mutants	57
3.1.3	Formation of large cell corpses requires the central apoptotic machinery	57
3.1.4	The <i>egl-1</i> 3'UTR harbors conserved binding sites for miR-35- and miR-58-family miRNAs	58
3.1.5	The <i>egl-1</i> 3'UTR directs downregulation of mRNA expression	59
3.1.6	Mothers and sisters of normal apoptotic cells die inappropriately in <i>mir-35</i> -family mutants	63
3.1.7	Penetrance of inappropriate cell death in <i>mir-35</i> -family mutants is dependent on both embryonic lineage and developmental stage	64
3.1.8	miR-35- and miR-58-family miRNAs cooperatively target <i>egl-1</i> mRNA to prevent precocious death of the RID neuroblast	65
3.1.9	<i>egl-1</i> mRNA copy number is buffered by the cooperative activity of miR-35- and miR-58-family miRNAs in the MSpaap lineage	69
3.2	RBP-mediated regulation of programmed cell death	74
3.2.1	Loss of <i>puf-8</i> , but not <i>puf-9</i> , produces an abnormal cell-death phenotype in embryos	74

CONTENTS

3.2.2	Large cell corpses in <i>puf-8(lf)</i> animals belong to both cell-death and non-cell-death lineages	76
3.2.3	The time required to form a refractile cell corpse is prolonged in <i>puf-8</i> mutants	77
3.2.4	Knockdown of <i>fbf</i> partially suppresses the large-cell-corpse phenotype in <i>mir-35</i> -family mutants	80
3.2.5	The 3'UTRs of <i>egl-1</i> , <i>ced-9</i> , <i>ced-4</i> , and <i>ced-3</i> harbor predicted PBEs and FBEs	81
3.2.6	Embryonic <i>ced-3</i> mRNA copy numbers are not elevated in <i>puf-8(lf)</i> embryos	85
3.2.7	Two FBEs in the 3'UTR of <i>egl-1</i> mediate repression of a transgenic reporter	85
4	Discussion	89
4.1	miRNA-mediated regulation of programmed cell death	90
4.1.1	miR-35 and miR-58 family miRNAs cooperatively repress <i>egl-1</i> <i>in vivo</i>	90
4.1.2	miR-35- and miR-58-family miRNAs mediate both translational repression and degradation of <i>egl-1</i> mRNA	91
4.1.3	Lineage-specific differences in <i>egl-1</i> transcription are buffered by miRNA activity	92
4.1.4	miR-35- and miR-58-family miRNAs ensure the continuous regulation of <i>egl-1</i> during development	94
4.2	RBP-mediated regulation of programmed cell death	96
4.2.1	<i>puf-8</i> possesses a novel activity required for cell-death specification and timing	96
4.2.2	PUF-8 activity prevents inappropriate death in both cell-death and non-cell-death lineage	97
4.2.3	Regulation via conserved secondary structure elements	98
4.3	Cooperative regulation of programmed cell death by PUF proteins and miRNAs	99
4.4	Conclusion and future perspectives	101
4.4.1	Summary and open questions	101
4.4.2	Emerging fields in post-transcriptional gene regulation	102

4.4.3 Purification of transcript-specific mRNP complexes	103
4.4.4 Medical implications of cell-death regulation	104
References	105
Curriculum vitae	133

ABSTRACT

ABSTRACT

Programmed cell death is an essential process during animal development. One type of cell death—apoptosis—is well understood at the molecular level, in large part due to genetic studies in the nematode *Caenorhabditis elegans*. The central apoptotic pathway in *C. elegans* consists of the four conserved genes *egl-1* (BH3-only), *ced-9* (Bcl-2), *ced-4* (Apaf-1), and *ced-3* (caspase), which act in a linear pathway. It is crucial that the activity of this pathway only triggers apoptosis in those cells programmed to die, and this requires regulation at multiple levels of gene expression. Although several studies have examined this regulation, post-transcriptional control of the pathway is still not well characterized. Here, I investigate regulation of the central apoptotic pathway by two prominent post-transcriptional mechanisms: microRNAs (miRNAs) and RNA-binding proteins (RBPs).

First, I present evidence that the miR-35 family and the miR-58 *bantam* family of miRNAs directly target conserved elements in the 3'UTR of *egl-1* mRNA and act cooperatively to repress its expression. This repression is crucial during embryogenesis, as loss of the *mir-35* family leads to the inappropriate death of cells that are not programmed to die, and this phenotype is enhanced by the additional loss of the *mir-58* family. These inappropriately dying cells are exclusively mothers and sisters of cells that are programmed to die, and their precocious and collateral deaths result in the formation of abnormally large cell corpses. Using single-molecule RNA FISH, I show that *egl-1* is already transcribed in mother cells, and that both miR-35- and miR-58-family miRNAs function to maintain the copy number of *egl-1* mRNA below a critical threshold—failure to do so results in precocious death of the mother cell. Furthermore, it seems that these two miRNA families are not required for the turnover of *egl-1* mRNA over time in the daughter that survives. Considering that *egl-1* transcription is controlled by numerous factors with varying modes of activity, the cooperative activity of miR-35- and miR-58-family miRNAs may buffer any lineage-specific differences in *egl-1* transcription, thereby ensuring EGL-1 activity only reaches a level sufficient to trigger death in daughter cells that are programmed to die.

Next, I describe a novel cell-death role for the gene *puf-8*, which encodes a conserved member of the Pumilio/FBF (PUF) family of RBPs. I show that animals lacking *puf-8* exhibit two contrasting cell-death abnormalities. First, some cells die inappropriately, and these cells belong to both cell-death and non-cell-death lineages. Second, programmed cell death is delayed during the first wave of embryonic cell death. These abnormalities are not present upon nor enhanced by the loss of closely related *puf-9*, nor is the phenotype present upon knockdown of another member of the PUF family, *fbf*; however,

fbf knockdown does suppress the large-cell-corpse phenotype in *mir-35*-family mutants. All four genes of the central apoptotic pathway harbor PUF-8-binding elements (PBEs) and/or FBF-binding elements (FBEs) in their 3'UTRs, and two FBEs in *egl-1* can mediate the repression of a transgenic reporter. Therefore, *puf-8* and *fbf* exhibit activity that both promotes and suppresses the cell-death pathway, and their prevailing activity might be regulated in a tissue- or cell-specific manner.

Taken together, these findings show complex regulation of the central apoptotic pathway by both miRNAs and RBPs, and mounting evidence in the field suggests these two mechanisms can function cooperatively in the regulation of common targets. Evidence of cell-death genes being targeted by miRNAs and RBPs in mammals supports the possibility of this regulation being conserved in higher animals, which could have implications for the medical field. Our understanding of programmed cell death and its regulation has already led to the development of drugs that trigger apoptosis in cancer cells, and furthering this understanding could aid in the development of novel disease treatments.

1

INTRODUCTION

1.1 Programmed cell death

1.1.1 Apoptosis

Life and development of an organism relies, counterintuitively, on cell death. Tens of billions of cells are generated in the human body every day, and the same number must be eliminated to maintain balance (reviewed in Nagata 2018). When executed in a programmed manner, cell death is crucial for tissue homeostasis, sculpting of organs, and culling of damaged cells (reviewed in Fuchs & Steller 2011). Hence, the perturbation of programmed cell death can have serious consequences. Neurological diseases, for example, can arise when cell death fails to eliminate excess neurons during development of the central nervous system (reviewed in Dekkers et al. 2013). The evasion of cell death is also a hallmark of tumorigenic cells and, ultimately, cancer (reviewed in Letai 2017). Programmed cell death is therefore an essential process; however, it must be restricted to specific cells while leaving others unscathed, and this requires tight regulation at multiple levels.

Several types of programmed cell death have been uncovered, and among them apoptosis has emerged as a prominent focus of research. First described in 1972, apoptosis was considered an opposing force to mitosis in the regulation of cell populations (Kerr et al. 1972). Apoptosis is a noninflammatory process that can be triggered by intrinsic factors, such as DNA damage, as well as extrinsic factors, such as growth factor depletion (reviewed in Fuchs & Steller 2015). Both pathways converge on the activation of caspases, a conserved class of cysteinyl aspartate proteases. Caspase activity leads to the cleavage of numerous substrates, triggering irreversible death and the ultrastructural characteristics of an apoptotic cell: cell shrinkage and separation, plasma membrane blebbing, nuclear condensation, and finally fragmentation into apoptotic bodies (reviewed in Taylor et al. 2008). These characteristics were noted by Kerr and colleagues, who also observed that the engulfment of apoptotic bodies by neighbouring cells prevented the release of cellular components (Kerr et al. 1972) (Fig. 1-1). In contrast to apoptosis, which is generally triggered by mild insults to the cell, more intense insults lead to a type of uncontrollable cell death called necrosis. Unlike apoptosis, necrosis involves cell swelling, membrane rupture, and elicitation of a local immune response (reviewed in Kolb et al. 2017).

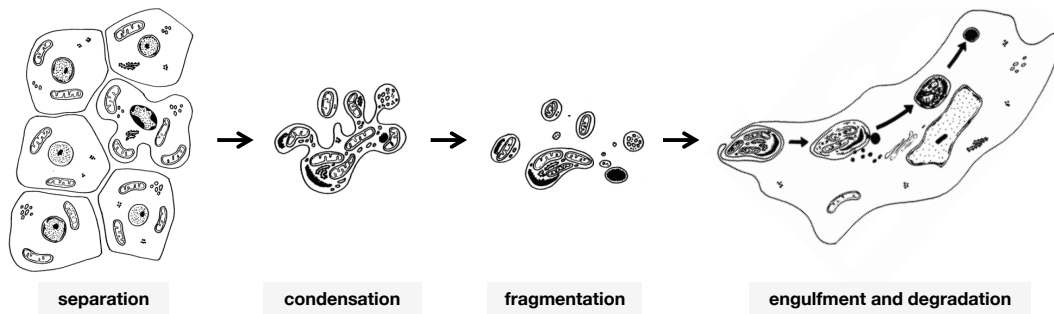


Fig. 1-1 | The morphological events of apoptosis. In 1972, J. Kerr, A. Wyllie, and A. Currie described the separation of apoptotic cells from the surrounding tissue as well as their condensation, fragmentation and eventual engulfment by macrophages (image adapted from Kerr et al. 1972).

Following the characterization of apoptosis, interest in the field took off in the 1980s when studies focused on the human gene *Bcl-2*. Researchers studying B-cell lymphoma discovered that a chromosomal translocation led to overactivity of the *Bcl-2* gene; however, the function of *Bcl-2* was initially unknown (Tsujimoto et al. 1983). When *Bcl-2* was found to be an inhibitor of cell death, it became the first example of an anti-apoptotic oncogene (Vaux et al. 1988). A genetic screen then uncovered a functional homolog of *Bcl-2* in nematode worms—the gene *ced-9*—that could also inhibit cell death (Hengartner et al. 1992). Furthermore, expression of human *Bcl-2* in worms significantly reduced the number of programmed cell deaths, demonstrating that *Bcl-2* can function in the nematode pathway and hinting at an evolutionarily conserved pathway for apoptosis in metazoans (Vaux et al. 1992). Soon thereafter, cloning of *ced-9* confirmed that it shares sequence and structural homology with *Bcl-2* (Hengartner & Horvitz 1994).

In the decades since, collective research has identified an entire family of proteins in the animal kingdom with homology to *BCL-2* and roles in apoptosis. These proteins contain one or more regions of amino-acid homology to *BCL-2*, termed *BCL-2* homology (BH) domains (reviewed in Delbridge et al. 2016), and can be categorized into three functional classes: 1) anti-apoptotic, multi-BH-domain; 2) pro-apoptotic, multi-BH-domain; and 3) pro-apoptotic, BH3-only (Fig. 1-2). It is the BH3-only proteins that act as initiators of the apoptotic pathway by sensing cellular stimuli. Their direct interaction with anti-apoptotic, multi-domain proteins, such as *BCL-2*, relay the signal further down the pathway, leading to the induction of pro-apoptotic, multi-domain proteins and, ultimately, the activation of caspases (reviewed in Youle & Strasser 2008). In essence, the

INTRODUCTION

life-or-death decision in a cell relies on the balance and net interactions of BCL-2-family proteins and their opposing activities.

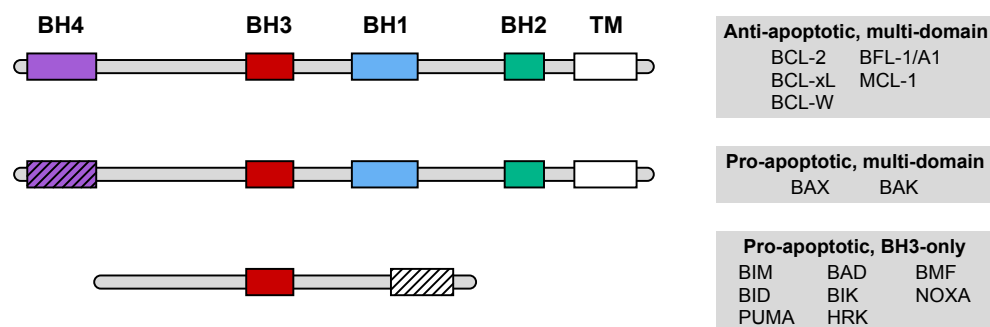


Fig. 1-2 | Domain structure of the three BCL-2-family protein classes. The presence of BH domains is illustrated for proteins in each of the three BCL-2-family classes. Mammalian proteins belonging to each class are given. Transmembrane (TM) domains are also indicated, when present. Domains that are not always present in the group are striped (BH4 in pro-apoptotic, multi-domain; TM in pro-apoptotic, BH3-only).

1.1.2 Programmed cell death during development in *C. elegans*

The underlying mechanisms of programmed cell death, and the role of BCL-2-family proteins, were revealed by groundbreaking genetic studies in the soil nematode *Caenorhabditis elegans*. These studies were not initially related to cell death; rather, they were designed to track cell divisions during animal development. *C. elegans* was used due to its small size and cell number, simple tissue organization, and transparency. This allowed researchers to view individual cells—as well as their divisions, migrations, and fates—using Nomarski differential interference contrast (DIC) optics (Robertson & Thomson 1982; Sulston & Horvitz 1977; Kimble & Hirsh 1979; Sulston et al. 1983).

John Sulston and H. Robert Horvitz meticulously tracked individual cell lineages during *C. elegans* development, noting little variation in the number and position of somatic cells between animals (Sulston & Horvitz 1977). Thus, they proposed that the development of *C. elegans* follows a rigidly fixed program and proceeded to derive the complete embryonic and post-embryonic cell-lineage trees (Sulston & Horvitz 1977; Sulston et al. 1983). Their efforts revealed that a total of 1090 somatic cells are generated during development of a *C. elegans* hermaphrodite; however, not all of these cells survive, and it was the observation of programmed cell death in the animal that led to the establishment of *C. elegans* as a powerful model for the field (Horvitz 2003). For this, the 2002 Nobel

Prize in Physiology or Medicine was awarded to Sulston and Horvitz, as well as Sydney Brenner—the man who established *C. elegans* as a model organism in biology.

Precisely 131 of the 1090 cells (~12%) that arise during *C. elegans* development are eliminated by programmed cell death—113 during embryogenesis and 18 during post-embryonic stages (Sulston & Horvitz 1977; Sulston et al. 1983). Furthermore, the identities of the 131 apoptotic cells are essentially invariant from animal to animal, producing a distinctive pattern of cell death. Many of these cells are the product of an asymmetric neuroblast division, with the larger daughter surviving and the smaller daughter undergoing programmed death. As they die, these cells round up and adopt a refractile morphology under DIC optics, making them discernible from living cells (Fig. 1-3B); they also exhibit condensed chromatin and a reduced cytoplasmic volume (Sulston et al. 1983; Shaham & Horvitz 1996a). Eventually, each cell corpse is engulfed by a neighbouring cell and its remnants are degraded inside the resulting phagosome (Fig. 1-3A).

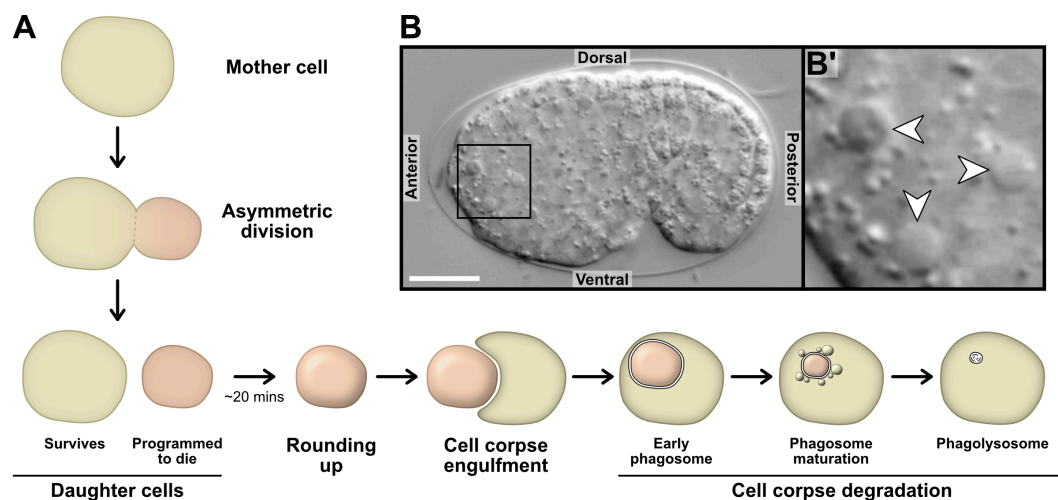


Fig. 1-3 | Formation and observation of cell corpses during *C. elegans* development. (A) Illustration of an asymmetric division that generates a small daughter cell programmed to die, followed by the rounding up, engulfment, and degradation phases. (B) DIC image of a developing *C. elegans* embryo, with three rounded-up, refractile cell corpses visible in the anterior region (boxed area magnified in B'; arrowheads indicate cell corpses). Scale bar 10 μm .

1.1.3 The central pathway of apoptosis

Researchers sought to uncover the molecular pathway of apoptosis and *C. elegans* was well-suited to forward genetic screening, making it possible to isolate genes responsible

INTRODUCTION

for the well-defined pattern of cell death. Moreover, apoptosis is not essential for *C. elegans* development and viability under laboratory conditions (Ellis & Horvitz 1986), so mutants exhibiting a general block in apoptosis can be maintained for study. In the end, the central apoptotic pathway was narrowed down to four genes: three pro-apoptotic (*egl-1*, *ced-4*, and *ced-3*) and one anti-apoptotic (*ced-9*) (reviewed in Conradt et al. 2016).

The *ced-3* and *ced-4* (*ced*, cell death abnormal) genes were first to be recognized, pulled out of a genetic screen when loss-of-function (*lf*) mutations in either gene lead to a general block in programmed cell death during development (Ellis & Horvitz 1986). The *ced-9* gene was identified next, when a dominant gain-of-function (*gf*) mutation in *ced-9* prevented cells from dying (Hengartner et al. 1992). Furthermore, *lf* mutations in *ced-9* caused the inappropriate death of cells that normally survive, resulting in embryonic lethality (Hengartner et al. 1992). Thus, *ced-9* was determined to be an essential gene for development, and its protective activity in cells differed from the pro-apoptotic activity of both *ced-3* and *ced-4*.

The *egl-1* (*egl*, egg-laying defective) gene was the final component of the central apoptotic pathway to be isolated. A prior screen had identified a number of genes regulating vulva development, and among these was *egl-1* (Trent et al. 1983). Dominant *gf* mutations in *egl-1* led to the inappropriate death of two neurons required for egg laying—the hermaphrodite-specific neurons (HSNs)—causing an *Egl* phenotype due to egg retainment in the mother (Trent et al. 1983). Since the HSNs normally undergo programmed death in male animals, initial findings limited the role of *egl-1* to the sexually dimorphic fate of these neurons (Trent et al. 1983; Desai et al. 1988). A decade passed before the true role of *egl-1* was uncovered. By mutagenizing *egl-1(gf)* animals and screening for suppression of the *Egl* phenotype, a *lf* mutation in *egl-1* was isolated that rescued HSN death (Conradt & Horvitz 1998). Surprisingly, loss of *egl-1* also blocked nearly all somatic cell death, indicating that *egl-1* had a general role in programmed cell death during development and its activity was not limited to the HSNs.

Epistatic analyses allowed researchers to arrange the four genes into a genetic pathway. First, ectopic cell death and lethality in *ced-9(lf)* animals could be suppressed by *lf* mutations in *ced-3* or *ced-4* (Hengartner et al. 1992) but not by *egl-1(lf)* (Conradt & Horvitz 1998). This placed *ced-9* upstream of *ced-3* and *ced-4* but downstream of *egl-1*. Second, overexpression of *ced-4* required *ced-3* activity to induce ectopic cell death, placing *ced-4* upstream of *ced-3* (Shaham & Horvitz 1996a). Taken together, these results implied a

simple linear pathway, with *egl-1* as the most upstream factor and antagonist of *ced-9* (Fig. 1-4). This pathway is conserved in the animal kingdom, from nematodes to humans, although the mammalian pathway possesses more redundancy and complexity (reviewed in Conradt 2009). Still, the presence of homologous cell-death genes in *C. elegans* and mammals underscored the importance of understanding the core apoptotic pathway and its regulation.

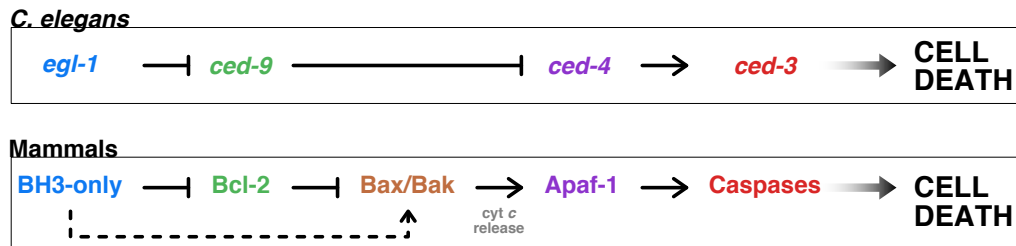


Fig. 1-4 | The conserved central apoptotic pathway. Homologous genes are similarly coloured. Positive interactions are indicated with an arrow; inhibitory interactions with a blunt line. The Bax/Bak-dependent release of cytochrome *c* (cyt *c*) from mitochondria in mammals has not been reported in *C. elegans*.

The *ced-9* and *egl-1* genes encode members of the BCL-2 family that have conserved roles in apoptosis. CED-9 is an anti-apoptotic protein with all four types of BH domains, as well as a transmembrane domain; it is homologous to other anti-apoptotic, multi-domain BCL-2-family proteins (Fig. 1-2). EGL-1 is a pro-apoptotic BH3-only protein, homologous to the eight BH3-only proteins that exist in mammals: BIM, BID, PUMA, BAD, BIK, HRK, BMF, and NOXA (Fig. 1-2). The two remaining genes in the central apoptotic pathway—*ced-4* and *ced-3*—do not encode members of the BCL-2 family. CED-4 is an APAF-1-like adapter protein, capable of oligomerizing to form the apoptosome complex (Ellis & Horvitz 1986; Yuan & Horvitz 1992; Yang et al. 1998; Qi et al. 2010), and CED-3 is a caspase, the founding member of a family of proteolytic enzymes with crucial roles in the execution of apoptosis (Ellis & Horvitz 1986; Yuan et al. 1993; Xue et al. 1996). Much like their mammalian counterparts, the CED-4 apoptosome recruits pro-CED-3 precursors and facilitates their activation to CED-3 caspase (Yang et al. 1998; Huang et al. 2013).

CED-9 resides on the outer mitochondrial membrane (Chen et al. 2000; Tan et al. 2007) and, under non-apoptotic conditions, physically binds and sequesters an asymmetric homodimer of CED-4, prohibiting its activity (Spector et al. 1997; Wu et al. 1997; Yan et al. 2005). In most of the 131 cells programmed to die during *C. elegans* development, EGL-1

INTRODUCTION

activity crosses a threshold and commits the cell to an apoptotic fate (reviewed in Nehme & Conradt 2008; Conradt et al. 2016). EGL-1 exerts its pro-apoptotic activity by interacting with CED-9, which is mediated by the helical BH3 domain of EGL-1 (Conradt & Horvitz 1998; del Peso et al. 1998; del Peso et al. 2000; Woo et al. 2003; Yan et al. 2004) (Fig. 1-5). Binding of EGL-1 induces a conformational change in CED-9, destabilizing the preexisting CED-4:CED-9 complex and displacing CED-4. Released into the cytosol, CED-4 dimers associate to form an octameric apoptosome that mediates the activation of CED-3. Finally, CED-3 cleaves a variety of downstream substrates that bring about the demise of the cell (Yuan et al. 1993; Xue et al. 1996; Taylor et al. 2007). One substrate is the Xkr8-like protein CED-8, whose activity mediates phosphatidylserine externalization on the plasma membrane as a phagocytic signal (Stanfield & Horvitz 2000; Suzuki et al. 2013).

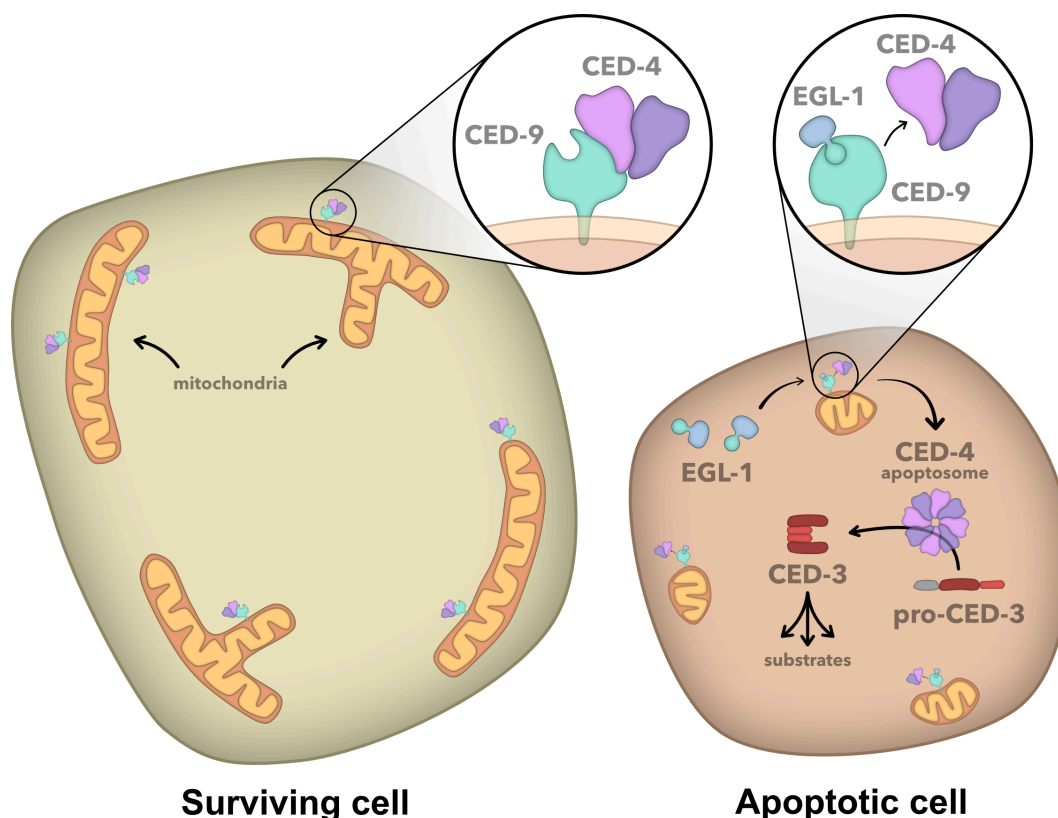


Fig. 1-5 | Molecular mechanism of cell death in *C. elegans*. The proteins and key steps of the central apoptotic pathway are illustrated in both a surviving and apoptotic cell. See text for further details.

There are examples of programmed cell death in *C. elegans* that are not dependent on the entire central pathway. For example, the tail-spike cell undergoes programmed cell death five hours after it arises (Sulston et al. 1983), and its death is thought to rely on the transcriptional activation of *ced-3*, bypassing the roles of *egl-1* and *ced-9* (Maurer et al. 2007). In another case, the linker cell is unaffected by mutations blocking apoptosis, and the morphological changes of this cell death differ from that of an apoptotic cell (Abraham et al. 2007; Blum et al. 2012). Linker cell-type death instead relies on multiple regulatory modules (Abraham et al. 2007; Blum et al. 2012; Malin et al. 2016). Cell death is also prevalent during maturation of the *C. elegans* germline, with more than half of all female germ cells undergoing physiological germ-cell death (Gumienny et al. 1999). However, germline apoptosis is a stochastic process without fixed cell identities, and the activity of EGL-1 is dispensable (Gumienny et al. 1999).

The four components of the central apoptotic pathway are functionally conserved across various members of the animal kingdom, but are seemingly absent in bacteria, fungi, and plants (reviewed in Zmasek & Godzik 2013). Among animals, there are differences in how programmed cell death is executed. In the fruit fly *Drosophila melanogaster*, Bcl-2-family genes have a surprisingly minor role, although at least two are encoded by the genome (Sevrioukov et al. 2007; Galindo et al. 2009; Tanner et al. 2011). Rather, programmed cell death in the fly depends on both internal and external stimuli that lead to the transcriptional upregulation of pro-apoptotic genes—namely Reaper, Hid, and Grim (RHG) (reviewed in Conradt 2009). In mammals, most BCL-2-family proteins control activity of the APAF-1 apoptosome by regulating the release of cytochrome *c* (cyt *c*) from mitochondria, which then facilitates apoptosome formation (Fig. 1-4); the release of cyt *c* from mitochondria has not been found in *C. elegans*. Regulation of apoptosis in mammals is also more complex, and the pathway itself is more robust due to a considerable amount of redundancy among components, including multiple BCL-2-family proteins and caspases. Despite this robustness, apoptosis can still go awry and lead to cancer, neurological disorders and autoimmune diseases (Fuchs & Steller 2011).

1.1.4 Regulation of *egl-1* and the apoptotic fate

The central apoptotic pathway is tightly regulated in *C. elegans* to avoid any unwanted (i.e. ectopic) cell death. In particular, the *egl-1* gene is under precise temporal and spatial control that restricts its activity to cell-death lineages (reviewed in Nehme & Conradt

2008; Conradt et al. 2016). This control occurs largely at the level of *egl-1* transcription, and rather than a universal set of *trans*-acting factors (i.e. transcriptional regulators) across all cells programmed to die, it seems that each cell-death lineage employs its own factors to control *egl-1* expression. Among these are the zinc-finger transcription factor TRA-1 in the HSNs (Conradt & Horvitz 1999), the Snail-like CES-1 and bHLH proteins HLH-2/HLH-3 in the neurosecretory motorneurons (NSMs) (Thellmann et al. 2003), and the Collier/Olf1/EBF1 (COE) transcription factor UNC-3 in the dopaminergic RID neuron lineage (Wang et al. 2015). Often, these factors have additional nonapoptotic roles within the same lineage. For example, CES-1 activity contributes to asymmetric division of the NSM neuroblast (Wei et al. 2017), and UNC-3 is involved in terminal differentiation of the RID neuron (Wang et al. 2015). *Trans*-acting factors of the *egl-1* gene may also have more general roles during development and regulate numerous targets, such as the Sp1-family transcription factor SPTF-3 and its role in vulval development, morphogenesis, and cell-fate determination (Ulm et al. 2011; Hirose & Horvitz 2013). Just as the central apoptotic pathway is evolutionarily conserved, many of these *trans*-acting factors have homologs in humans that have been implicated in cancer and cell death regulation (reviewed in Potts & Cameron 2011).

To accommodate *cis*-regulatory elements (i.e. binding sites) for various transcription factors, the *egl-1* genomic locus has evolved to be extensive and complex. The regulatory elements described to date are located both up- and downstream of the *egl-1* transcription unit, even extending beyond neighbouring genes; mutations in these elements affect *egl-1* expression and the invariant pattern of programmed cell death (Conradt & Horvitz 1999; Thellmann et al. 2003; Liu et al. 2006; Potts et al. 2009; Hirose et al. 2010; Winn et al. 2011; Hirose & Horvitz 2013; Jiang & Wu 2014; Wang et al. 2015). The most distant *cis*-regulatory element described to date is the binding site for TRA-1 that controls HSN survival, which resides 5.6 kilobases (kb) downstream of *egl-1* (Conradt & Horvitz 1999). Furthermore, a comparative genome sequence alignment of the locus across other species of *Caenorhabditis* revealed several regions of conservation that span across ~14.5 kb, and all known *cis*-acting elements of *egl-1* are found within these regions (Conradt et al. 2016) (Fig. 1-6).

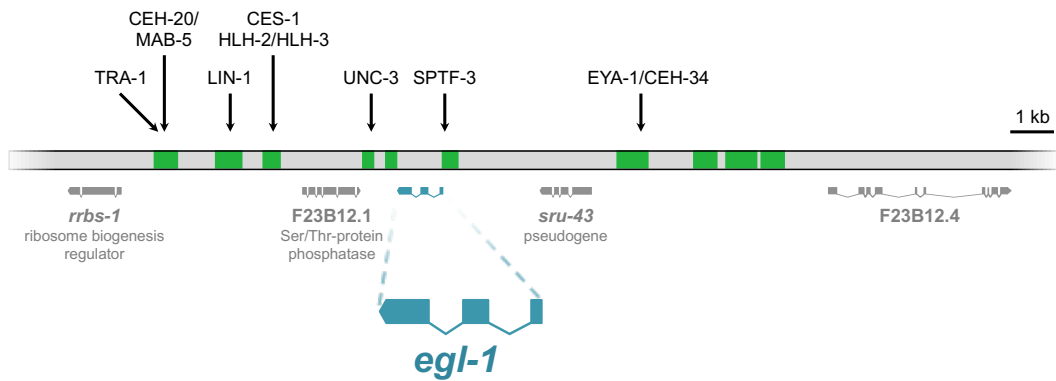


Fig. 1-6 | The complex genomic locus of *egl-1*. The *egl-1* gene resides on the negative strand of chromosome V (i.e. linkage group V, LGV). The *egl-1* transcription unit (1050 bp) is enlarged and coloured in blue. Neighbouring transcription units on both strands are illustrated in grey. Blocks of sequence conserved in other nematodes are highlighted in green. Transcription factors of *egl-1* with validated binding elements are shown above their respective sites (image taken from Conradt et al. 2016).

It is clear that transcriptional regulation is crucial for the proper expression of *egl-1*, and this holds true for BH3-only genes in mammals. For example, upon DNA damage, the tumour suppressor P53 upregulates three BH3-only genes to trigger apoptosis; Puma is the main target, while Noxa and Bik are minor targets (Oda et al. 2000; Nakano & Vousden 2001; Mathai et al. 2002; Villunger et al. 2003). Mutations in p53 are therefore common among human cancers (reviewed in Kasthuber & Lowe 2017). Puma, Noxa and Bik, as well as Hrk, are also regulated by the transcription factor E2F1 (Hershko & Ginsberg 2004), while Bim is a target of the transcription factors FOXO3a and CHOP (Dijkers et al. 2000; Puthalakath et al. 2007). Consequently, the genomic loci of mammalian BH3-only genes need to accommodate multiple transcription-factor binding sites to coordinate gene activity in response to the cellular state—similar to the locus of *egl-1*.

Regulation of BH3-only genes also occurs at the post-translational level in mammals. Phosphorylation of all eight BH3-only proteins has been reported, which can positively or negatively alter their activity based on the modified residue (reviewed in Happo et al. 2012). For example, phosphorylation of BIM by ERK reduces its pro-apoptotic activity and targets it for ubiquitylation and proteasomal degradation, whereas phosphorylation by JNK enhances its activity (reviewed in Sionov et al. 2015). BH3-only proteins are also controlled by interactors that sequester and inhibit their pro-apoptotic activity, such as the binding of BAD to 14-3-3 scaffold proteins (Zha et al. 1996), or the interaction of BIM

INTRODUCTION

and BMF with cytoskeletal motor complexes (Puthalakath et al. 1999, 2001). Finally, BID is regulated post-translationally by Caspase-8 to generate the active cleavage product termed truncated BID (tBID), which then interacts with other BCL-2 family members (Luo et al. 1998; Li et al. 1998).

Regulation that takes place at the post-transcriptional level also contributes to the precise execution of programmed cell death; however, our knowledge of such regulation lags behind that of other levels. Recent advances in the field are changing this, including the discovery of additional post-transcriptional mechanisms and the development of transcriptome-wide analyses. Considering that the central apoptotic pathway and several of its regulators are conserved between *C. elegans* and humans, exploring how the pathway is regulated post-transcriptionally is an open and interesting question.

In the next section, I introduce mechanisms of post-transcriptional regulation and discuss the subject as it pertains to the aim of this study. Since the major mechanisms are largely identical across eukaryotic cells (reviewed in Schaefer et al. 2018), post-transcriptional regulation of the core apoptotic pathway in *C. elegans* could be paralleled in higher organisms.

1.2 Post-transcriptional regulation of gene expression

1.2.1 Mechanisms of post-transcriptional regulation

Regulation of eukaryotic gene expression is a complex process, encompassing all mechanisms that induce or repress the expression of a gene. These mechanisms act at multiple points along the pathway from DNA to messenger RNA (mRNA) to protein, ensuring that genes are expressed in a cell at the correct time and at the proper level (Fig. 1-7).

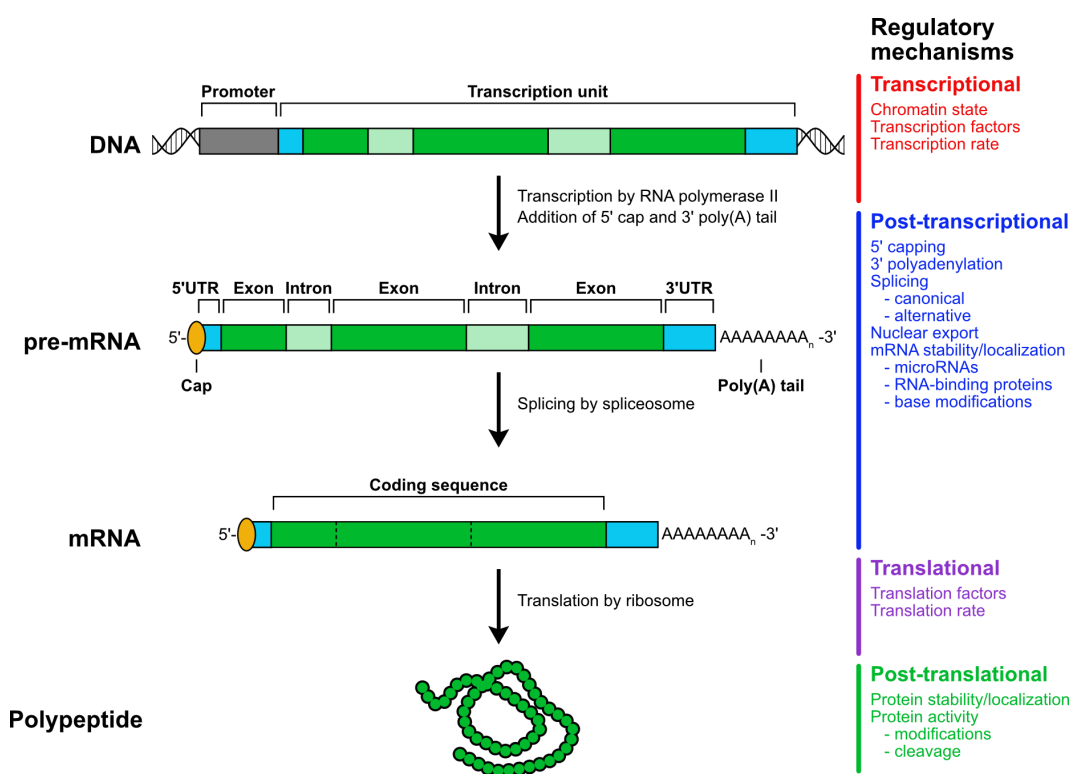


Fig. 1-7 | Principal stages of gene regulation. From DNA to protein, transcription to translation, the intermediate molecules are illustrated and annotated to highlight major features. The key regulatory mechanisms affecting each step are summarized on the right.

The first point of regulation is at the transcriptional level, where the chromatin status and activity of transcription factors control the rate and efficiency of pre-mRNA synthesis. The final point of regulation occurs post-translation, where modifications and turnover affect the stability and activity of the encoded protein. Between these two stages, post-transcriptional regulation provides cells with a chance to fine-tune gene expression after a gene has already been transcribed, but before translation of the mRNA into a

INTRODUCTION

polypeptide. The stability, chemical nature, and localization of an mRNA molecule can all be controlled, ultimately determining if translation is favoured or not. This level of regulation is particularly crucial during adaptation to stress, since it makes use of preexisting mRNAs to induce changes in the proteome more rapidly than transcriptional upregulation (reviewed in Harvey et al. 2017). Furthermore, studies often find a poor correlation between mRNA and protein levels in eukaryotic cells, and this is partially attributed to the activity of post-transcriptional mechanisms (reviewed in Liu et al. 2016).

The mechanisms of post-transcriptional regulation are diverse and take place in multiple compartments of the cell (reviewed in Schaefer et al. 2018). It begins with pre-mRNA processing in the nucleus, where capping enzymes and poly(A) polymerases add the 5' cap and poly(A) tail, respectively. This is important for stability of the molecule, as the first step in mRNA decay is shortening of the poly(A) tail by deadenylases and/or removal of the 5' cap by decapping enzymes (reviewed in Schoenberg & Maquat 2012). Next, large spliceosome complexes assemble on the pre-mRNA and catalyze the excision of introns; concurrently, they splice together the remaining exons to yield a mature mRNA molecule (Fig. 1-7). All three of these processes—capping, polyadenylation, and splicing—can be regulated by the cell to modify genetic output. One notable example of this is alternative splicing, where exons are differentially spliced together to direct the synthesis of multiple protein isoforms.

Mature mRNA molecules need to be exported from the nucleus to the cytoplasm where ribosomes await. Translocation through nuclear pore complexes and across the nuclear membrane is an active process, facilitated by a host of co-factors (reviewed in Carmody & Wentz 2009). Once in the cytoplasm, mRNAs are susceptible to post-transcriptional regulatory machinery that controls their localization, stability, and translatability. The precise fate of an mRNA is largely dictated by *cis*-regulatory elements contained within the nucleotide sequence itself. These elements serve as binding sites for *trans*-acting factors, namely microRNAs (miRNAs), RNA-binding proteins (RBPs), and other small non-coding RNAs. The regulatory actions of these factors are detailed in Section 1.3 (miRNAs) and Section 1.4 (RBPs).

1.2.2 Post-transcriptional regulation via the 3'UTR

Flanking each end of the mRNA coding sequence (CDS) are untranslated regions (UTRs), whose nucleotide sequences do not code for amino acids in the final polypeptide (Fig. 1-8). UTRs are less conserved than CDSs overall, however 3'UTRs still contain regions of highly-conserved sequence that are often enriched for miRNA- and RBP-binding elements (Siepel et al. 2005; Friedman et al. 2009). This makes 3'UTRs—and to a lesser degree, 5'UTRs—hotspots of post-transcriptional regulation, with key roles in determining the fate of an mRNA molecule (reviewed in Mayr 2017).

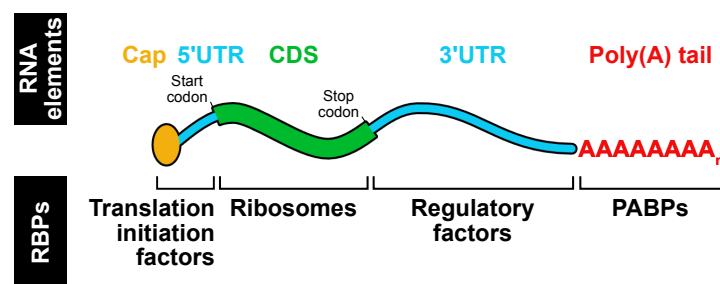


Fig. 1-8 | Anatomy of an mRNA molecule. The key elements are indicated above the illustration, while RBPs known to interact with each element are given below (PABPs, poly(A)-binding proteins).

The regulatory potential of a 3'UTR is held in its sequence and *cis*-regulatory-element composition, which define the pool of *trans*-acting factors that can directly target the mRNA. This pool is then further specified by the cellular state, meaning that the propensity of a factor to bind a given *cis*-regulatory element depends on the local environment (reviewed in Singh et al. 2015). Often, the *trans*-acting factors themselves interact with diverse sets of cofactors, so each regulatory element has the potential to carry out different functions depending on the factors recruited. In addition, mRNAs are not simple linear molecules—they can adopt intricate secondary and tertiary structures. Local and long-distance base pairing can create structural elements such as stem-loops, pseudoknots and complex junctions (reviewed in Bevilacqua et al. 2016). These structures influence the binding of *trans*-acting factors, particularly when occlusive mRNA structures are formed that reduce the accessibility of *cis*-regulatory-elements (Agarwal et al. 2015; Taliaferro et al. 2016). Thus, 3'UTR-mediated post-transcriptional regulation is highly dynamic and should be considered in the context of bound factors at a given time.

1.2.3 Post-transcriptional regulation of the cell death pathway

In mammals, post-transcriptional regulation of several Bcl-2-family genes has been documented. Alternative splicing of Bcl-xL and Mcl-1 is mediated by the spliceosome and RBPs, resulting in protein isoforms that have opposing activity to the dominant gene products (Boise et al. 1993; Bae et al. 2000; Kim et al. 2009). Bim is also alternatively spliced, generating three protein isoforms that have different potentials for phosphorylation (O'Connor et al. 1998; Clybouw et al. 2012). Targeting of Bcl-2-family transcripts by both RBPs and miRNAs has also been reported. Bcl-2, Mcl-1, and Bcl-xL are all targeted by stabilizing and/or destabilizing RBPs, depending on the cellular state; they are also targeted by multiple miRNAs, as are Bcl-w, Bax, and Bim (reviewed in Cui & Placzek 2018).

In *C. elegans*, at least two of the four central-apoptotic genes are regulated at the post-transcriptional level. First, *ced-4* pre-mRNA can be alternatively spliced to produce a second, longer transcript called *ced-4L* (Shaham & Horvitz 1996b). Both mRNA variants are present in whole animals, although *ced-4L* mRNA is only expressed at one-tenth the level of *ced-4* (Shaham & Horvitz 1996b). Contrary to CED-4, the activity of CED-4L is anti-apoptotic due to its dominant interference in apoptosome assembly. The second example was recently reported, showing that *ced-3* mRNA is post-transcriptionally repressed by RBPs in the germline of adults (Subasic et al. 2016). Prior to the study I present in this thesis, post-transcriptional regulation of neither *egl-1* nor *ced-9* had not been demonstrated *in vivo*, although an *in vitro* study demonstrated that the *egl-1* 3'UTR is capable of binding miRNAs (Wu et al. 2010).

1.3 Post-transcriptional regulation by miRNAs

1.3.1 Biogenesis and function of miRNAs

First discovered in *C. elegans*, miRNAs are small non-coding RNAs, approximately 22 nucleotides (nt) in length, with a conserved role in post-transcriptional gene regulation (Lee et al. 1993; Lau et al. 2001; Lee & Ambros 2001; reviewed in Ambros 2004 and Bartel 2009). miRNAs play a major regulatory role in eukaryotic cells, whereas the role of small RNAs in prokaryotic cells is less evident; the first example of a functional, miRNA-size molecule in bacteria was only recently described (Nejman-Faleńczyk et al. 2015). In *C. elegans*, over 140 miRNA-coding genes have been uncovered with wide-ranging regulatory roles in biological processes, including developmental timing, metabolism, stress responses, and behaviour (reviewed in Ambros & Ruvkin 2018).

miRNAs are first generated as a hairpin-containing primary miRNA (pri-miRNA) transcript by RNA polymerase II (Fig. 1-9). The pri-miRNA is processed in the nucleus by Drosha (DRSH-1 in *C. elegans*) to yield a single hairpin precursor miRNA (pre-miRNA), which is then exported to the cytoplasm (Lee et al. 2003). The pre-miRNA is processed once more by Dicer (DCR-1 in *C. elegans*) to generate the mature, single-stranded miRNA (Bernstein et al. 2001). The mature miRNA is then incorporated into the miRNA-induced silencing complex (miRISC), where it directly associates with a member of the ArgonAUT protein family (ALG-1/2 in *C. elegans*). The miRNA then guides the miRISC to specific sequences in target mRNAs—often in the 3'UTRs—that complement the miRNA seed region (nucleotides 2–7); additional imperfect complementarity may also exist outside the seed region (Brancati & Großhans 2018). Ultimately, the binding of the miRISC to its target mRNA inhibits translation while also promoting deadenylation, decapping, and degradation of the mRNA (reviewed in Jonas & Izaurralde 2015).

Due to the imperfect binding of miRNAs to their targets, some interactions are more stable than others, leading to the classification of miRNA-binding sites that differ in strength. For nematodes in particular, several types of miRNA sites have been defined, but only the strongest six are preferentially conserved (Fig. 1-10) (Jan et al. 2011). These include two sites that are nematode specific (i.e. not observed in vertebrates)—an octamer site (8mer-U1) and a hexamer site (6mer-A1).

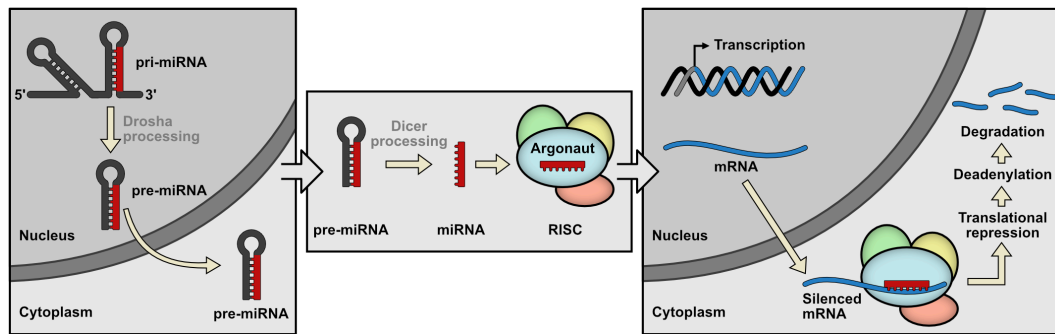


Fig. 1-9 | miRNA biogenesis pathway and miRISC-mediated mRNA silencing. See text for details.

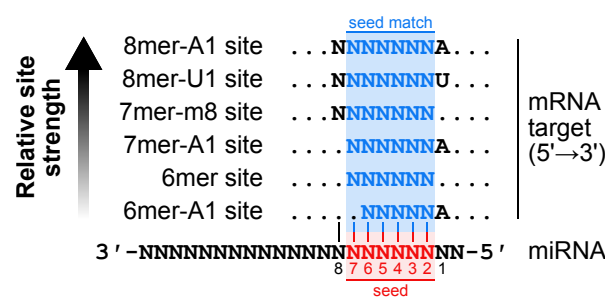


Fig. 1-10 | Relative strength of miRNA-seed binding in nematodes. These six types of miRNA-binding sites are preferentially conserved in nematode 3'UTRs, ordered from strongest (8mer-A1) to weakest (6mer-A1). The seed region of the miRNA is highlighted in red, and seed-matched nucleotides in the mRNAs are highlighted in blue. Image adapted from Jan et al. (2011).

Initially, the miRISC was thought to silence gene expression by blocking the initiation step of protein translation on target mRNAs (Wightman et al. 1993; Olsen & Ambros 1999). It was later discovered that the miRISC also promotes mRNA decay via the recruitment of destabilizing factors (Bagga et al. 2005; Lim et al. 2005; reviewed in Iwakawa & Tomari 2015). First, the miRISC can recruit deadenylases, such as those associated with the Ccr4-Not complex, which shorten the poly(A) tail and decrease the half-life of the mRNA molecule (Giraldez et al. 2006; Wu et al. 2006; Eulalio et al. 2009). Second, they can recruit decapping enzymes which catalyze removal of the protective 5' cap, rendering the mRNA susceptible to degradation by exonucleases (Rehwinkel et al. 2005; Behm-Ansmant et al. 2006). Less understood is exactly how miRNAs direct the repression of translation, despite long-standing knowledge that this repression exists. The prominent view is that the miRISC mediates the displacement of poly(A)-binding proteins (PABPs) from the poly(A) tail, as well as cap-binding proteins from the 5' cap (Moretti et al. 2012). This destabilizes the closed-loop structure of the target mRNA,

thereby disrupting translation re-initiation. More recently, it was proposed that the miRISC can promote the formation of a unique, inhibitory closed-loop formation that blocks translation (Chapat et al. 2017). Undoubtedly, the miRNA silencing pathway employs both deadenylation and decapping machinery to inhibit translation and promote mRNA decay, although the precise mechanisms still need to be affirmed.

How one mechanism—translational repression or mRNA decay—is selected over the other is another topic of debate. Certain conditions may dictate the relative contribution of each mechanism, such as the concentration of miRISC components, the miRNA-seed binding strength, the number of binding sites per mRNA, or the type of cell (reviewed in Jonas & Izaurralde 2015). Furthermore, evidence suggests that translational repression often precedes mRNA decay, but the latter still accounts for the majority of overall silencing (Guo et al. 2010; Bazzini et al. 2012; Djuranovic et al. 2012; Eichhorn et al. 2014). Finally, degradation may not be the terminal fate of miRNA-targeted mRNAs; in some cases, repression may be relieved at a later point, allowing translation to re-initiate. This relief may be achieved via the degradation of specific miRISC components or dissociation of the miRISC from target mRNAs (Bhattacharyya et al. 2006; Kundu et al. 2012).

1.3.2 miRNA-mediated regulation of programmed cell death

miRNAs can regulate diverse cellular processes, including programmed cell death (reviewed in Alberti & Cochella 2017). This was first revealed by studies on the *bantam* miRNA in *Drosophila*, which targets the pro-apoptotic gene *hid* (Brennecke et al. 2003). Hid is an RHG protein that promotes apoptosis by binding to and neutralizing inhibitor-of-apoptosis proteins (IAPs), resulting in caspase activation (Grether et al. 1995; reviewed in Steller 2008). A later study uncovered two members of the *Drosophila* miR-2 family, miR-6 and miR-11, which also target RHG genes and reduce levels of apoptosis during embryonic development; accordingly, *mir-6/11* double mutants exhibit strong embryonic lethality (Ge et al. 2012).

Mammalian studies have uncovered numerous miRNAs that regulate the intrinsic and extrinsic apoptotic pathways (reviewed in Su et al. 2016). Although much of this regulation is indirect, some direct targets do include pro- and anti-apoptotic genes of the Bcl-2 family, namely: Bcl-2 (Cimmino et al. 2005; Zhu et al. 2010), Bax (Adlakha & Saini 2011; Hamada et al. 2014), Bcl-xL (Nakano et al. 2010; Zhang et al. 2014), Mcl-1 (Mott et al.

2007; Li et al. 2016), and Bcl-w (Gong et al. 2013). When it comes to pro-apoptotic BH3-only genes, regulation occurs predominantly at the transcriptional and post-translational levels (reviewed in Happo et al. 2012). Nevertheless, extensive post-transcriptional regulation by miRNAs has been shown for at least one mammalian BH3-only gene. Bim—a key initiator of the intrinsic apoptotic pathway—is directly targeted by several different miRNAs to precisely regulate its activity (Ventura et al. 2008; Qian et al. 2011; Pernaute et al. 2014; reviewed in Sionov et al. 2015). One of these miRNAs in particular, miR-29b, is also capable of targeting the BH3-only genes Bmf, Hrk, and Puma (Kole et al. 2011). Two other BH3-only genes, Puma and Noxa, were reported as direct targets of both miR-23a and miR-27a in the brain tissue of mice (Sabirzhanov et al. 2014).

1.3.3 miR-35- and miR-58-family microRNAs

Prior to the work presented in this study, direct regulation of the central apoptotic pathway by miRNAs in *C. elegans* had not been reported. However, the 3'UTR of *egl-1* was investigated *in vitro* as a potential target of miRNAs from the miR-35 and miR-58 families (Wu et al. 2015). The miR-35 family has eight members, referred to collectively as miR-35-42, with each having the same 5'-CACCGGG-3' seed sequence. The genes encoding these miRNAs reside in two loci on chromosome II: seven of the eight genes (*mir-35-41*) are clustered at a single locus and transcribed together—a so-called miRNA operon—yielding a complex pri-mRNA (Fig. 1-11); the eighth gene (*mir-42*) is located ~350 kb away and transcribed separately. No sequence homology exists between the miR-35 family and miRNAs higher animals, so it is considered to be nematode specific. On the other hand, the miR-58 family is homologous to *bantam* in *Drosophila* and consists of six members: miR-58.1, miR-58.2, miR-80-82, and miR-2209.1. All members of the miR-58 family contain the seed sequence 5'-CGAUCUC-3'.

Many miRNAs are maternally inherited; that is, they are loaded into oocytes prior to fertilization and therefore already present in the 1-cell embryo. The miR-35 family is inherited in this manner, and is the most abundant miRNA family in oocytes and early embryos (Stoeckius et al. 2009; Jan et al. 2011; Alberti & Cochella 2017). Although miR-35 family miRNAs continue to be transcribed, their abundance declines as development progresses (Martinez et al. 2008; Kato et al. 2009; Stoeckius et al. 2009; Alvarez-Saavedra & Horvitz 2010; Wu et al. 2010; Jan et al. 2011) (Fig. 1-12).

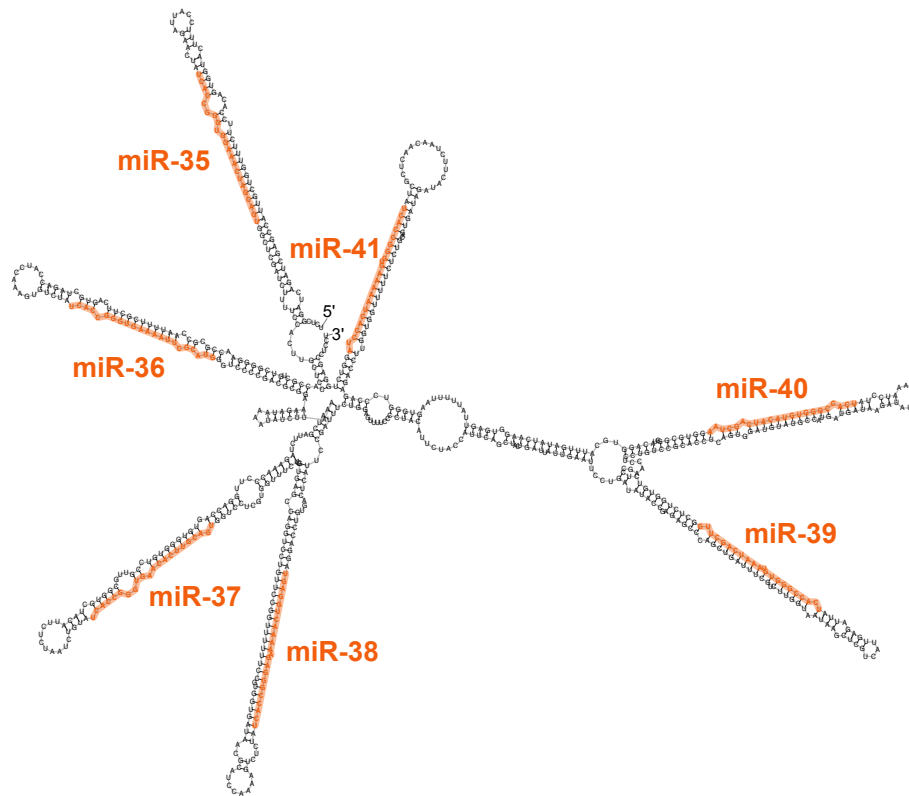


Fig. 1-11 | The *mir-35-41* primary transcript. Seven of the eight genes encoding miR-35 family miRNAs are clustered into a miRNA operon, resulting in a highly structured pri-miRNA transcript. Secondary structure prediction was generated by the RNAfold web server (v2.4.6, <http://ma.tbi.univie.ac.at>; Lorenz et al. 2011).

The miR-58 family is the most abundant in *C. elegans* when considering all stages of development, accounting for more than 30% of the total miRNA pool and reaching their highest levels post-gastrulation (Alvarez-Saavedra & Horvitz 2010; Isik et al. 2010; Wu et al. 2010; Jan et al. 2011) (Fig. 1-12). Moreover, the six members of the miR-58 family are differentially expressed—four are abundant (miR-58.1 and miR-80-82) whereas two are scarce (miR-58.2 and miR-2209.1) at all stages of development (Friedländer et al. 2008; Jan et al. 2011). Notably, miR-58.1 exhibits the highest expression of any single miRNA at all developmental stages and across multiple tissues, with the exception of the nervous system (Lim et al. 2003; Kato et al. 2009; Isik et al. 2010).

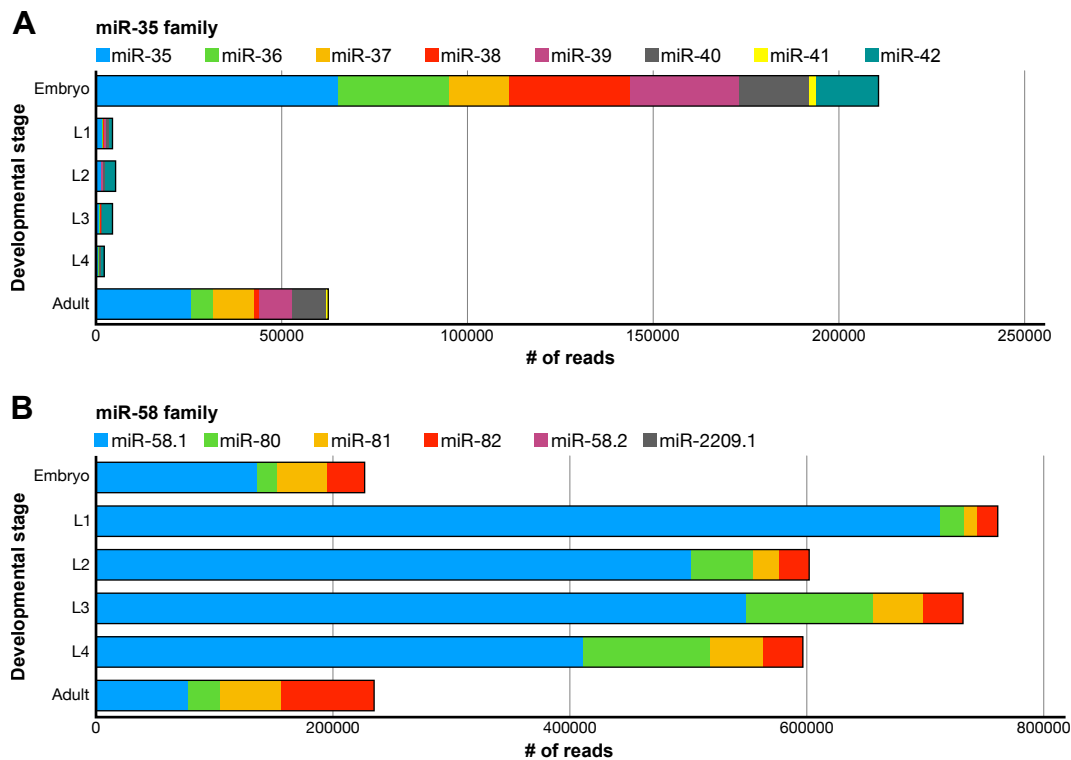


Fig. 1-12 | Developmental expression profile of miR-35- and miR-58-family miRNAs. (A–B) Illumina sequencing reads for individual miRNAs of the (A) miR-35 and (B) miR-58 families, from libraries of six developmental stages (embryo, L1, L2, L3, L4, adult). Data generated by Jan et al. (2011).

Grouping miRNAs into families reflects their identical seed regions as well as redundancy of their activity, since severe phenotypes generally arise only when all members of a family are lacking (Miska et al. 2007; Alvarez-Saavedra & Horvitz 2010). For example, a loss of seven *mir-35*-family members in *mir-35-41(nDf50)* animals results in altered sensitivity to RNA interference (RNAi) (Massirer et al. 2012), reduced fecundity (McJunkin & Ambros 2014), impaired responsiveness to hypoxia (Kagias & Pocock 2015), and improper sex determination (McJunkin & Ambros 2017), but only a partially penetrant temperature-sensitive lethality (Alvarez-Saavedra & Horvitz 2010). It is only when all eight members are deleted in *mir-35-41(nDf50) mir-42(nDf49)* animals—herein referred to as “*mir-35*-family mutants”—that development is irreversibly perturbed, resulting in 100% embryonic lethality (Alvarez-Saavedra & Horvitz 2010). The *mir-35* family is one of only two families—the other being the *mir-51* family (Shaw et al. 2010)—known to produce a fully penetrant embryonic lethal phenotype when all members are knocked-out. Although lethality in *mir-35*-family mutants is likely the consequence of several misregulated genes and pathways, it was recently shown that a single miR-35-

family binding site in the 3'UTR of the TRIM-NHL gene *nhl-2* is essential for viability (McJunkin & Ambros 2017).

When all four abundant members of the *mir-58* family are deleted in *mir-80(nDf53); mir-58.1(n4640); mir-81-82(nDf54)* animals—herein referred to as “*mir-58*-family mutants”—defects in both locomotion and dauer formation become apparent and body size is reduced (Alvarez-Saavedra & Horvitz 2010). Interestingly, *bantam* mutations in *Drosophila* also result in a smaller body size (Hipfner et al. 2002, Raisin et al. 2003). *C. elegans* mutants lacking all six *mir-58*-family members have not yet been described.

A previous study reported that miR-35- and miR-58-family miRNAs could bind the 3'UTR of *egl-1* mRNA *in vitro* and promote deadenylation (Wu et al. 2010). Furthermore, a loss of the *mir-58* family was linked to apoptosis abnormalities in the *C. elegans* germline, however no direct target was identified (Subasic et al. 2015). Thus, a firm link between these miRNAs and the regulation of programmed cell death remains to be shown.

1.4 Post-transcriptional regulation by RBPs

1.4.1 Function of RBPs

RBPs provide yet another level of post-transcriptional control over gene expression. RBPs contain an RNA-binding domain that facilitates their direct interaction with target mRNA molecules, unlike the miRISC which requires miRNA as a guide. Upon binding, RBPs may influence the translation, localization, or stability of the target mRNA (reviewed in Glisovic et al. 2008). Several RBPs can target the same mRNA simultaneously, forming a complex messenger ribonucleoprotein (mRNP) whose composition is governed by the affinity of individual RBPs for the mRNA and each other (reviewed in Müller-McNicoll & Neugebauer 2013). Therefore, the components of an mRNP can be controlled to coordinate and fine-tune expression, if needed.

Studies primarily identify genome-wide targets of specific RBPs by one of two methods. The first is RNP immunoprecipitation and microarray chip analysis (RIP-Chip), in which RBPs are purified together with associated RNAs, then RNAs are identified by microarray analysis (Keene et al. 2006). The second is crosslinking and immunoprecipitation (CLIP), in which RNA fragments that crosslink to a specific RBP are purified and sequenced (Ule et al. 2005). One advantage of CLIP over RIP-Chip is the ability to map crosslink sites with individual-nucleotide resolution—a variation of the method known as iCLIP (Huppertz et al. 2014).

RBPs can be recruited to their target mRNA in several ways and with varying degrees of specificity (reviewed in Jankowsky & Harris 2015) (Fig. 1-13). First, RBPs may directly bind a sequence motif in the mRNA molecule. These motifs can be specific, such as the motif recognized with high affinity by the Pumilio RBP in *Drosophila* (5'-UGUAHAUA-3'; H = A, U or C) (Gerber et al. 2006), or they can be nonspecific, such as the loosely defined U- and AU-rich motifs recognized by Human antigen R (HuR) (Lebedeva et al. 2011). Other RBPs rely on the presence of structural elements that arise from the folding of mRNA molecules. One such example, Staufen, binds to double-stranded (dsRNA) regions in a largely sequence-independent manner (Wickham et al. 1999; LeGendre et al. 2013). RBPs can also be recruited by proteins that have already associated with the mRNA, as with components of the splicing machinery and translation initiation factors.

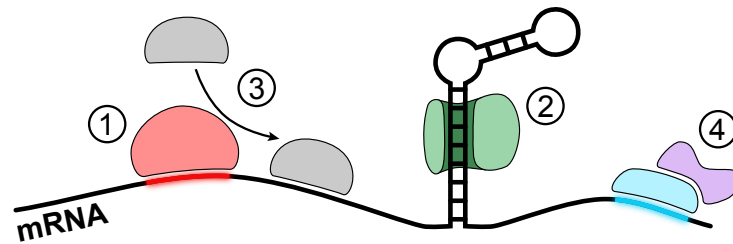


Fig. 1-13 | Modes of mRNP assembly. Four conventional ways that cytoplasmic RBPs associate with target mRNAs are: 1) direct recognition of a nucleotide sequence motif; 2) binding to a structural element, such as dsRNA regions within a stem-loop; 3) recruitment to the mRNA by a currently-bound RBP (or other factor); and 4) interaction with a currently-bound RBP, or binding as a pre-formed complex.

Sequence motifs recognized by RBPs are enriched and most often conserved in 3'UTRs (Ray et al. 2013), although they can also occur in the CDS and 5'UTR (Dominguez et al. 2018). The location of a motif can also determine which regulatory mechanism is promoted by the RBP; as shown for *C. elegans* GLD-1, binding to the 3'UTR of target mRNAs largely promotes degradation, whereas binding to the CDS contributes more to translational repression (Brümmer et al. 2013). The accessibility of a binding site is also important, and RBPs that recognize single-stranded motifs are impeded when the motif is involved in base pairing, such as in the dsRNA region of a stem-loop (Brümmer et al. 2013; Taliaferro et al. 2016). Once bound the target mRNA, RBPs can recruit stabilizing or destabilizing factors to the mRNP, commonly poly(A) polymerases or deadenylases (reviewed in Glisovic et al. 2008).

1.4.2 PUF family of RBPs

PUF (Pumilio/FBF) proteins are a conserved family of RBPs present in eukaryotes. The name comes from the first two members of the family to be characterized in detail: *Drosophila* Pumilio (Murata & Wharton 1995) and *C. elegans* FBF-1/2 (Zhang et al. 1997). Mammals express two PUF proteins (PUM1 and PUM2), *Drosophila* one (Pumilio), yeast six (Puf1-6p), *C. elegans* at least eleven, and *Arabidopsis* up to twenty-six (reviewed in Wang et al. 2018). All PUF proteins have a conserved RNA-binding domain called the Pumilio homology domain (Pum-HD), which is made up of eight imperfect Puf repeats of ~36 amino acids that each fold into three α -helices and together form an arched structure (Zamore et al. 1997; Wang et al. 2001) (Fig. 1-14). The sequence motif recognized by the Pum-HD consists of a conserved UGUR (R = A or G) tetranucleotide followed by downstream sequences that vary among PUF proteins. For example, *Drosophila* Pumilio,

INTRODUCTION

mammalian PUM1, yeast Puf3p, and *C. elegans* PUF-8 are orthologs that bind the sequence motif 5'-UGUAN_nAUA-3' (n = any nucleotide) (Gerber et al. 2004; Opperman et al. 2005; Gerber et al. 2006; Galgano et al. 2008).

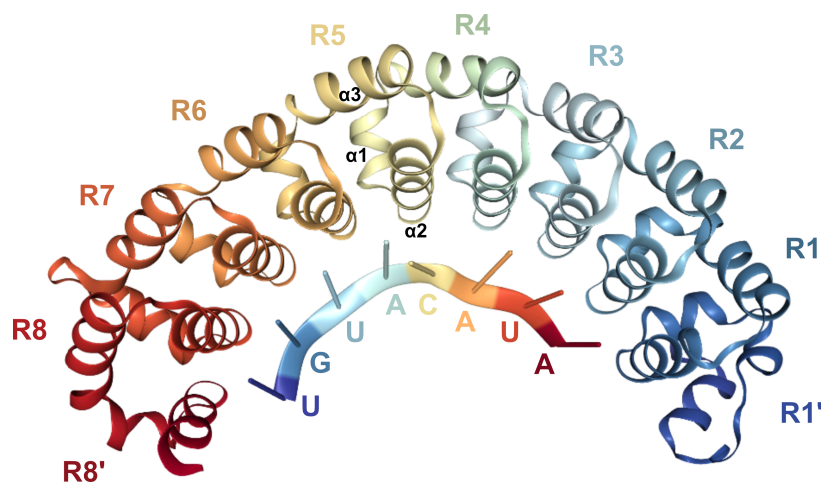


Fig. 1-14 | Crystal structure of *Drosophila* Pumilio Pum-HD in complex with RNA. Cartoon depiction of the arched Pum-HD from *Drosophila* Pumilio in complex with its recognition element (5'-UGUACAUA-3') in the 3'UTR of *hunchback* mRNA. Puf repeats (R1–R8) and pseudo repeats (R1' and R8') are indicated; α -helices 1–3 are labeled for repeat R5. Structure obtained from Protein Data Bank (ID: 5KLA; Weidmann et al. 2016).

Studies on PUF proteins in metazoans have uncovered a conserved role in stem-cell maintenance as well as diverse roles in embryonic patterning, cell-cycle control, and neural adaptation (Murata & Wharton, 1995; Crittenden et al. 2002; Kadyrova et al. 2007; Kaye et al. 2009). Although they are often regarded as negative regulators of gene expression, there are also examples of positive regulation mediated by PUFs (reviewed in Quenault et al. 2011). This dual nature of PUF activity is not inherent to the proteins themselves, but is rather attributed to their interactors. Recruitment of the deadenylase complex is a conserved function of PUF proteins (Goldstrohm et al. 2007), and interference with assembly of the translation initiation complex has also been reported (Deng et al. 2008). In promoting gene expression, PUF proteins can recruit poly(A) polymerases or cytoplasmic polyadenylation element binding protein (CPEB) to increase stability of the mRNA (Piqué et al. 2008; Suh et al. 2009). PUF proteins may also compete for binding to target mRNAs with other regulators, thereby hindering their regulatory functions (Archer et al. 2009).

1.4.3 PUF proteins in *C. elegans*

The PUF family is greatly expanded in *C. elegans*, with at least eleven members arranged into five subgroups based on sequence similarity, binding motif preference, and evolutionary divergence (Liu et al. 2012) (Fig. 1-15). Two additional genes contain a Pum-HD but are predicted to be non-functional—*puf-4* (similar to *puf-3/11*) lacks two Pumilio repeats, and *puf-10* (similar to *puf-5/6/7*) is a pseudogene. Moreover, *puf-2* exists in other nematodes but not in *C. elegans* (Liu et al. 2012). Redundancy among PUF proteins belonging to the same subgroup has been demonstrated (Lamont et al. 2004; Lublin & Evans 2007), as well as among PUFs of different subgroups (Bachorik & Kimble 2005). All *C. elegans* PUF proteins recognize a UGU-containing motif, with slight variations in the remaining nucleotides among the subgroups. For example, a single nucleotide differentiates the PUF-8/9-binding element (PBE) from the FBF-binding element (FBE) (Opperman et al. 2005) (Fig. 1-15).

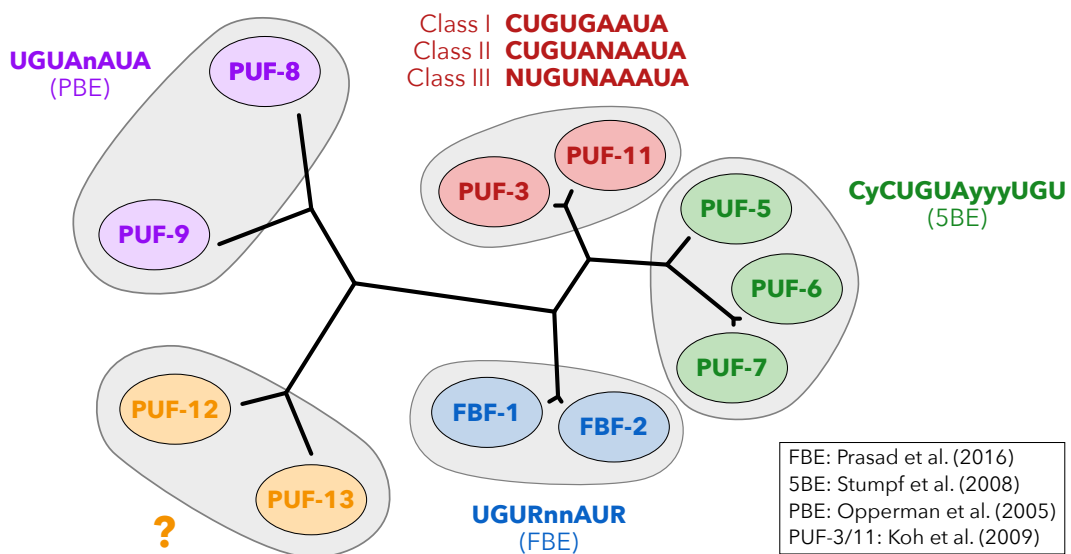


Fig. 1-15 | The subgroups of PUF proteins in *C. elegans*. Eleven PUF proteins can be classified into five subgroups, based on amino-acid and binding-motif similarities. References are given for the characterization of binding elements; PUF-12 and PUF-13 (gene ID: ZK792.5) remain to be characterized. Binding motifs are written 5' to 3', with the following letter codes: R = A or G; y = pyrimidine; n = any nucleotide. Image adapted from Koh et al. (2009) and Liu et al. (2012).

The roles of PUF proteins discovered so far in *C. elegans* are germline centric. The two nearly identical proteins FBF-1 and FBF-2 (collectively referred to as FBF) function

redundantly in the distal region of the germline to maintain a stem-cell niche by repressing regulators of meiotic entry (Crittenden et al. 2002; Eckmann et al. 2004; Lamont et al. 2004). FBF also binds to and negatively regulates *fem-3* mRNA, which controls the sperm-to-oocyte switch in *C. elegans* hermaphrodites (Zhang et al. 1997). On top of these roles, FBF is also a major regulator of other RNA-binding proteins and cross-regulates other PUFs, even participating in autoregulation—*fbf-1* and *fbf-2* mRNAs are regulated by each other's proteins (Lamont et al. 2004; Prasad et al. 2016).

Similar to FBF, PUF-8 activity promotes germline stem-cell mitosis and is critical for the sperm-to-oocyte switch (Bachorik & Kimble 2005; Ariz et al. 2009). Loss of *puf-8* leads to the formation of germline tumors due to the proliferation of dedifferentiated primary spermatocytes (Subramaniam & Seydoux 2003). PUF-8 also acts in the germline to repress genes involved in somatic differentiation (Mainpal et al. 2011), while also functioning redundantly with *tcer-1*—a component of the RNA processing machinery—to maintain proper levels of germline mRNAs by promoting mRNA processing and export (Pushpa et al. 2013).

To date, few somatic roles have been described for PUF proteins in *C. elegans*. FBF-1 promotes expression of the cyclic GMP-dependent protein kinase *egl-4* in olfactory sensory neurons (Kaye et al. 2009), FBF and PUF-8 function in the vulval cells to inhibit vulval development (Walser et al. 2006), and PUF-9 functions in seam cell morphology and adult cuticle formation (Nolde et al. 2007). Hence, the characterization of additional somatic roles for PUF proteins, if they exist, would be important for the field.

1.4.4 Interaction between miRNA- and PUF-mediated post-transcriptional regulation

Post-transcriptional regulation by RBPs and miRNAs has generally been regarded as two distinct mechanisms. However, functional miRNA binding sites are most prevalent in 3'UTRs, the same region of mRNA targeted by many RBPs, and there is a growing body of evidence that supports broad interactions between these two post-transcriptional mechanisms. The interactions can be cooperative or competitive, as well as direct or indirect, in the regulation of gene expression (Fig. 1-16).

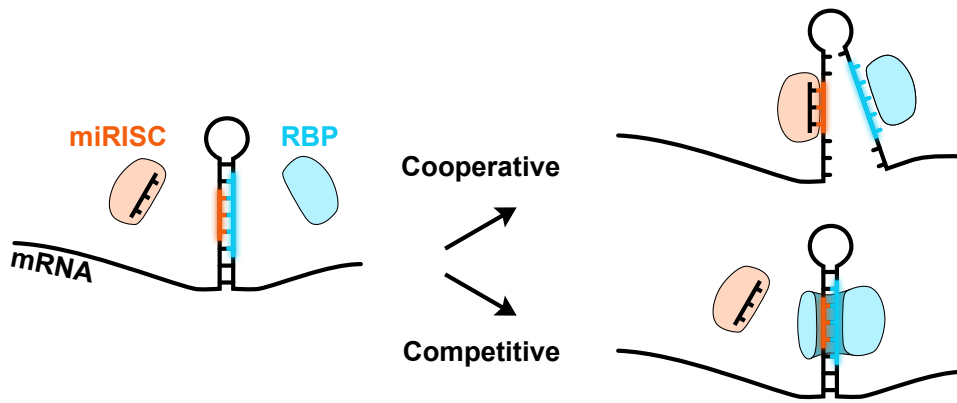


Fig. 1-16 | Modes of direct interaction between an RBP and the miRISC at an mRNA stem-loop. In the cooperative mode, binding of an RBP to its motif disrupts the local RNA structure element, liberating a miRNA binding site. In the competitive mode, binding of an RBP stabilizes the structural element, prohibiting miRISC binding.

One of the first observations that RBPs could functionally interact with miRNAs came from a study in *C. elegans*, where loss of *puf-9* enhanced the developmental phenotypes and lethality caused by mutations in the *let-7* miRNA (Nolde et al. 2007). It was found that PUF-9 and *let-7* share the common mRNA target *hbl-1*, a zinc-finger transcription factor with essential roles in the timing of post-embryonic development. Interestingly, *hbl-1* is the ortholog of *Drosophila hunchback*, a known target of Pumilio repression, and *let-7* is highly conserved in both invertebrate and vertebrate organisms (Pasquinelli et al. 2000). Therefore, the authors hinted towards an evolutionarily conserved mechanism by which miRNAs and PUF proteins cooperate to regulate common mRNA targets. Galgano and colleagues reached the same conclusion following their identification of human PUM1 and PUM2 targets (Galgano et al. 2008). They found PUM binding motifs to be enriched around predicted miRNA binding sites in 3'UTRs, further suggesting an interaction between the two pathways. More recently, a transcriptome-wide study found both cooperative and antagonistic interactions between the miRNA machinery and PUM proteins in human cells (Sternburg et al. 2018).

Several studies have shed light on the underlying mechanisms of interaction. Direct functional interaction was demonstrated by Kedde et al. (2010), using human primary cells to show that PUM1 and miR-221/miR-222 compete for binding to the 3'UTR of *p27*, a tumour suppressor that inhibits cell-cycle progression. Both binding motifs are sequestered within the dsRNA region of a stem-loop, however PUM1 binding induces a local change in RNA structure that liberates the miRNA binding site. In this way, PUM1 activity represses *p27* by enhancing miRNA association. Direct physical interaction

INTRODUCTION

between PUF proteins and the miRISC has also been found. In one study, PUF and Argonaut proteins were isolated in complex with a core translation elongation factor (Friend et al. 2012). These complexes—FBF-1-CSR-1-EFT-3 in *C. elegans* and PUM1-AGO-eEF1A in mammals—inhibited translation initiation and demonstrated a conserved PUF-miRISC interaction.

Instances of competitive interaction have also been reported. In *Drosophila*; the conserved RBP Dnd1 binds to U-rich regions and hinders miRNA association, thereby protecting target mRNAs from degradation (Kedde et al. 2007). In humans, the RBP HuR not only competes with miRNA binding, but can also redirect the mRNA to polysomes for active translation (Tominaga et al. 2011). HuR is also unique in that it can bind miRNAs directly, preventing their activity (Poria et al. 2015).

1.5 Aim of this study

The molecular mechanism of programmed cell death has been elucidated in the decades since its discovery, but questions still remain. Specifically, how is the pathway's activity kept at bay in non-dying cells and, perhaps more importantly, can we exploit the pathway's activity, or its regulators, for the targeted treatment of cancer cells? Triggering apoptosis specifically in cancer cells is an attractive approach, and the recent emergence of BH3 mimetics is a promising solution. These small molecules mimic the structure of the BH3 domain, and they are being used as drugs to inhibit the activity of anti-apoptotic BCL-2-family proteins in cancer cells. Such novel approaches to drug development and cancer therapy would not have been possible were it not for seminal studies on programmed cell death in *C. elegans*. Focus now turns to unraveling the complex regulatory networks that govern the core apoptotic pathway, knowing that a full understanding of these networks may aid the development of more selective and effective drugs.

The aim of this study is, therefore, to uncover regulatory mechanisms of the central apoptotic pathway during *C. elegans* development. The tools afforded by studying cell death in *C. elegans* make it an attractive model, and the conservation of core apoptotic factors make any findings relevant to higher animals. I focus on the potential for miRNA- and RBP-mediated post-transcriptional regulation via the 3'UTRs of core cell-death genes, and I compile the results into two sections.

First, in Section 3.1, my colleagues S. Lühr, N. Memar and I provide evidence that *egl-1* mRNA is a direct *in vivo* target of both miR-35- and miR-58-family miRNAs. Loss of the *mir-35* family leads to the appearance of abnormally large cell corpses in embryos, and this phenotype is enhanced upon subsequent knockout of *mir-58*-family genes. The formation of these large cell corpses is dependent on the central cell-death pathway, as loss of either *egl-1* or *ced-3* blocks the formation of large cell corpses in *mir-35*-family mutants. Furthermore, these large cell corpses are identified as precociously dying mothers and collaterally dying sisters of cells normally programmed to die. Using a series of 3'UTR reporters, *egl-1* mRNA is shown to be a direct target of miR-35- and miR-58-family miRNAs, which bind to conserved sites in the 3'UTR and mediate its repression. Finally, by closely studying two different cell-death lineages, miRNAs of the miR-35 and miR-58 families are found to cooperate in buffering the copy number of *egl-1* mRNA,

INTRODUCTION

thereby preventing EGL-1 activity from crossing a threshold that would trigger precocious and/or collateral cell death.

Then, in Section 3.2, my colleague K. Ikegami and I explore regulation of the central apoptotic pathway by PUF proteins and the potential for interaction with the miRNA pathway. I present a novel somatic function for *puf-8* in regulating programmed cell death, showing that animals lacking *puf-8* exhibit two opposing cell-death phenotypes. First, mothers of cells programmed to die undergo precocious death during embryogenesis and, additionally, cells in non-cell-death lineages undergo ectopic death. Second, cells that are programmed to die during the first wave of cell death take longer to form a refractile corpse. These phenotypes are not affected by the loss of closely-related *puf-9*, nor upon knockdown of *fbf*; however, *fbf* knockdown does suppress the large-cell-corpse phenotype exhibited by *mir-35*-family mutants. All four genes of the central apoptotic pathway have PBEs and/or FBEs in their 3'UTRs, and two FBEs in *egl-1* show functionality by mediating the repression of a transgenic reporter. Together, these findings indicate complex regulation of the central apoptotic pathway by PUF-protein and miRNA activity during development, with roles in both cell-death and non-cell-death lineages.

Finally, I conclude by discussing emerging fields in post-transcriptional gene regulation. I also summarize recent advances in the medical field pertaining to BH3 mimetics, and speculate how an increased knowledge of cell-death regulation could impact the development of targeted therapies.

2

MATERIALS AND METHODS

2.1 Strains and general maintenance of *C. elegans*

Strains of *C. elegans* were maintained using standard procedures, as previously described (Brenner 1974). Animals were grown at 20°C on nematode growth medium (NGM) plates with *E. coli* OP50 bacterial lawns. Experiments were conducted at 25°C, unless stated otherwise. The Bristol N2 strain was used as wild type. The alleles, balancers, and transgenes used in this study are summarized in Tables 2-1 and 2-2.

Table 2-1 | Alleles and balancers used in this work.

Allele/balancer	Gene(s) affected	Chromosome (LG)	Reference
<i>mIn1</i>	(balancer)	II	Edgley & Riddle 2001
<i>nDf50</i>	<i>mir-35-41</i>	II	Miska et al. 2007
<i>nDf49</i>	<i>mir-42-44</i>	II	Miska et al. 2007
<i>ok302</i>	<i>puf-8</i>	II	<i>C. elegans</i> Deletion Mutant Consortium 2012
<i>q725</i>	<i>puf-8</i>	II	Bachorik & Kimble 2005
<i>ok91</i>	<i>fbf-1</i>	II	Crittenden et al. 2002
<i>q704</i>	<i>fbf-2</i>	II	Crittenden et al. 2002
<i>q738</i>	<i>fbf-2</i>	II	Lamont et al. 2004
<i>ed3</i>	<i>unc-119</i>	III	Maduro & Pilgrim 1995
<i>nDf53</i>	<i>mir-80</i>	III	Miska et al. 2007
<i>n4640</i>	<i>mir-58.1</i>	IV	Miska et al. 2007
<i>n717</i>	<i>ced-3</i>	IV	Shaham et al. 1999
<i>n3330</i>	<i>egl-1</i>	V	This study (generated by B. Conradt)
<i>n4535</i>	<i>mir-230</i>	X	Miska et al. 2007
<i>nDf54</i>	<i>mir-81-82</i>	X	Miska et al. 2007
<i>ok1136</i>	<i>puf-9</i>	X	<i>C. elegans</i> Deletion Mutant Consortium 2012

Table 2-2 | Transgenes and extrachromosomal arrays used in this work.

Allele/array	LG	Transgene	Plasmid	Reference
<i>bcSi25</i>	I	$P_{mai-2gfp}::h2b::mai-2$ 3'UTR	pBC1483	This study (generated by M. Basch, N. Memar, and S. Lühr)
<i>bcSi26</i>	I	$P_{mai-2gfp}::h2b::egl-1^{wt}$ 3'UTR	pBC1484	This study (generated by M. Basch, N. Memar, and S. Lühr)
<i>bcSi27</i>	I	$P_{mai-2gfp}::h2b::egl-1^{mut\ mir-35}$ 3'UTR	pBC1485	This study (generated by M. Basch, N. Memar, and S. Lühr)
<i>bcSi45</i>	I	$P_{mai-2gfp}::h2b::egl-1^{mut\ FBE-1}$ 3'UTR	pBC1650	This study (generated by me)
<i>bcSi46</i>	I	$P_{mai-2gfp}::h2b::egl-1^{mut\ mir-58}$ 3'UTR	pBC1653	This study (generated by M. Basch, N. Memar, and S. Lühr)
<i>bcSi47</i>	II	$P_{mai-2gfp}::h2b::egl-1^{mut\ mir-35\ mir-58}$ 3'UTR	pBC1654	This study (generated by M. Basch, N. Memar, and S. Lühr)
<i>bcSi49</i>	I	$P_{mai-2gfp}::h2b::egl-1^{mut\ FBE-1\ FBE-2}$ 3'UTR	pBC1651	This study (generated by me)
<i>bcSi60</i>	IV	$P_{egl-1egl-1(n3082)}::mNeonGreen::egl-1$ 3'UTR	pBC1712	This study (generated by me)
<i>nEx1187</i>	-	<i>mir-35 (genomic) + sur-5::gfp</i>	-	Alvarez-Saavedra & Horvitz 2010
<i>xdEx1091</i>	-	$P_{unc-3unc-3::gfp} + P_{sur-5rfp}$	-	Wang et al. 2015

2.2 Cloning and single-copy integration of *egl-1* 3'UTR reporters: miRNA binding-site variants

The plasmids pBC1483 and pBC1484 were made by M. Basch, N. Memar, and S. Lühr, by a series of overlap-extension PCRs. The first fragment, P_{mai-2} (1763 bp), was defined as the sequence upstream of the *mai-2* start codon, stopping at the neighbouring transcription unit for B0546.4. The primers used to amplify P_{mai-2} were:

5'-agatctGGAAAAAATCGATA-3' (lowercase indicates BglII site)

5'-GAAAAGTTCTTCTCCTTTACTCATTCTGAAAATTGAGTGAATTAG-3'

The second fragment, *gfp::h2b* (1287 bp), was amplified from the plasmid pCM1.35 (a gift from G. Seydoux; Addgene plasmid no. 17248), and fused to P_{mai-2} . The primers used to amplify *gfp::h2b* were:

MATERIALS AND METHODS

5'-CTAATTCACTCAATTTTCAGAATGAGTAAAGGAGAAGAAGCTTTT-3'

5'-GCTCGCGTTCCTGTACTGCAAATTACTTGCTGGAAGTGTACTTG-3'

The third and final fragment differed between the two plasmids. For pBC1483, the *mai-2* 3'UTR (142 bp) was used, and for pBC1484 the *egl-1* 3'UTR (172 bp) was used. This fragment was fused to $P_{mai-2gfp::h2b}$ to yield the final transgene. The primers used to amplify the *mai-2* 3'UTR were:

5'-CAAGTACACTTCCAGCAAGTAATTTGCAGTACAAGAACGCGAGC-3'

5'-TcttaagTTCGCTAAAAACTA-3' (lowercase indicates AflII site)

The primers used to amplify the *egl-1* 3'UTR were:

5'-CAAGTACACTTCCAGCAAGTAAGTGATCAAATCTCCAACCTTTTC-3'

5'-TcttaagAAAAAAACCATATTTATTATTAG-3' (lowercase indicates AflII site)

As an intermediate step, each transgene was bluntly ligated into the EcoRV site of pBluescript II KS+. At this point, the region of the *egl-1* 3'UTR harboring the miR-35-family binding site was mutated from 5'-GATTTCTCATAATACCCGGT-3' to 5'-CTAATCTCATAATCGCCGA-3' using PCR site-directed mutagenesis, generating a third pBluescript-based intermediate. The mutagenic primers used for this were:

5'-TCTAATCTCATAATCGCCGAGTTTTTCTTCATTTGTGATTATTTTC-3'

5'-CTCGGCGATGTATGAGATTAGATGGTACAAATTGGAGAAAAG-3'

Each transgene was then excised using BglII/AflII double digestion and ligated into the BglII/AflII site of the final destination mosSCI vector pCFJ350 (a gift from Erik Jorgensen; Addgene plasmid no. 34866), which harbors the *cb-unc-119(+)* rescue fragment. The final plasmids were named pBC1483 (*mai-2* 3'UTR transgene), pBC1484 (*egl-1^{wt}* 3'UTR transgene), and pBC1485 (*egl-1^{mut mir-35}* 3'UTR transgene).

The two plasmids pBC1653 (*egl-1^{mut mir-58}* 3'UTR transgene) and pBC1654 (*egl-1^{mut mir-35 mir-58}* 3'UTR transgene) were constructed using PCR site-directed mutagenesis with the templates pBC1484 and pBC1485, respectively. The region of the *egl-1* 3'UTR harboring the miR-58-family binding site was mutated from 5'-GAGAGATCGAAAA-3' to 5'-CACTGTACCATAT-3'. The mutagenic primers used for this were:

5'-CACTGTACCATATATAATCACAAATGAAGAAAAAACAC-3'

5'-ATATGGTACAGTGCGTCTCCAACCTCCCCT-3'

Single-copy integrations of all five plasmids were generated by S. Lühr using mosSCI (Frøkjær-Jensen et al. 2014) and germline microinjection as previously described (Mello et al. 1991). The strain EG8078 [*oxTi185; unc-119(ed3)*] was used for targeted mosSCI integrations on LGI of the transgenes from pBC1483, pBC1484, pBC1485, and pBC1653, creating the alleles *bcSi25*, *bcSi26*, *bcSi27*, and *bcSi46*, respectively. The strain EG6699 [*ttTi5605; unc-119(ed3)*] was used for targeted mosSCI integration on LGII of the transgene from pBC1654, creating the allele *bcSi47*.

2.3 Cloning and single-copy integration of *egl-1* 3'UTR reporters: FBE variants

The plasmid pBC1650 was generated by K. Ikegami using PCR site-directed mutagenesis, using pBC1485 as a template. Primers were designed to introduce a point-mutation in the critical UGU trinucleotide of e1-FBE-1 (5'-TGTACCATA-3' to 5'-AGTACCATA-3'). The mutagenic primers used for this were:

5'-CCCCTCAATATTAGTACCATAGTCC-3'

5'-GGACTATGGTACTAATATTGAGGGG-3'

The plasmid pBC1651 was also generated by K. Ikegami using PCR site-directed mutagenesis, using pBC1650 as a template. A point-mutation was introduced in the UGU trinucleotide of e1-FBE-2 (5'-TGTACCATG-3' to 5'-AGTACCATG-3'). The mutagenic primers used for this were:

5'-CCAACTTTTCTCCAATTAGTACCATGATTTTC-3'

5'-GAAATCATGGTACTAATTGGAGAAAAGTTGG-3'

I used the strain EG8078 [*oxTi185; unc-119(ed3)*] for germline microinjection and targeted mosSCI integrations on LGI of the transgenes from pBC1650 and pBC1651, creating the alleles *bcSi45* and *bcSi49*, respectively.

2.4 Cloning and single-copy integration of *egl-1* translational reporter

I constructed the *egl-1* translational reporter plasmid pBC1712 as an in-frame fusion of mNeonGreen in exon 2 of *egl-1(n3082)*. The plasmid was made using four-fragment Gibson Assembly (Gibson et al. 2009).

MATERIALS AND METHODS

The first fragment (6221 bp) contained *egl-1(n3082)* sequence downstream of the mNeonGreen insertion site, as well as the *egl-1* 3'UTR and downstream intergenic sequence. The template for this PCR was the plasmid pBC63 (made by B. Conradt), which is identical to pBC08 (Conradt & Horvitz 1998) but harbors a 5-bp deletion defined by the *n3082* allele in exon 3 of *egl-1* (5'-GATGACTCTGGAGATCAGCAGCATCG-3', deletion underlined). The primers used for this PCR were:

5'-ctggtagcctctagtagcaaggCCCTAACATATTTCTCAAAGATAC-3'

5'-tacaagaacgTTTTTGACGTTCAATCTTC-3'

The second fragment (862 bp) contained the CDS for mNeonGreen, amplified from the plasmid pOD2065 (a gift from K. Oegema). The primers used for this were:

5'-acgtcaaaaaCGTTCTTGTAGAGCTCGTC-3'

5'-gtccaacggtGTCTCCAAGGGAGAGGAG-3'

The third fragment (8194 bp) contained *egl-1* sequence upstream of the mNeonGreen insertion site, as well as the *egl-1* 5'UTR and upstream intergenic sequence. The template for this PCR was the WRM0630cB06 fosmid (Source Bioscience; Cat. no. UBC_f80D1130Q), and the primers used were:

5'-ccttgagacAACGTTGGACATTGGTAG-3'

5'-gtaatacgaactacttaaggAACTAGAACAAAAACATTAGATCAAG-3'

The destination vector was pCFJ909 (a gift from Erik Jorgensen; Addgene plasmid no. 44480), which harbors the *cb-unc-119(+)* rescue fragment. A four-fragment Gibson Assembly was performed using commercial reagents (New England Biolabs; Cat No. e2611), the three PCR fragments, and StuI-linearized vector to generate the final plasmid pBC1712. Finally, the strain HT1593 [*unc-119(ed3)*] was used for germline microinjection and miniMos integration of the transgene from pBC1712 on LGIV, creating the allele *bcSi60*.

2.5 4D microscopy and lineage analysis of embryonic cell death

Prior to analysis, L4 larvae were grown to the adult stage overnight at 25°C. The following day, two- or four-cell embryos were collected from the young adults, mounted on 4.5% agarose pads and covered with a cover slip (Carl Roth GmbH; 18 x 18 mm, #1 thickness; Cat. no. 0657.2). 4D recordings were made throughout embryonic development

as described previously (Schnabel et al. 1997, 2006) using a Zeiss Axio Imager.M2 and Time to Live software (Caenotec), capturing 25 DIC z-stacks every 35 sec at 25°C with intermittent fluorescence scans as required.

Lineage analysis of the 4D recordings was performed using Simi BioCell software (Simi Reality Motion Systems GmbH; <http://www.simi.com>). The “time to die” for first-wave cell deaths was measured as the number of minutes post-birth required to form a refractile cell corpse.

2.6 RNAi knockdown of *fbf* by injection of dsRNA

For RNAi knockdown of *fbf-1*, I injected dsRNA corresponding to nucleotides +186 to +2484 (relative to AUG start codon) of *fbf-1*. This dsRNA is predicted to trigger degradation of both *fbf-1* and *fbf-2* (Zhang et al. 1997). The template for the production of *fbf-1* dsRNA was clone II-4F05 (Source Bioscience; Cat. no. CUUkp3301F054Q) from the Ahringer *C. elegans* RNAi Collection (Kamath et al. 2003). A T7-promoter primer (5'-TAATACGACTCACTATAGGG-3') was used to amplify the gene specific fragment of *fbf-1* with flanking T7 promoters, and subsequently 1 μ g of this PCR product was used as a template for *in vitro* transcription using the MEGAscript RNAi Kit (Ambion; Cat. no. AM1626) in a reaction volume of 20 μ l. dsRNA was purified using the MEGAclean Transcription Clean-Up Kit (Ambion; Cat. no. AM1908). After final elution in Elution Buffer (supplied with kit), 3X Soaking Buffer (32.7 mM Na₂HPO₄, 16.5 mM KH₂PO₄, 6.3 mM NaCl, 14.1 mM NH₄Cl) was added to a final concentration of 1X.

Injection of *fbf-1* dsRNA was made into the gut of either *fbf-2(q738)* or *mir-35-42(nDf50 nDf49)* L4 animals at a concentration of 750 ng/ μ l, as previously described (Fire et al. 1998). After 24 hours at 25°C, embryos were collected (4-hour layoff) and examined for cell-death defects by 4D microscopy. Any embryos remaining from the layoff were allowed to grow to the adult stage at 25°C for confirmation of *fbf* knockdown by analysis of germline morphology.

2.7 smRNA FISH

Single-molecule RNA fluorescent *in situ* hybridization (smRNA FISH) was performed as previously described (Raj et al. 2008; Raj & Tyagi 2010), with slight modifications. Stellaris

MATERIALS AND METHODS

FISH Probes (Biosearch Technologies) were designed against the mature mRNA of interest using the Stellaris Probe Designer (version 4.2; www.biosearchtech.com/stellaris-designer). The *egl-1* probe set contained 23 TAMRA-labeled oligonucleotides and was used at 250 nM (Table 2-3). The probe set to target *unc-3::gfp* contained 48 fluorescein-labeled oligonucleotides and was used at 500 nM (Table 2-4). The probe set to target *gfp::h2b* contained 30 TAMRA-labeled oligonucleotides and was used at 500 nM (Table 2-5). The *ced-3* probe set contained 48 Quasar-670-labeled oligonucleotides and was used at 500 nM (Table 2-6).

Table 2-3 | Sequences of probes used for *egl-1* smRNA FISH (TAMRA labeled).

Probes 1–8 (5' to 3')	Probes 9–16 (5' to 3')	Probes 17–23 (5' to 3')
CGGTGTGAATGTTTTGGGTG	AAGAATCTTCACACGAGGAG	GTTGGAGATTTTGATCACTT
AAGAGAAGTTAGAATACGAC	AAAAAATCCCGAGTCGTCGG	CATGGTACAAATGGAGAA
AGCATCAGCATATCAACTGA	CGATGCTGCTGATCTCAGAG	CACCGGTATTATGAGAA
ATCCGAAGAGGTTGAGGCAA	ATTGCTGCTAGCTTGGAGCC	TAATCACAAATGAAGAAAA
AAACGTTGGACATGGTAGA	GAGCATCGAAGTCATCGC	TGGAGACGGAGAGATCGAAA
AAAACGGAAGATTGAACGTC	TGGGCCGAGTAGGACATCAT	TGGTACAAATATTGAGGGGA
ACATGTTCTTTTCGTTGT	GAAGAGGCTTCTGTCGGAAG	AATATGAGCAATAAAGGAC
GTCCTGAGACGAGGAGTA	GCGAAAAAGTCCAGAAGACG	

Table 2-4 | Sequences of probes used for *unc-3::gfp* smRNA FISH (fluorescein labeled).

Probes 1–16 (5' to 3')	Probes 17–32 (5' to 3')	Probes 33–48 (5' to 3')
CATTTTTCTGAGCTCGGTA	GTGTCCAAGAATGTTCCAT	CGAGATGTCTGATGACAGCG
CTTACGTTCTTCTTTGGAG	GTGAGTTATAGTTGTATCC	GGACTTAGAAGTCAGAGGCA
TACTCATTTTTTCTACCGGT	GTCTGCCATGATGTATACAT	AGAGCATGTAGGGATGTTGA
CCAGTGAAAAGTTCTTCTCC	CTTTGATTCCATTCTTTTGT	AAAATAGGGGGTGGGAGCAC
CCCATTAACATCACCATCTA	CCATCTTCAATGTTGTGTCT	TTTCATTGTTAGAGGTGACT
CCTCTCCACTGACAGAAAAT	ATGGTCTGCTAGTTGAACGC	GGGAGGGAGCACAATTTTTT
GTAAGTTTTCCGTATGTTGC	CGCCAATTGGAGTATTTTGT	GTGTACACAGAACATTGTGT
GTAGTTTTCCAGTAGTGCAA	GTCTGGTAAAAGGACAGGGC	GTATTTTGTGTGCGGTTTTT
ACAAGTGTGGCCATGGAAC	AAGGGCAGATTGTGTGGACA	GCGGTCATAAACTGAAACGT
GGTATCTCGAGAAGCATTGA	TCTTTTCGTTGGGATCTTTC	CCCAGACGTGCGAAGAAATA
TCATGCCGTTTCATATGATC	TCAAGAAGGACCATGTGGTC	CGATGAGCATGATTTGACGT
GGGCATGGCACTTTGAAAA	AATCCCAGCAGCTGTTACAA	GGGGAAACCCCAAAAAGCAA
TTCTTTCCTGTACATAACCT	TATAGTTCATCCATGCCATG	AAGAAAAACGCCGTCTCGA
GTTCCCGTCATCTTTGAAAA	GCTCAGTTGGAATICTACGA	TGCATCGTGCTCATCAATAC
TGACTTCAGCACGTGTCTTG	CAAGTTGGTAATGGTAGCGA	CTCAAACCCAAACCTTCTTC
TAACAAGGGIATCACCTTCA	CCCTATTATTTTGACACCA	ATCAACTTCTACTCACCTTC

Table 2-5 | Sequences of probes used for *gfp::h2b* smRNA FISH (TAMRA labeled).

Probes 1–10 (5' to 3')	Probes 11–20 (5' to 3')	Probes 21–30 (5' to 3')
AAAGTTCTTCTCCTTTACTCA	CGGGCATGGCACTCTTGAAAA	AGTTAACTTTGATTCCATTCT
AAGAATTGGGACAACCTCCAGT	AGTTCTTCTGTACATAACC	TTCCATCTTCAATGTTGTGTC
CCCATTAACATCACCATCTAA	GTTCCCGTCATCTTTGAAAA	TGATAATGGTCTGCTAGTTGA
CCTCTCCACTGACAGAAAATT	TTGACTTCAGCACGTGTCTTG	ATCGCCAATTGGAGTATTTTG
TAAGTTTTCCGTATGTTGCAT	TAACAAGGGTATCACCTCAA	TGTCTGGTAAAAGGACAGGG
AGTTTTCCAGTAGTGCAAATA	ATACCTTTTAACTCGATTCTA	CAGATTGTGTGGACAGGTAAT
AAGTGTGGCCATGGAACAGG	GTTCCATCTTCTTTAAAATC	TTTTCGTTGGGATCTTTCGAA
CACCATAACAGAAAGTAGTGA	ATTCCAATTGTGTCCAAGAA	CAAGAAGGACCATGTGGTCTC
GGGTATCTCGAGAAGCATTGA	ACATTGTGTGAGTTATAGTTG	AATCCAGCAGCTGTTACAAA
GTCATGCCGTTTCATATGATC	TTGTTGTCTGCCATGATGTA	ATTGTATAGTTCATCCATGC

Table 2-6 | Sequences of probes used for *ced-3* smRNA FISH (Quasar-670 labeled).

Probes 1–16 (5' to 3')	Probes 17–32 (5' to 3')	Probes 33–48 (5' to 3')
CTTCTATCTTGACGCATCAT	TATTGAGTTGGTCCAGAAGC	CTCGACAAGCCTGCACAAAA
CATAATGTTCTCTCTAGCA	TCATATCCTTTCATGGAAT	AATCCATTGTCACGACGTTT
ACACTTGTTTTGGCGATGAGA	ATGGTTGGTGCATCGACAAA	AGGAACTCCGTCGACAGAAT
CGAACCGTTCACATGAATT	TTTCTCGTCGAAAACACGGC	CCCATCCACGACGAAGAAAT
CATAAAACGCGTCGAACGCC	AGGACTCGAGAAGTTTCTGT	AAATTGAACAATGGCCCGTC
GGCGAGAGGTTCAAGAACTT	TTATGATGAGGCACATTCCA	TTTCTCCACACTTGCTGAAC
CGACAGCATTGAGTCAACA	GCATCTGCTCAAAGTGTCA	AATCAGAATGTCAGCTTGGC
GGTGACATTGGACACTCGAA	TGGTAAGATTGTCCTTGTGCG	TATTGAGCTGTGCTTGCCTA
GACTGTAAGAGACGCTGTC	TATAGCCCATGCATCTGAAC	AGCACTGTTTCTCCACGAAA
GCTCTTGAGTAGATATCCTG	GTCAGATTGTCCTTGCAAAT	CAGACGGCTTGAATGAACCA
CACGCGATCGAGAACGAGAT	TCTCGAATTGTCAGGAGCAT	TTTGCGTGTGTCGAGAACAC
TGTGTCGATCCGATGAATGA	GTGTGATTCGTGTTGGCAA	AGTCAGCAGCTCAACAACAT
GGAAATGCGTTGACTGGAGG	TCACGAGTATCGCAGAATCT	AAGCGACCTTCTTATTGACT
AAGAGTTGGCGGATGAAGGT	TAATCACATTCTTCTCCG	ATCCCTGTGATGTCTGAAAT
AGAGAAGAGCATCCGGTGAA	CTCGTGTGTAATAATCGGTA	TCTCTGGCATCTGTTTCAAA
GCGATTACGACTTGAAGTGT	CCGCGTTGAGAAGATCATAT	TCCGGCCAAAAGTAGAACTT

Embryos were harvested by dissolving healthy adults in bleaching solution (Table 2-7) for ~8 min. Embryos were pelleted by centrifugation at 1500 $\times g$, then resuspended in M9 buffer (22 mM KH_2PO_4 , 42 mM Na_2HPO_4 , 86 mM NaCl, 1 mM MgSO_4) and permitted to develop at 25°C until the desired stage was reached. Embryos were then pelleted and resuspended in fixation solution (Table 2-8) and mixed by rotation at room temperature for 15 mins. The tube was then briefly vortexed and submerged in liquid nitrogen for 1

MATERIALS AND METHODS

min to freeze-crack eggshells, then allowed to slowly thaw in room-temperature water; once thawed, the tube was placed on ice for 20 mins. Embryos were then washed twice with 1X PBS, then resuspended in 70% ethanol (to permeabilize membranes) and incubated overnight at 4°C with rotation. The following day, embryos were pelleted then resuspended in wash buffer (Table 2-9) and allowed to stand for 5 min at room temperature. Embryos were pelleted again and resuspended in 100 μ l hybridization buffer (Table 2-10) supplemented with desired Stellaris® FISH Probes, then incubated overnight in the dark at 30°C. The following day, 1 ml wash buffer was added directly to the tube, then embryos were pelleted, resuspended again in wash buffer and incubated at 30°C for 30 min. Embryos were then pelleted and resuspended in wash buffer supplemented with 5 ng/ml DAPI for nuclear counterstaining, incubated at 30°C for 30 mins, and finally resuspended in VECTASHIELD Antifade Mounting Medium (Vector Laboratories; Cat. no. H-1000-10).

Table 2-7 | Bleaching solution.

Component	Supplier, catalog number	Final concentration
NaHOCl (12 %)	Roth, 9062.3	0.6%
NaOH (10 N)	Roth, 9356.1	0.7 N
Nuclease-free H ₂ O	Millipore, H20MB0106	→ add to final volume

Table 2-8 | Fixation solution.

Component	Supplier, catalog number	Final concentration
Formaldehyde (37%)	Roth, 4979.1	3.7%
10X PBS (nuclease free)	Invitrogen, AM9624	1X
Nuclease-free H ₂ O	Millipore, H20MB0106	→ add to final volume

Table 2-9 | Wash buffer.

Component	Supplier, catalog number	Final concentration
Formamide (deionized)	Invitrogen, AM9342	10%
SSC (20X, nuclease free)	Invitrogen, AM9770	2X
Nuclease-free H ₂ O	Millipore, H20MB0106	→ add to final volume

Table 2-10 | Hybridization buffer.

Component	Supplier, catalog number	Final concentration
Dextran sulfate ¹	Sigma-Aldrich, D8906	10%
Ribonucleic acid, transfer (from <i>S. cerevisiae</i>)	Sigma-Aldrich, R8759	1 mg/ml
Ribonucleoside vanadyl complex (200 mM)	NEB, S1402S	2 mM
BSA (50 mg/mL, nuclease free)	Invitrogen, AM2616	200 µg/ml
SSC (20X, nuclease free)	Invitrogen, AM9770	2X
Formamide ² (deionized)	Invitrogen, AM9342	10%
Nuclease-free H ₂ O	Millipore, H20MB0106	→ add to final volume

¹ Mix the dextran sulfate in ~2 ml of nuclease-free water with gentle agitation at room temperature until dissolved, then add other components. Store in 100 µl aliquots at -20°C.

² Hybridization stringency can be adjusted via formamide—the higher the concentration, the higher the stringency. Previously opened formamide was deionized with Mixed Bed Resin (Sigma-Aldrich, M3082) by adding 1 g resin to 10 ml formamide (resin will turn from blue to yellow). Single-use aliquots were stored at -20°.

For imaging, embryos were briefly vortexed to resuspend, then 1.5 µl were applied to a round German glass cover slip (Electron Microscopy Sciences; 8 mm diameter, #1.5 thickness; Cat. no. 72296-08). A square cover slip (Carl Roth GmbH; 22 x 22 mm, #1 thickness; Cat. no. H874.2) was then gently touched to the drop, effectively sandwiching the embryos between the two glass surfaces. Next, a silicon isolator was adhered to a standard glass microscope slide (Grace Biolabs; Cat. no. 664504), and the square cover slip was adhered on top of the silicon isolator, such that the round cover slip was hanging upside-down inside the airtight chamber (Fig. 2-1).

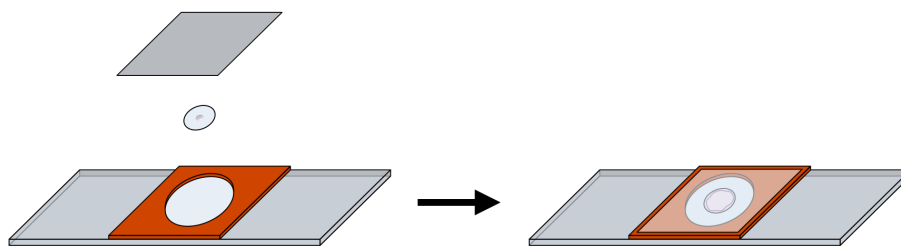


Fig. 2-1 | Assembly of imaging chamber for whole-mount embryos. See text for details.

Imaging was performed using a Leica TCS SP5 II confocal microscope with 63x oil-immersion lens and a z-spacing of 500 nm to capture diffraction-limited spots over several z-slices. Leica LAS AF software was used with default settings, aside from following adjustments: pinhole, 95.53 (Airy 1); line average, 3; resolution, 1024x512 (whole embryo), 128x128 (single cell); zoom factor, 3.5 (whole embryo), 12 (single cell); bidirectional scanning.

2.8 Quantification of mRNA copy number from smRNA FISH images

Image analysis was performed using Fiji software (Schindelin et al. 2012). The number of nuclei in a given embryo was determined using Multiview Reconstruction Software (Preibisch et al. 2010). For this, a confocal z-series of the DAPI signal from a fixed embryo was subjected to interest point detection using the software, with manual corrections as required.

The pipeline used to quantify the mRNA copy number in a cell of interest is illustrated (Fig. 2-2). A three-dimensional region of interest (ROI) was defined for the cell-of-interest and background signal was subtracted. Next, the total smRNA FISH signal intensity was measured for this ROI from a z-projection summing the slices. Finally, the mRNA copy number for the cell-of-interest was calculated, dividing the total signal intensity of the ROI by the average intensity of a single diffraction-limited mRNA spot. Cellular volumes were calculated by assuming sphericity and measuring the average diameter of the cell-of-interest from confocal image stacks. For presentation, maximum intensity z-projection images were smoothed (Gaussian Blur, radius = 1.5) and the DAPI signal of neighbouring nuclei was removed.

Quantification of *gfp::h2b* mRNA in transgenic embryos was performed on a maximum intensity z-projection of the smRNA FISH signal generated for the whole embryo. Then, a background subtraction (radius = 4) and Gaussian Blur filter (radius = 1.5) were applied and the resulting image was watershedded. Finally, the number of particles were determined using the Analyze Particles tool (size > 15, circularity 0.2–1.0).

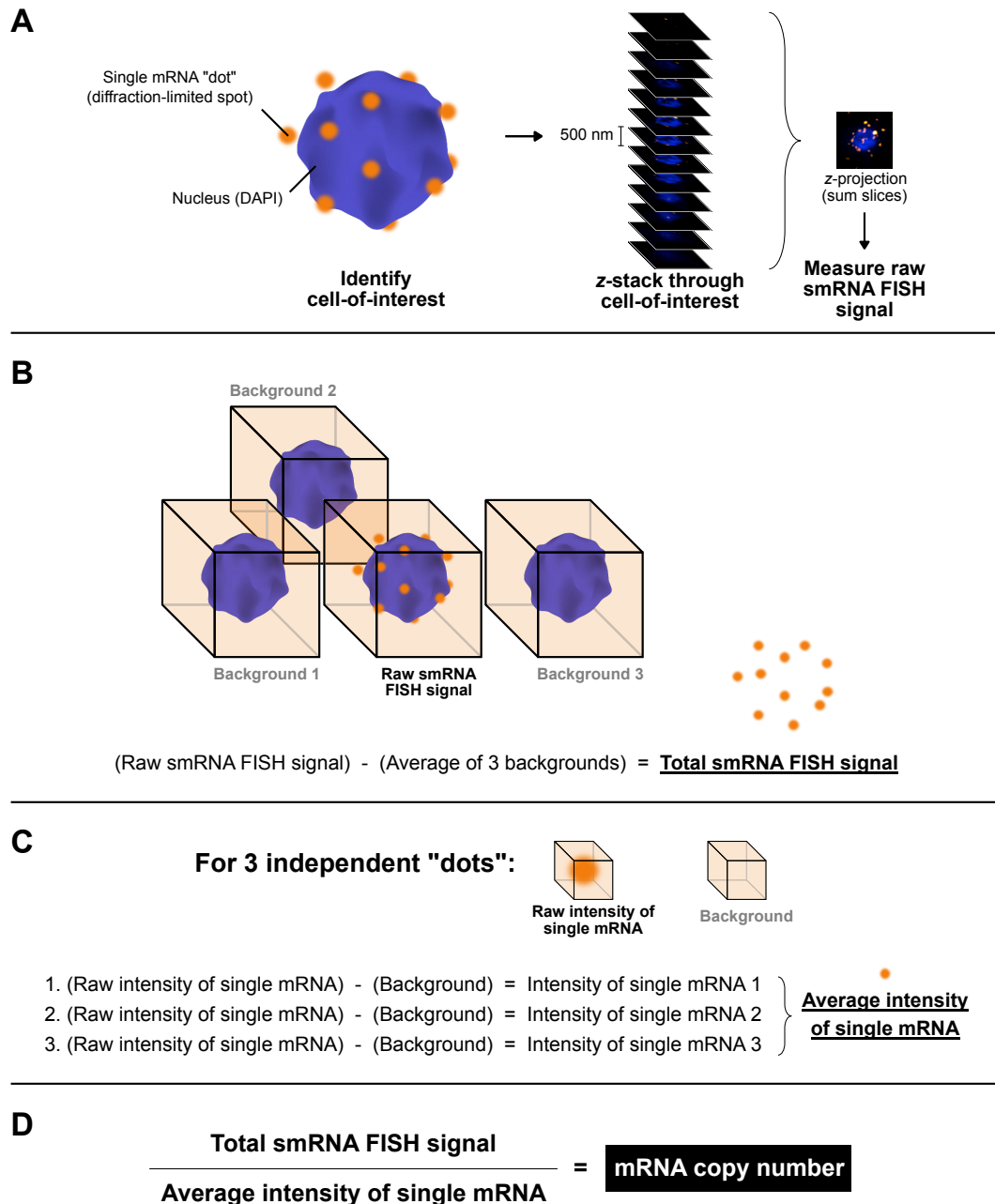


Fig. 2-2 | Quantification of single-cell mRNA copy numbers. See text for details. Figure taken from Sherrard et al. (2017), supplemental material.

3

RESULTS

Results: Preface

The results presented in Section 3.1 were the combined effort of S. Lühr, N. Memar, and me. This work was published in the January 15, 2017, issue of *Genes & Development* as:

Sherrard R, Luehr S, Holzkamp H, McJunkin K, Memar N & Conradt B (2017).
miRNAs cooperate in apoptosis regulation during *C. elegans* development. *Genes
Dev* 31, 209–222.

The results presented in Section 3.2 were the combined effort of K. Ikegami and me. As of the present time, this work has not been published in any source.

3.1 miRNA-mediated regulation of programmed cell death

3.1.1 Abnormally large cell corpses are present in *mir-35*-family mutants

The first cell division of *C. elegans* embryogenesis is asymmetric and produces two blastomeres: the anteriorly positioned AB cell and the posteriorly positioned P1 cell. Successive divisions of these cells often occur along the anterior-posterior axis, giving rise to daughter cells that are named accordingly. For example, the anterior and posterior daughters of the AB blastomere are called ABa and ABp, respectively. Descendants of the AB blastomere differentiate into neuronal, hypodermal and pharyngeal cells. In this process, a total of 98 cells in the AB lineage undergo programmed cell death, and the death of these cells occurs in three temporal waves during embryogenesis. Specifically, 13 cells die following the ninth round of cell division and belong to the “first wave of AB cell death”; 55 cells die during the second wave and 30 during the third wave, which follow the tenth and eleventh rounds of cell division, respectively (Fig. 3-1).

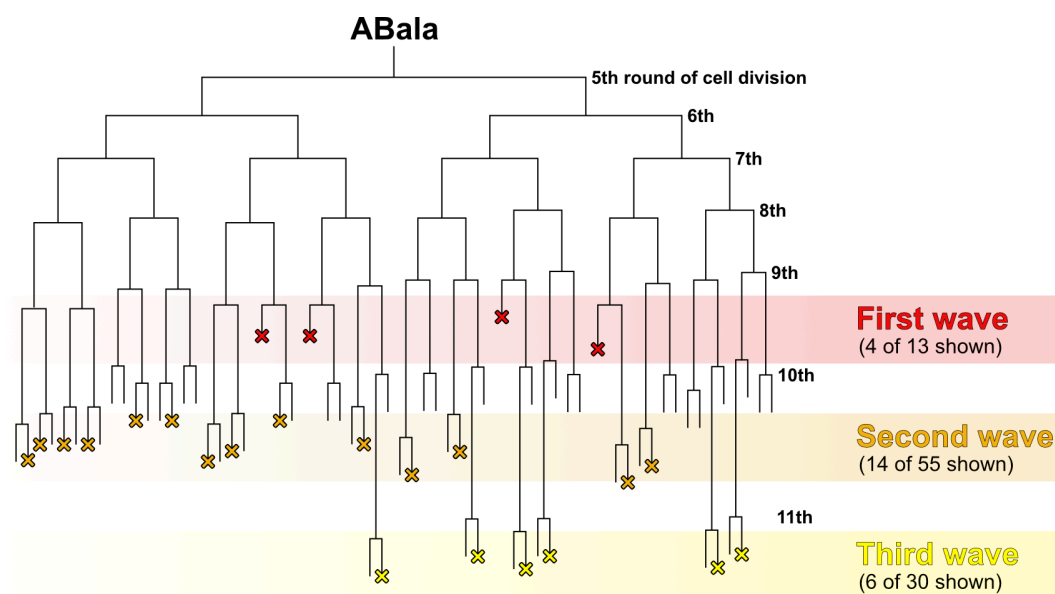


Fig. 3-1 | Cell death in the AB lineage occurs in three temporal waves during *C. elegans* embryogenesis. A representative portion of the AB lineage, the ABa sub-lineage, is shown. Cells programmed to die are indicated by X's. Those that die following the 9th round of embryonic cell division are classified as first-wave cell deaths (red). Cells that die following the 10th or 11th round of embryonic cell division are classified as second-wave (orange) or third-wave (yellow) cell deaths, respectively.

RESULTS

To investigate the role of miR-35- and miR-58 family miRNAs in programmed cell death, S. Lühr, N. Memar, and I screened embryos from wild-type (+/+), *mir-35*-family-mutant, and *mir-58*-family-mutant populations for cell-death abnormalities during development at 25°C using four-dimensional (4D) microscopy (Schnabel et al. 1997, 2006). Specifically, the first 13 cell deaths of the first wave of AB cell death were scored for appropriate death by lineage analysis. All 13 cell deaths were detected in wild-type embryos, each rounding up to form a refractile cell corpse $\sim 2.5 \mu\text{m}$ in diameter (Figs. 3-2A, 3-3A). In *mir-35*-family mutants, all 13 cell deaths were also detected (Fig. 3-3A); however, abnormally large cell corpses were also present, having a diameter ~ 1.5 -fold larger than that of a normal cell corpse (Fig. 3-2B). Although these large cell corpses had the characteristics of a normal cell corpse (e.g. rounded up, increased refractility, detachment from surrounding cells), they were not always engulfed by neighbouring cells; they often persisted in the embryo or were eventually extruded (Fig. 3-4). The number of large cell corpses was quantified in *mir-35*-family mutants, using ventral enclosure of the epidermal cells as a developmental endpoint (~ 330 min at 25°C). An average of 4.6 large cell corpses were detected per embryo, the first arising after ~ 180 min of embryonic development (Fig. 3-3A,B). Moreover, the formation of large cell corpses increased during development, with peaks at ~ 225 and ~ 300 min, implying that their formation is most prevalent at these time points (Fig. 3-3B). The formation of these large corpses was specifically attributed to the loss of *mir-35*-family miRNAs, since a transgene harboring a wild-type copy of *mir-35* (*nEx1187* extrachromosomal array) completely rescued the large-cell-corpse phenotype—only normal corpses were present in these transgenic embryos (Figs. 3-2C, 3-3A).

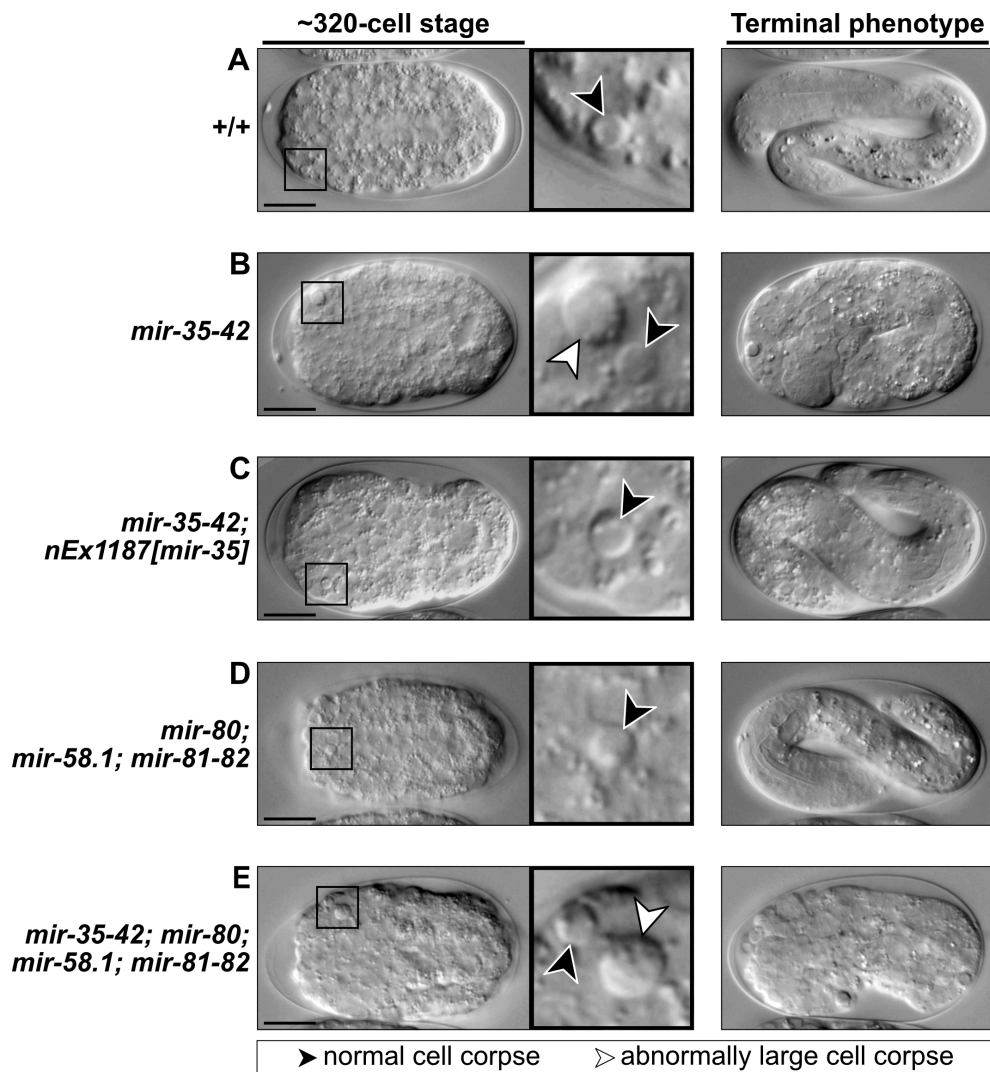


Fig. 3-2 | *mir-35*-family mutants display a large-cell-corpse phenotype. (A–E) DIC microscopic images of developing embryos. Genotypes are indicated to the left of each panel. The left-most image of each panel shows a bean-stage embryo (~320-cells), with representative cell corpses enlarged in the insets. Normal cell corpses (black arrowheads) are present in all genetic backgrounds, whereas large cell corpses (white arrowheads) are also present in (B) *mir-35*-family mutants and (E) *mir-35 mir-58* double-family mutants. The right-most image of each panel shows the terminal embryonic phenotype. Embryos depicted in panels A, C, and D survived to hatching, whereas those in panels B and E arrested. Scale bars: 10 μ m. Figure adapted from Sherrard et al. (2017).

A

Genotype	# of normal first-wave AB cell deaths (n)	# of abnormally large cell corpses (n)
+/+	13 (5)	0 (5)
<i>mir-35-41(nDf50) mir-42(nDf49)</i>	13 (10)	4.6 ± 0.7 (10)
<i>mir-35-41(nDf50) mir-42(nDf49); nEx1187[mir-35]</i>	13 (5)	0 (5)
<i>mir-80(nDf53); mir-58.1(n4640); mir-81-82(nDf54)</i>	13 (5)	0 (5)
<i>mir-35-41(nDf50) mir-42(nDf49); mir-80(nDf53); mir-58.1(n4640); mir-81-82(nDf54)</i>	13 (10)	10.7 ± 0.8 (10)
<i>ced-3(n717)</i>	0 (5)	0 (5)
<i>mir-35-41(nDf50) mir-42(nDf49); ced-3(n717)</i>	0 (5)	0 (5)
<i>egl-1(n3330)</i>	0 (5)	0 (5)
<i>mir-35-41(nDf50) mir-42(nDf49); egl-1(n3330)</i>	0 (5)	0 (5)

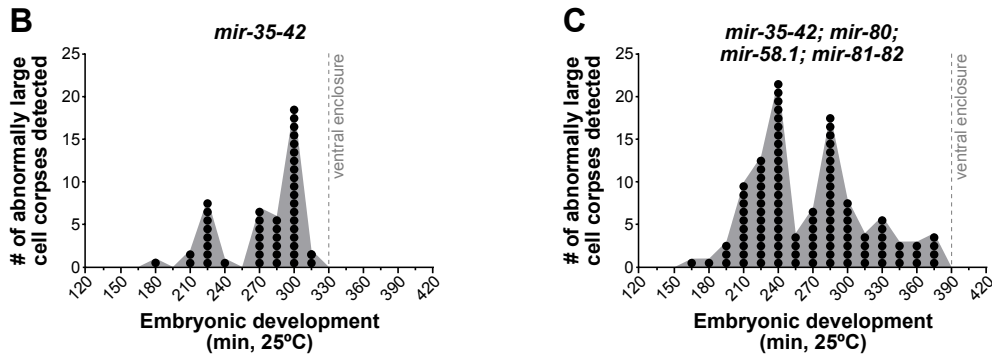


Fig. 3-3 | The large-cell-corpse phenotype in *mir-35*-family mutants is enhanced upon loss of *mir-58*-family miRNAs. (A) The number of normal first-wave AB cell deaths, as well as the number of abnormally large cell corpses appearing before ventral enclosure, was determined per embryo for the indicated genotypes. Values are mean ± SEM when applicable. (****) $P \leq 0.0001$ by Student's *t*-test. **(B–C)** The time at which each large cell corpse formed in **(B)** *mir-35*-family mutants (46 large corpses from 10 embryos) and **(C)** *mir-35 mir-58* double-family mutants (107 large corpses from 10 embryos) is indicated. Detection times were grouped into 15 min bins, ending at the point of ventral enclosure. Figure taken from Sherrard et al. (2017).

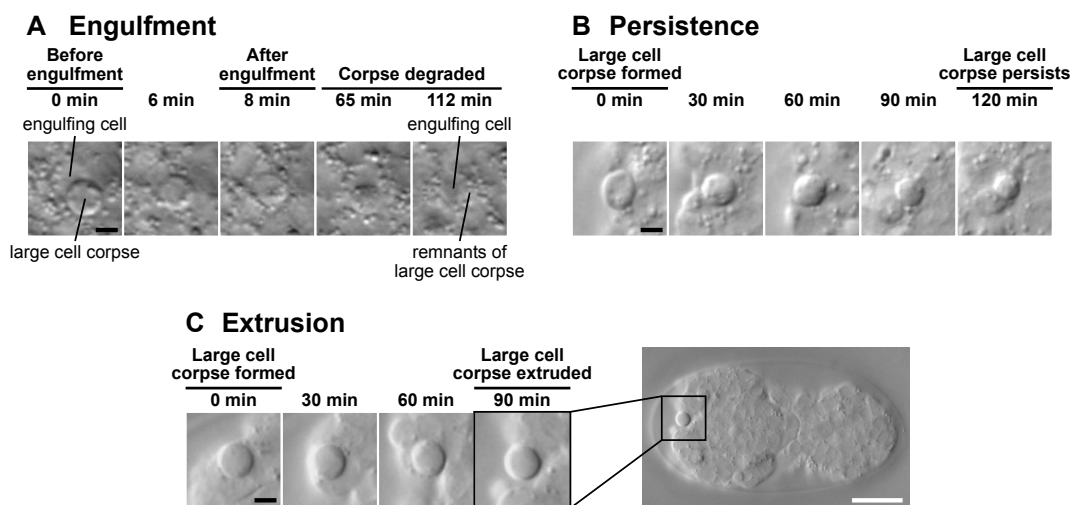


Fig. 3-4 | Large cell corpses in *mir-35*-family mutants meet various fates. (A–C) Large cell corpses may be engulfed or not (persistent), or they can be extruded from the embryo. **(A)**

Engulfment: a large cell corpse is engulfed by a neighbouring cell. After 112 min, only granular remnants of the large cell corpse can be seen in the engulfing cell. **(B)** Persistence: a large cell corpse is not engulfed and still present in the embryo 120 min after forming. **(C)** Extrusion: a large cell corpse initially persists, but is later extruded from the embryo after 90 min. Black scale bars: 2 μm . White scale bar: 10 μm . Figure adapted from Sherrard et al. (2017), supplemental material.

3.1.2 Loss of *mir-58*-family miRNAs enhances the large-cell-corpse phenotype in *mir-35*-family mutants

Cell-death abnormalities were next studied in *mir-58*-family mutants. During embryogenesis, only normal cell corpses were detected, including all 13 of the first wave of AB cell death (Figs. 3-2D, 3-3A). No large cell corpses were observed in *mir-58*-family mutants, and embryos survived to hatching (Fig. 3-2D). Having examined *mir-35*- and *mir-58*-family mutants separately, mutants lacking miRNAs of both families were generated. In these *mir-35 mir-58* double-family mutants [*mir-35-41(nDf50) mir-42(nDf49); mir-80(nDf53); mir-58.1(n4640); mir-81-82(nDf54)*] (strain made by N. Memar), all 13 cell deaths of the first wave of AB cell death were detected (Fig. 3-3A). Similar to *mir-35*-family mutants, all *mir-35 mir-58* double-family mutants arrested during embryogenesis and abnormally large cell corpses were present (Fig. 3-2E). Quantification revealed 10.7 large cell corpses per embryo in *mir-35 mir-58* double-family mutants prior to ventral enclosure—a significant 2.3-fold increase over *mir-35*-family mutants alone (Fig. 3-3A). The formation of large cell corpses began ~165 min into embryonic development and became more frequent as embryogenesis progressed, peaking at ~240 and again at ~285 min (Fig. 3-3C). These were similar to the peaks observed in *mir-35*-family mutants. Thus, although *mir-58*-family mutants themselves do not exhibit a large-cell-corpse phenotype, loss of the *mir-58*-family enhances the phenotype in *mir-35*-family mutants.

3.1.3 Formation of large cell corpses requires the central apoptotic machinery

Apart from size, the large cell corpses present in *mir-35*-family mutants resembled normal cell corpses—they rounded up, coinciding with an increase in refractility, and they could be engulfed by neighbouring cells. This suggested that the large cell corpses were dying by apoptosis. To determine whether the central apoptotic pathway is required for the formation of large cell corpses in *mir-35*-family mutants, homozygous loss-of-function alleles were introduced for either *ced-3* caspase or *egl-1* BH3-only. Both of these alleles,

RESULTS

ced-3(n717) and *egl-1(n3330)*, block most of the 131 programmed cell deaths that normally occur during *C. elegans* development (Ellis & Horvitz 1986; Conradt & Horvitz 1998), including all 13 of the first wave of AB cell death. In both *mir-35-42; ced-3* and *mir-35-42; egl-1* animals (strains generated by S. Lühr), no cell corpses were detected; that is, the 13 first-wave cell deaths of the AB lineage were absent, as were large cell corpses (Fig. 3-3A). This finding demonstrates that the central apoptotic pathway is required for the formation of large cell corpses in *mir-35*-family mutants, and that miRNAs of the miR-35 family act upstream of or in parallel to *egl-1* to suppress the formation of large cell corpses. Furthermore, blocking the central apoptotic pathway did not rescue lethality in either *mir-35-42; ced-3* or *mir-35-42; egl-1* embryos (Fig. 3-5), meaning that the large-cell-corpse phenotype is not the underlying cause of embryonic arrest in *mir-35*-family mutants.

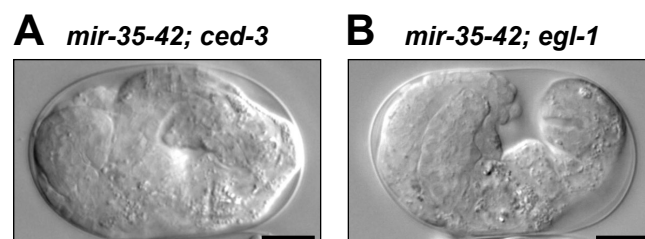


Fig. 3-5 | Blocking apoptosis does not prevent embryonic lethality in *mir-35*-family mutants. (A–B) DIC images of the terminal phenotype for *mir-35*-family mutant embryos additionally homozygous for either (A) *ced-3(n717)* or (B) *egl-1(n3330)*. Scale bars: 10 μ m. Figure adapted from Sherrard et al. (2017), supplemental material.

3.1.4 The *egl-1* 3'UTR harbors conserved binding sites for miR-35- and miR-58-family miRNAs

To determine if *egl-1* mRNA is a target of miR-35 and/or miR-58 family miRNAs, the 3'UTR of *egl-1* was analyzed for potential binding sites. According to the TargetScanWorm prediction tool (www.targetscan.org/worm, release 6.2; Jan et al. 2011), the 3'UTR of *egl-1* is 172 nt in length and contains a highly conserved binding site for each family (Fig. 3-6). The miR-35 family binding site (5'-CCCGGUG-3'; nucleotides 53–59) is classified as a 8mer-U1 site—the second-strongest site possible in nematodes. The miR-58 family binding site (5'-CGAUCUC-3'; nucleotides 86–92) has two classifications: first, as an 8mer-U1 site for miR-58.1; and second, as a 6mer site for the remaining family members (miR-80-82, miR-58.2, and miR-2209.1). Moreover, a 57 bp region (nucleotides

40–96) of the *egl-1* 3'UTR was reported to bind ALG-1 Argonaut in an iPAR-CLIP experiment (Grosswendt et al. 2014). This region overlaps with both the miR-35- and miR-58-family binding sites, lending evidence to these sites being functional and targeted by the miRISC *in vivo*.

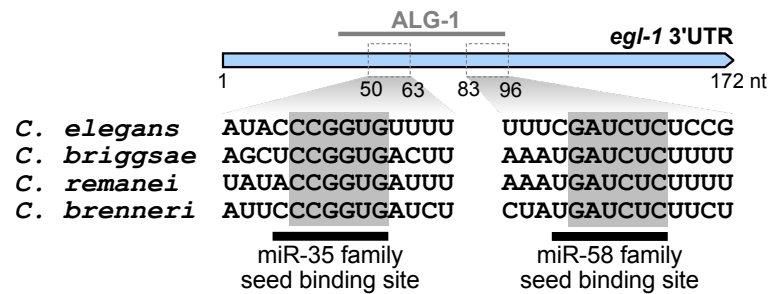


Fig. 3-6 | The *egl-1* 3'UTR is a predicted target of miR-35- and miR-58-family miRNAs. The *egl-1* 3'UTR is illustrated in blue, with the location of an ALG-1 Argonaut interaction site indicated above, as reported by Grosswendt et al. (2014). The positions and sequences of the predicted miR-35- and miR-58-family binding sites are shown, as well as their conservation across three other *Caenorhabditis* species. Nucleotides shaded in grey are perfectly conserved within the miRNA seed binding region. Figure adapted from Sherrard et al. (2017).

3.1.5 The *egl-1* 3'UTR directs downregulation of mRNA expression

To assay the functionality of the miRNA binding sites in the *egl-1* 3'UTR, five reporter constructs were generated by M. Basch, S. Lühr, and N. Memar. Each contained green fluorescent protein (GFP) fused to histone H2B under transcriptional control of the *mai-2* promoter ($P_{mai-2gfp::h2b}$), thereby ensuring constitutive expression in all cells during development (Ichikawa et al. 2006). The five constructs only differed in their 3'UTRs (Fig. 3-7A), and were as follows:

- 1) *mai-2* 3'UTR, not predicted to harbor conserved, functional miRNA binding sites;
- 2) *egl-1^{wt}* 3'UTR, the wild-type variant with both miRNA binding sites intact;
- 3) *egl-1^{mut mir-35}* 3'UTR, with the predicted miR-35-family binding site mutated (Fig. 3-7B);
- 4) *egl-1^{mut mir-58}* 3'UTR, with the predicted miR-58-family binding site mutated (Fig. 3-7B);
- 5) *egl-1^{mut mir-35 mir-58}* 3'UTR, with both predicted miRNA binding sites mutated.

These were used by S. Lühr to generate five transgenic strains, each with one of the constructs integrated into the *C. elegans* genome using Mos1-mediated single-copy insertion (mosSCI) (Frøkjær-Jensen et al. 2008, 2012). The expression pattern of each

RESULTS

transgene was then analyzed by S. Lühr and N. Memar in embryos at three developmental time points: 4-cell stage (early), ~320-cell stage (mid), and ~500-cell stage (late).

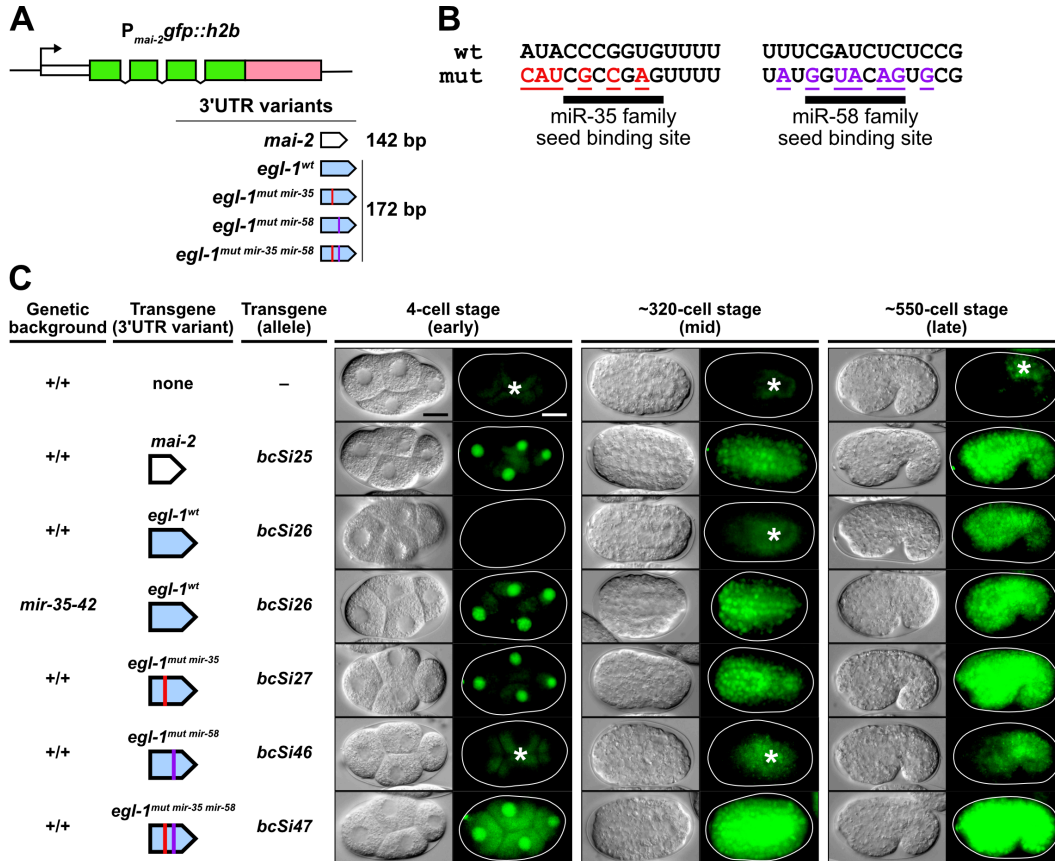


Fig. 3-7 | The *egl-1* 3'UTR mediates repression of a transgene in a miRNA-dependent manner. (A) Five reporter constructs were generated, each consisting of $P_{mai-2}gfp::h2b$ and one of the *egl-1* 3'UTR variants. (B) In cases where the miR-35- and/or miR-58-family binding site were mutated in the construct, the corresponding nucleotide changes (mut) are shown below the wild-type (wt) sequence. (C) Expression of the indicated $P_{mai-2}gfp::h2b$ transgene (3'UTR variant) at single-copy levels in embryos of the indicated genetic background. DIC and fluorescence images are shown for embryos at the 4-, ~320-, and ~550-cell stages. Transgenic strains were homozygous for *unc-119(ed3)* and the *cb-unc-119(+)* selection marker. Asterisks (*) indicate autofluorescence. Scale bar: 10 μ m. Figure adapted from Sherrard et al. (2017).

First, the *mai-2* 3'UTR transgene was ubiquitously expressed at all embryonic stages examined (Fig. 3-7C). Second, the *egl-1^wt* 3'UTR transgene was suppressed in early- and mid-stage embryos, but became detectable in late-stage embryos (Fig. 3-7C). This pattern of repression reflects the timing of *mir-35-42* expression, which peaks in early embryos and decreases post-gastrulation (Stoekius et al. 2009; Alvarez-Saavedra & Horvitz 2010;

Wu et al. 2010). Third, the *egl-1^{mut mir-35}* 3'UTR transgene was derepressed and resembled the *mai-2* 3'UTR transgene; expression was ubiquitous at all stages (Fig. 3-7C). Similarly, the *egl-1^{wt}* 3'UTR transgene in a *mir-35*-family mutant background was also ubiquitously expressed (Fig. 3-7C). Fourth, the *egl-1^{mut mir-58}* 3'UTR transgene resembled that of the *egl-1^{wt}* 3'UTR transgene, in that expression was only detected in late-stage embryos (Fig. 3-7C). Finally, expression of the *egl-1^{mut mir-35 mir-58}* 3'UTR transgene was ubiquitous and strong at all stages (Fig. 3-7C). Taken together, these data demonstrate the ability of the *egl-1* 3'UTR to mediate suppression of a transgene in a manner dependent on the miR-35 family, while miR-58-family miRNAs enhance this suppression.

To determine the mechanism by which the *egl-1* 3'UTR directs miRNA-dependent repression, smRNA FISH was used to directly label *gfp::h2b* mRNA in transgenic embryos. If repression is due to a block in translation, then *gfp::h2b* mRNA levels from the *egl-1^{wt}* 3'UTR transgene should not differ significantly from those of the control *mai-2* 3'UTR transgene. If, however, repression is due to mRNA degradation, then *gfp::h2b* mRNA levels from the *egl-1^{wt}* 3'UTR transgene should be lower than those of the control *mai-2* 3'UTR transgene; moreover, levels should positively correlate with GFP::H2B fluorescence (i.e. absent in early embryos and increasing during embryogenesis). First, *gfp::h2b* mRNA was quantified in whole, fixed embryos expressing the *mai-2* 3'UTR transgene. From the 50-cell to the 340-cell stage, *gfp::h2b* mRNA increased from ~360 copies to ~460 copies (Fig. 3-8). In embryos expressing the *egl-1^{wt}* 3'UTR transgene, the corresponding copy numbers were ~200 and ~270, consistently and significantly lower than the control ($P = 0.0059$ and 0.0015 , respectively, by Student's *t*-test) (Fig. 3-8). This decrease in mRNA copy number suggests that the *egl-1^{wt}* 3'UTR directs mRNA degradation. However, mRNA from the *egl-1^{wt}* 3'UTR transgene was still present at all stages examined—even in early embryos when GFP::H2B fluorescence is not detectable (Fig. 3-7C)—suggesting that the mRNA present at this time is translationally repressed. Taken together, these results provide evidence that miR-35- and miR-58-family miRNAs repress *egl-1* expression by promoting mRNA degradation as well as inhibiting translation.

RESULTS

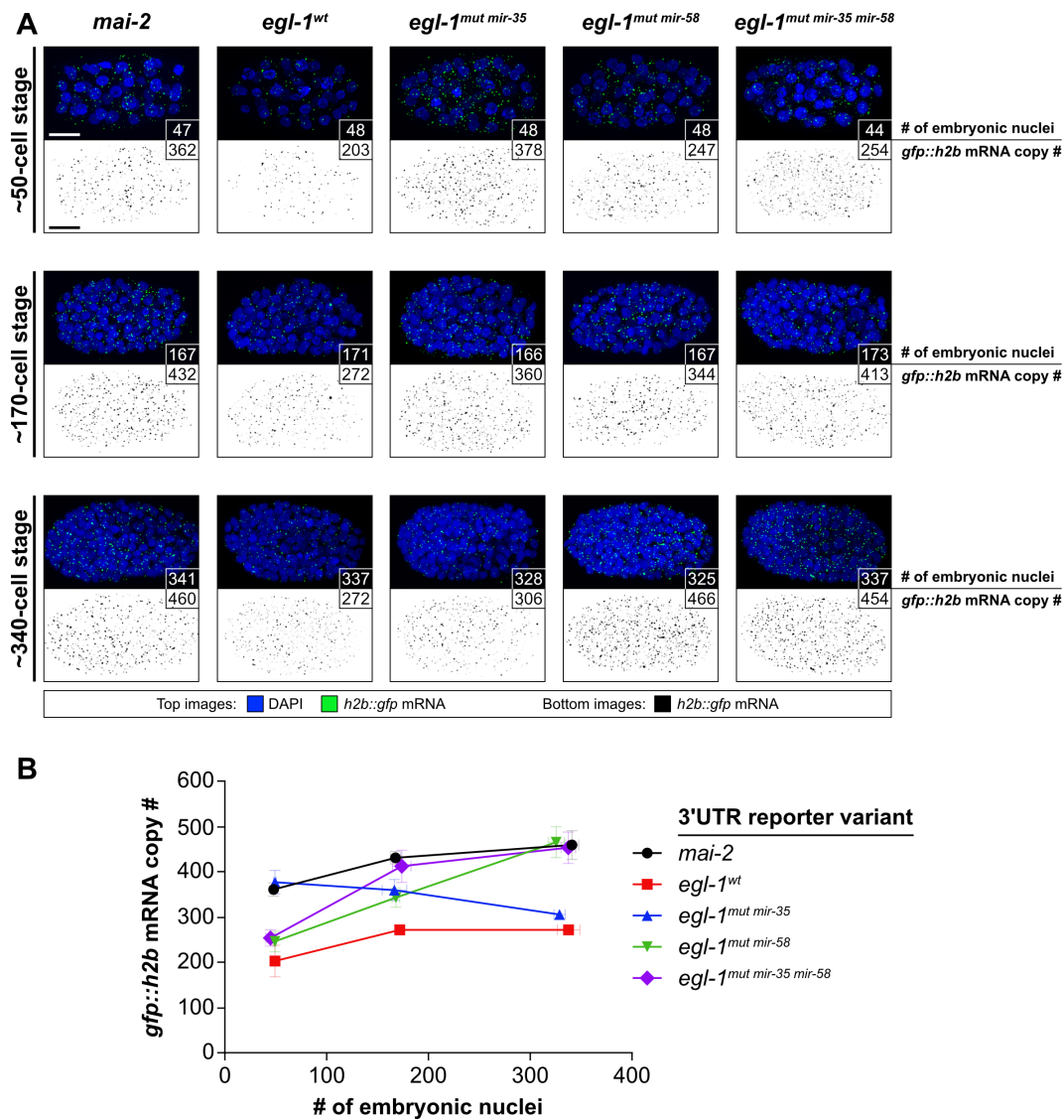


Fig. 3-8 | The *egl-1* 3'UTR mediates both translational repression and mRNA decay of a transgenic reporter. (A) Representative transgenic embryos are shown which express one of the five $P_{mai-2}gfp::h2b$ 3'UTR-variant transgenes, indicated above each image sequence. Embryos belong to one of three developmental stages (~50-cell, ~170-cell, and ~340-cell stage), and the smRNA FISH signal for *gfp::h2b* mRNA is shown together with DAPI (top images, green) or isolated (bottom images, black). All images are maximum intensity z-projections from whole embryos. Transgenic strains were homozygous for *unc-119(ed3)* and the *cb-unc-119(+)* selection marker. Scale bars: 10 μ m. (B) Quantification of total *gfp::h2b* mRNA in embryos at each stage of interest. $n = 3-6$ for each data point. Averages are plotted \pm SEM. Figure adapted from Sherrard et al. (2017), supplemental material.

The copy number of *gfp::h2b* mRNA was also quantified at the 50-cell and 340-cell stages in transgenic embryos harboring the remaining three 3'UTR variants. For the *egl-1^{mut mir-35}* 3'UTR transgene, mRNA copy numbers between these two stages decreased from ~380 to ~300 (Fig. 3-8). Comparing these values to those of the *egl-1^{wt}* 3'UTR transgene (~200 and

~270) shows that a mutation in the miR-35-family binding site leads to an increased amount of mRNA in early embryos, such that the amount is similar to that of the control *mai-2* 3'UTR transgene (~360). Furthermore, quantification of mRNA from the *egl-1^{mut} mir-58* 3'UTR transgene (~250 and ~470) shows that a mutation in the miR-58-family binding site leads to an increased amount of mRNA in later embryos, again reaching levels similar to that of the *mai-2* 3'UTR transgene (~460) (Fig. 3-8). These data reveal a pattern of 3'UTR-dependent *egl-1* mRNA degradation that is consistent with the known timings of *mir-35*- and *mir-58*-family expression. That is, *mir-35*-family genes are predominantly expressed in early embryos, and *mir-58*-family genes are predominantly expressed in late embryos and L1 larvae (Stoeckius et al. 2009; Isik et al. 2010; Wu et al. 2010).

Finally, mRNA from the *egl-1^{mut} mir-35 mir-58* 3'UTR transgene was quantified. Despite strong GFP::H2B fluorescence in early embryos expressing this transgene (Fig. 3-7C), the corresponding mRNA copy number in early embryos was low (~250) and comparable to that of the *egl-1^{wt}* 3'UTR (~200) and *egl-1^{mir-58}* 3'UTR (~250) transgenes. Therefore, mutation of both sites together has an effect on mRNA copy number that does not reflect *mir-35*- and *mir-58*-family expression, which may hint at a cooperative activity of the two miRNA families on the *egl-1* 3'UTR that involves not only mRNA degradation but also translational repression.

3.1.6 Mothers and sisters of normal apoptotic cells die inappropriately in *mir-35*-family mutants

The presence of abnormally large cell corpses has previously been observed in *C. elegans* embryos and was attributed to the death of physically larger cells, which can arise due to a prematurely active cell-death program (i.e. prior to division) or a reversal of size asymmetry during division (Hengartner et al. 1992; Sugimoto et al. 2001; Frank et al. 2005). To characterize the large cell corpses in *mir-35*-family mutants, I used 4D microscopy and lineage analyses to identify inappropriately dying cells. These analyses revealed that, in all instances, inappropriately dying cells were either the mother or the sister of a cell normally programmed to die in the embryo (Fig. 3-9A). Therefore, inappropriately dying cells in *mir-35*-family mutants are not purely ectopic deaths, as each occurs in relation to a normal programmed cell death. Specifically, large cell corpses were either precociously dying mothers (37/46; ~80%) or collaterally dying sisters (13/46; ~28%) (Fig. 3-9A,B). Moreover, precociously dying mother cells always died prior to their

RESULTS

expected time of division, and collaterally dying sister cells exhibited expected sizes, timing and polarity, often dying with similar kinetics to their respective apoptotic sister. Taken together, I conclude that abnormally large cell corpses in *mir-35*-family mutants arise due to a prematurely or collaterally active cell-death program, or stated more generally, a misregulation of the central apoptotic pathway in cell-death lineages.

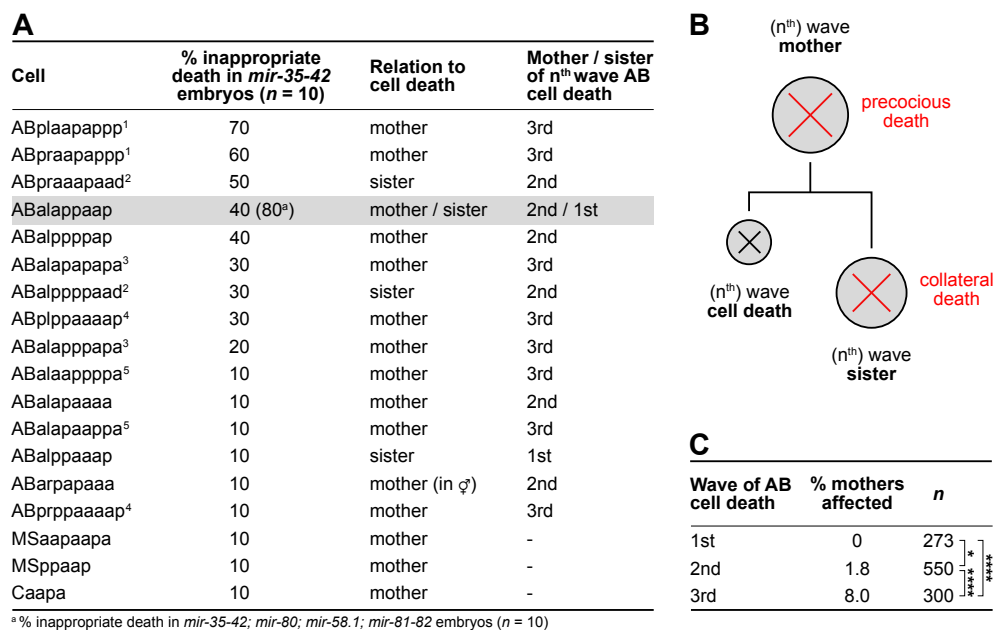


Fig. 3-9 | Large cell corpses in *mir-35*-family mutants are precociously dying mothers and collaterally dying sisters of cells programmed to die. (A) All 46 large cell corpses across ten *mir-35*-family mutant embryos were identified. Numerical superscripts in the first column indicate five pairs of bilaterally symmetric cells. The RIDnb (ABalappaap) was used for single-cell assays described later, and is highlighted in the table. (B) Schematic of a cell-death lineage, indicating a precocious and collateral cell death. (C) The percentage of precociously dying mother cells associated with each wave of cell death in the AB lineage was calculated, according to the data presented in panel A. (*) $P \leq 0.05$; (****) $P \leq 0.0001$ by Fisher's exact test. Figure adapted from Sherrard et al. (2017).

3.1.7 Penetrance of inappropriate cell death in *mir-35*-family mutants is dependent on both embryonic lineage and developmental stage

One cell that inappropriately dies in *mir-35*-family mutants, the RID neuroblast (RIDnb; i.e. ABalappaap), is both the mother and sister of a programmed cell death, and is therefore included in both classifications. Whereas the RIDnb dies inappropriately in 40% of *mir-35*-family mutants, that number doubles to 80% in *mir-35 mir-58* double-family mutants ($n = 10$ embryos) (Fig. 3-9A). This increase in precocious death of the RIDnb

demonstrates that loss of the *mir-58* family can enhance inappropriate cell death in a *mir-35* mutant background—consistent with conclusions from the 3'UTR reporter assay (Fig. 3-7C).

Interestingly, five pairs of bilaterally symmetric cells—functionally identical cells with left-right symmetry in the animal—exhibited similar incidences of inappropriate death. For example, the two most frequent inappropriate cell deaths in *mir-35*-family mutants were ABplapappp (70% inappropriate death) and ABpraapappp (60%) (Fig. 3-9A). These cells are bilaterally symmetric mothers of the ASIL/R amphid neurons and a cell programmed to die. The four other cell pairs were:

- 1) ABalpppaad (30%) and ABpraapaad (50%), ADLL/R amphid neurons and sisters of a cell death;
- 2) ABalapapapa (30%) and ABalappapa (20%), mothers of OLQDL/R sensory neurons and a cell death;
- 3) ABplppaaaap (30%) and ABprppaaaap (10%), mothers of RICL/R interneurons and a cell death;
- 4) ABalapaappa (10%) and ABalaappppa (10%), mothers of IL1L/R sensory neurons and a cell death.

This finding hints at the employment of similar, or identical, cell-death programs in bilaterally symmetric cells, making them equally susceptible to inappropriate cell death in *mir-35*-family mutants.

Finally, the prevalence of precocious cell death increased with each successive wave in the AB lineage. Of the 13 mothers that give rise to first-wave AB cell deaths, none (0%) died precociously in *mir-35*-family mutants (Fig. 3-9C). This number increased for second-wave mothers (1.8%), of which there are 55 per embryo, and was greatest for third-wave mothers (8.0%), of which there are 30. Therefore, mother cells show an increased susceptibility as embryogenesis progresses, with third-wave mother cells dying precociously about four times more often than those of the second wave.

3.1.8 miR-35- and miR-58-family miRNAs cooperatively target *egl-1* mRNA to prevent precocious death of the RID neuroblast

smRNA FISH was used to quantify endogenous *egl-1* mRNA in fixed embryos, specifically in three cells of the RID lineage. These cells were the RIDnb and its two

RESULTS

daughters, the RID neuron (ABalappaapa) and a cell programmed to die (ABalappaapp). It was previously demonstrated that programmed death of the ABalappaapp daughter cell is dependent on transcriptional upregulation of *egl-1* by UNC-3, a COE-family transcription factor (Wang et al. 2015). Therefore, I utilized an extrachromosomal *unc-3* reporter from this study, *xdEx2019* ($P_{unc-3}unc-3::gfp$), to label cells of the RID lineage during embryogenesis (Fig. 3-10A,B). Single-cell quantification of *egl-1* mRNA was achieved by confocal microscopy and image analysis.

In a wild-type background, *egl-1* mRNA was largely absent from the RIDnb, with only 0.2 copies (0.01 copies per μm^3) detected on average (Fig. 3-10C). Similarly, the copy number in a *mir-58*-family mutant background was negligible and not significantly different from wild type, at 0.5 copies (0.01 copies per μm^3) on average (Fig. 3-10C). In both of these genetic backgrounds the RIDnb never dies precociously. In the two remaining genetic backgrounds, where the RIDnb dies precociously, the average cellular *egl-1* mRNA copy numbers were significantly greater at 2.0 and 5.1 (0.05 and 0.13 copies per μm^3) in *mir-35*-family mutants and *mir-35 mir-58* double-family mutants, respectively (Fig. 3-10C). Since the RIDnb dies precociously in 40% and 80% of *mir-35*-family mutants and *mir-35 mir-58* double-family mutants, respectively, a proportional number of embryos should contain sufficient amounts of *egl-1* mRNA to trigger precocious death. This makes it possible to calculate an *egl-1* mRNA copy-number threshold, above which there is sufficient EGL-1 activity to trigger the precocious death of the RIDnb. This threshold was found to be 2–3 copies (0.05–0.08 copies per μm^3) of *egl-1* mRNA (Fig. 3-10C). Collectively, these data demonstrate the importance of miR-35-family and miR-58-family miRNAs in the RIDnb to repress *egl-1*, since only a few copies of *egl-1* mRNA are sufficient to trigger its precocious death.

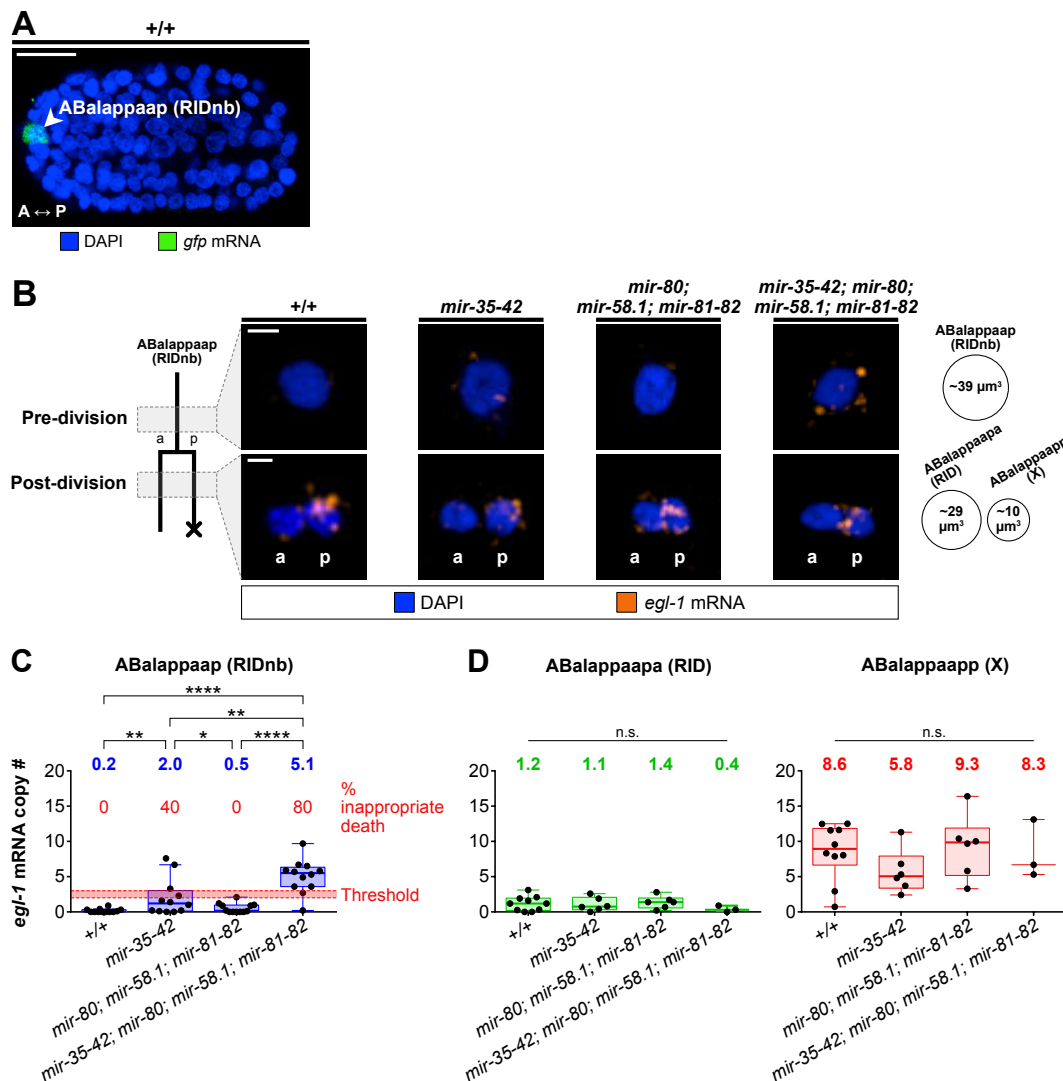


Fig. 3-10 | miR-35- and miR-58-family miRNAs prevent the precocious death of RIDnb by keeping *egl-1* mRNA levels below a critical threshold. (A) A fixed wild-type embryo expressing a *P_{unc-3unc-3::gfp}* reporter (*xdEx1091*) and stained with smRNA FISH probes specific to *gfp* mRNA, thereby labeling the RID lineage. The RIDnb (ABalappaap) is indicated, as well as anterior-posterior axis. Scale bar: 10 μm . (B) smRNA FISH staining of *egl-1* mRNA in the RIDnb and its two daughters in fixed embryos of the indicated genotypes. A schematic of the RID lineage is shown at the left, with the approximate times of analysis (pre- and post-division) highlighted. Representative images are shown for each cell in each genetic background. The surviving daughter (a, anterior) and dying daughter (p, posterior) are labeled. The estimated volume of each cell is indicated to the right in cubic micrometers (μm^3). Scale bars: 2 μm . (C–D) Single-cell quantification of *egl-1* mRNA copy numbers in the (C) RIDnb and (D) its two daughters across the indicated genotypes. For panel C, the observed percentage of precocious death is given for each genotype, and the red line illustrates the predicted threshold of 2–3 *egl-1* mRNA copies for triggering precocious death of the RIDnb. Mean values are given above each data set. Box-and-whiskers plots were generated according to Tukey’s test. (n.s.) not significant; (*) $P \leq 0.05$; (**) $P \leq 0.01$; (****) $P \leq 0.0001$ by Mann-Whitney test. Figure adapted from Sherrard et al. (2017).

RESULTS

To determine if loss of the *mir-35* family not only affects *egl-1* mRNA copy numbers but also EGL-1 protein levels, I analyzed an EGL-1 translational reporter, *bcSi60* [*P_{egl-1egl-1(n3082)::mNeonGreen::egl-1}* 3'UTR], at single-copy levels in the RIDnb. This reporter encodes the n3082 variant of EGL-1, where a 5 bp deletion in exon 3 causes a frameshift that disrupts the BH3 domain, rendering EGL-1 inactive and cytoplasmic (Conradt & Horvitz 1998). In a wild-type background, fluorescent signal was not detected in the RIDnb ($n = 5$), whereas in a *mir-35*-family mutant background, signal was detected in 40% of cases ($n = 10$) (Fig. 3-11). These values match the percentage of inappropriate death of the RIDnb in these two genetic backgrounds (Fig. 3-9A). Thus, the increased levels of *egl-1* mRNA in a *mir-35*-family mutant background correlate with higher amounts of EGL-1 protein, which is sufficient to trigger precocious death of the RIDnb.

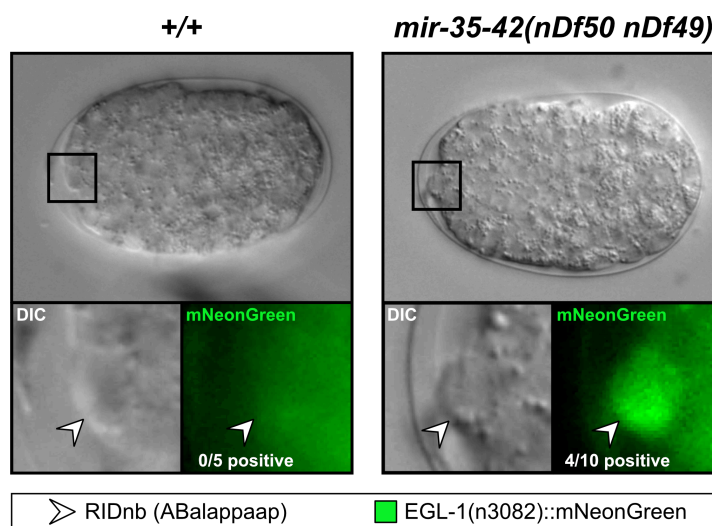


Fig. 3-11 | Loss of the *mir-35* family leads to increased expression of an EGL-1 translational reporter in RIDnb. Representative DIC images of a wild-type and *mir-35*-family mutant embryo are shown. The boxed region is enlarged below each image to show the RIDnb in both the DIC and fluorescence channels. The frequency of signal detection in the RIDnb is given for each genetic background. Both embryos harbor the *bcSi60* [*P_{egl-1egl-1(n3082)::mNeonGreen::egl-1}* 3'UTR] single-copy EGL-1 translational reporter.

Finally, the two daughter cells of the RIDnb were examined and *egl-1* mRNA was quantified in each cell. In the RID neuron, only low copy numbers of *egl-1* mRNA were detected in any genetic background (range 0.4–1.4) (Fig. 3-10D). Since this cell never died inappropriately in the mutant backgrounds, these copy numbers of *egl-1* mRNA represent below-threshold values. Conversely, in the daughter programmed to die, ABalappaapp, greater copy numbers of *egl-1* mRNA were present (range 5.8–9.3), representing above-

threshold values (Fig. 3-10D). For both daughter cells, *egl-1* mRNA copy numbers were not significantly different across the various genotypes. Taken together, these data indicate a predominant role for miR-35- family and miR-58-family miRNAs in the mother cell, RIDnb, to prevent its precocious death, with no evidence that these miRNAs are crucial for the life-or-death fate of its daughter cells.

3.1.9 *egl-1* mRNA copy number is buffered by the cooperative activity of miR-35- and miR-58-family miRNAs in the MSpaap lineage

The dynamics of *egl-1* mRNA were investigated in a second cell-death lineage—the MSpaap lineage—for which loss of the *mir-35* and *mir-58* families does not trigger inappropriate death. Cells of this lineage were identified in fixed embryos by *egl-1* smRNA FISH staining alone, without the need of a transgenic reporter (Fig. 3-12A). The MSpaap mother cell divides at the 180-cell stage, giving rise to an anterior daughter (MSpaapa) that survives and a posterior cell (MSpaapp) that dies. Notably, MSpaapp is the first programmed cell death to occur during *C. elegans* development.

smRNA FISH was used to quantify the amount of *egl-1* mRNA at three points in the MSpaap lineage: 1) pre-division; 2) during division; and 3) post-division. Pre-division, *egl-1* mRNA was already present in the MSpaap cell in all genotypes (Fig. 3-12B). In wild-type embryos, an average of 12.5 copies (0.11 copies per μm^3) of *egl-1* mRNA were detected (Fig. 3-12C). This number increased slightly in *mir-35* family mutants (18.3 copies; 0.16 copies per μm^3) and *mir-35 mir-58* double-family mutants (18.0 copies; 0.16 copies per μm^3) (Fig. 3-12C). Since MSpaap never died precociously in these mutants, these reported *egl-1* mRNA copy numbers and concentrations are considered as below threshold for this cell. In comparison, the threshold value for the RIDnb was only 2–3 copies of *egl-1* mRNA, or 0.05 to 0.08 copies per μm^3 . Data therefore indicate that the MSpaap cell can withstand at least double this concentration without succumbing to precocious death.

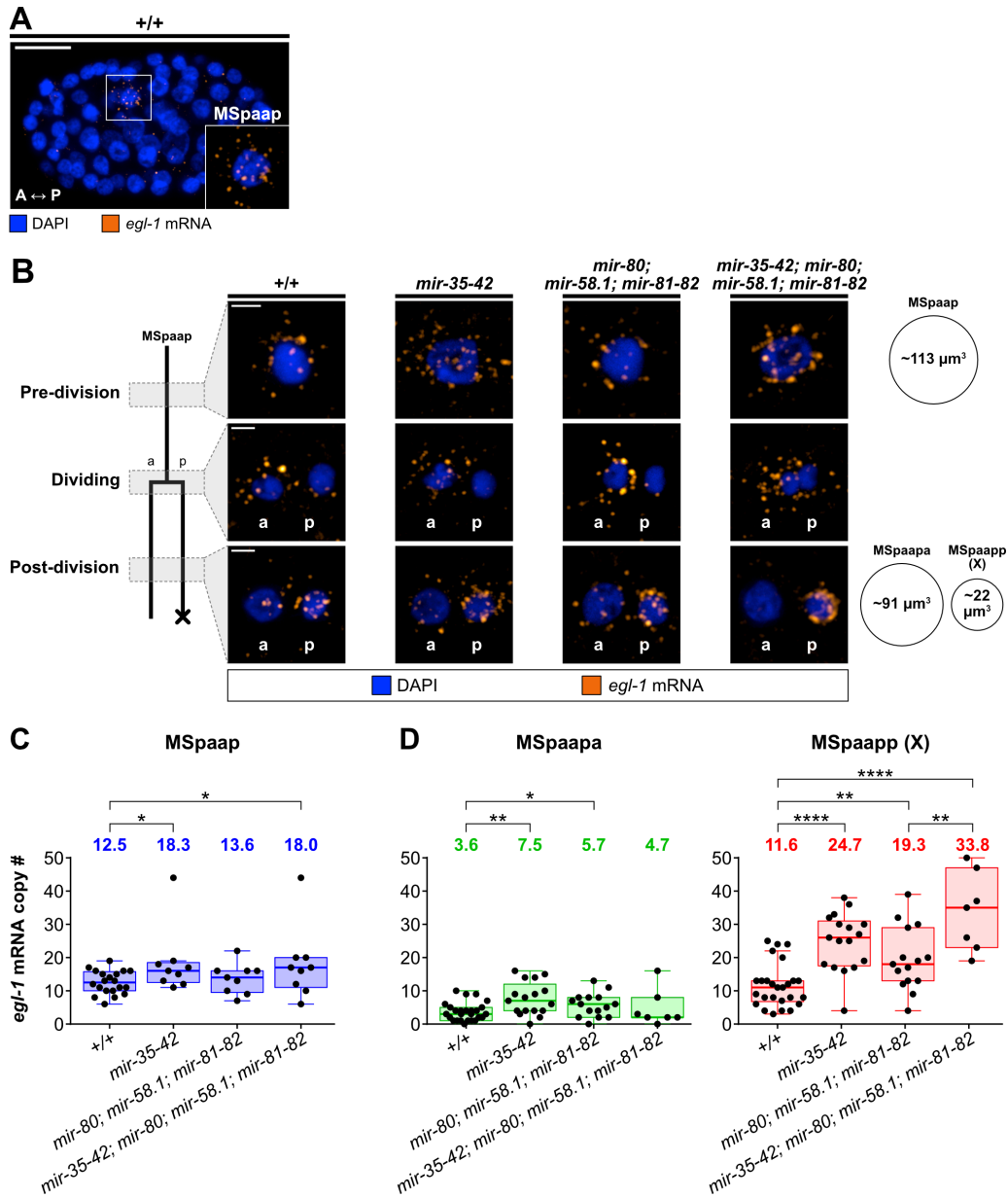


Fig. 3-12 | *egl-1* mRNA is more abundant in the MSpaap lineage in *mir-35-* and *mir-58-* family mutants. (A) A fixed wild-type embryo at the 167-cell stage, stained with smRNA FISH probes specific to *egl-1* mRNA, thereby labeling the MSpaap cell (inset). Anterior-posterior axis (A ↔ P) is indicated. Scale bar: 10 μm . **(B)** smRNA FISH staining of *egl-1* mRNA in the MSpaap cell and its two daughters in fixed embryos of the indicated genotypes. A schematic of the MSpaap lineage is shown at the left, with the approximate times of analysis (pre-, during, and post-division) highlighted. Representative images are shown for each cell in each genetic background. The surviving daughter (a, anterior) and dying daughter (p, posterior) are labeled. The estimated volume of each cell is indicated to the right in cubic micrometers (μm^3). Scale bars: 2 μm . **(C–D)** Single-cell quantification of *egl-1* mRNA copy numbers in the **(C)** MSpaap cell and **(D)** its two daughters across the indicated genotypes. The mean value is given above each data set. Box-and-whiskers plots were generated according to Tukey’s test. (*) $P \leq 0.05$; (**) $P \leq 0.01$; (****) $P \leq 0.0001$ by Mann-Whitney test. Figure adapted from Sherrard et al. (2017).

During division of the MSpaap cell, *egl-1* mRNA was detected in both prospective daughter cells (i.e. distributed throughout the common cytoplasm) in all genotypes (Fig. 3-12B). This suggests that *egl-1* mRNA transcribed in the mother cell is inherited by the daughter cells; however, low-level transcription may occur during mitosis, as recently reported in human hepatoma cells (Palozola et al. 2017), and cannot be ruled out as the source of *egl-1* mRNA in the dividing MSpaap cell.

Post-division, *egl-1* mRNA copy numbers in the surviving MSpaapa cell were only slightly different across genotypes, ranging from 3.6 copies (0.04 copies per μm^3) in wild-type embryos to 7.5 copies (0.08 copies per μm^3) in *mir-35*-family mutants (Fig. 3-12D). As MSpaapa never died collaterally, these *egl-1* mRNA copy numbers and concentrations are considered to be below threshold for this cell. Greater copy numbers and differences were measured in the dying MSpaapp cell, ranging from 11.6 copies (0.53 copies per μm^3) in wild-type embryos to 33.8 copies (1.54 copies per μm^3) in *mir-35 mir-58* double-family mutants (Fig. 3-12D). As MSpaapp is programmed to die, these *egl-1* mRNA copy numbers and concentrations are all considered to be above threshold for this cell.

Data from the MSpaap lineage was replotted according to developmental stage (i.e. number of nuclei), thus revealing the temporal dynamics of *egl-1* concentrations over time (Fig. 3-13A). In the mother cell, MSpaap, the concentration of *egl-1* mRNA remained steady at ~ 0.1 copies per μm^3 in all genotypes (Fig. 3-13B). The only fluctuation was a slight increase from the 170- to 180-cell stage, signifying an upregulation in *egl-1* transcription just prior before division. In wild-type embryos this increase in *egl-1* mRNA was approximately 1.5-fold, whereas in *mir-35*-family, *mir-58*-family, and *mir-35 mir-58* double-family mutants this increase was closer to 2-fold (Fig. 3-13B). Following division, the concentration of *egl-1* mRNA in the surviving MSpaapa cell diminished, reaching negligible levels around the 190-cell stage (Fig. 3-13B). This was observed across all genotypes, suggesting that miR-35- and miR-58-family miRNAs are not required for degradation of *egl-1* mRNA in the surviving daughter, and that this degradation might be due to normal mRNA turnover. In contrast, the concentration of *egl-1* mRNA in the dying MSpaapp cell increased sharply and significantly, reflecting full onset of *egl-1* transcription. The magnitude of this transcriptional boost varied across genotypes and was greatest in *mir-35 mir-58* double-family mutants, peaking at 37 copies (1.7 copies per μm^3); in comparison, the boost in wild-type animals peaked at 19 copies (0.85 copies per μm^3) (Fig. 3-13B). Despite these different boosts in *egl-1* transcription, the kinetics of MSpaapp death was independent of miR-35- and miR-58-family activity—the time

RESULTS

required to form a refractile corpse was the always the same (~25 min at 25°C) (Fig. 3-13C). Thus, miR-35- and miR-58-family miRNAs cooperate to buffer levels of *egl-1* mRNA in the MSpaap lineage, although loss of these miRNAs does not trigger inappropriate death nor does it affect cell-death kinetics in this lineage.

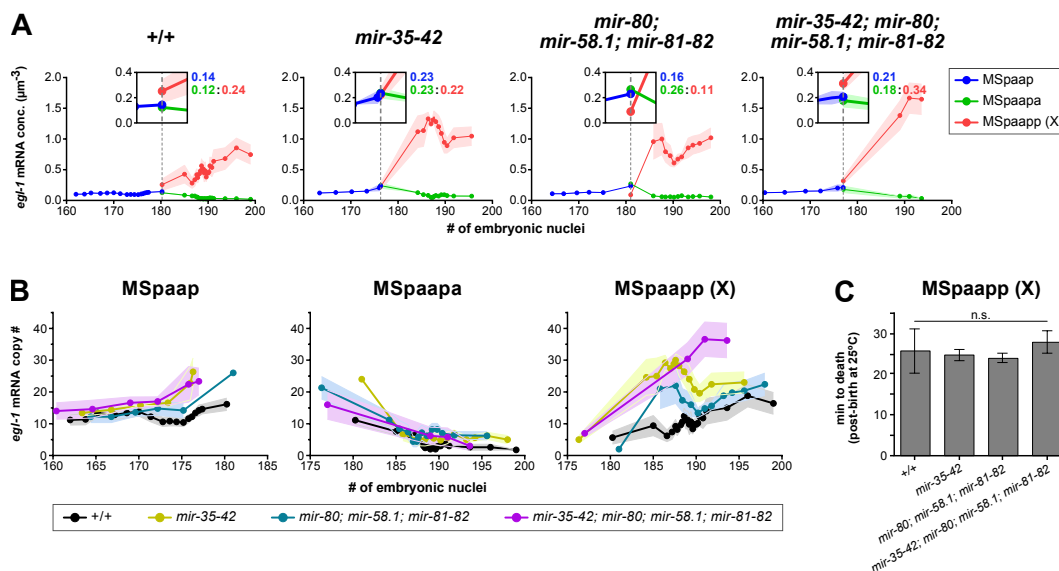


Fig. 3-13 | Loss of *mir-35* and *mir-58* families boosts the *egl-1* mRNA copy number in MSpaapp, but not the time required to die. (A) Concentration of *egl-1* mRNA in the MSpaap lineage over time in embryos of the indicated genotypes. The MSpaap cell (blue) divides around the 180-cell stage (vertical dashed line), giving rise to the surviving MSpaapa (green) and dying MSpaapp (red). The concentration of *egl-1* mRNA in all cells at the time of division is magnified in the insets, with the corresponding values given. Graphs were generated from raw data with a centered moving average of order 5. Shaded areas represent SEM, when applicable. **(B)** The copy number of *egl-1* mRNA is replotted for the MSpaap cell and its two daughters over a developmental time-course for the indicated genotypes. Shaded areas represent SEM, when applicable. **(C)** The time needed for MSpaapp to die (i.e. form a refractile corpse) post-birth was measured in each of the indicated genotypes. Averages are plotted \pm SEM. (n.s.) not significant. Figure adapted from Sherrard et al. (2017).

Finally, the average concentration of *egl-1* mRNA in both the RID and the MSpaap lineages were directly compared across the four genotypes of interest (Fig. 3-14). In the RID lineage, always-surviving cells had an *egl-1* mRNA concentration of ≤ 0.05 copies per μm^3 or less, whereas that of always-dying cells was ≥ 0.58 copies per μm^3 . When the *egl-1* mRNA concentration of a cell fell between those two values, that cell could survive or die, as evidenced by the RIDnb in both *mir-35*-family mutants (Fig. 3-14A, blue square) and *mir-35 mir-58* double-family mutants (Fig. 3-14A, blue diamond). In the MSpaap

lineage, the concentration of *egl-1* mRNA in always-surviving and always-dying cells was ≤ 0.16 and ≥ 0.53 copies per μm^3 , respectively (Fig. 3-14B). This means that a cell in the MSpaap lineage having an *egl-1* mRNA concentration of 0.16 copies per μm^3 could always survive, whereas this concentration is capable of triggering precocious cell death in the RID lineage. Taken together, these data reaffirm the correlation between *egl-1* mRNA concentration and the likelihood of cell death, while also demonstrating lineage-specific differences in the cell-death threshold.

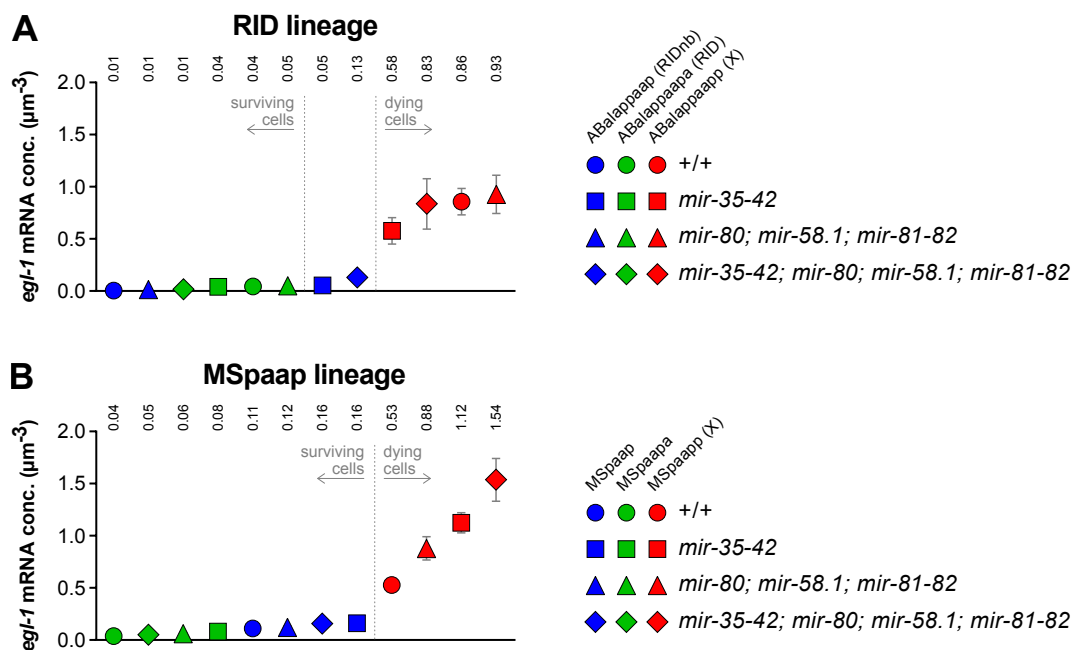


Fig. 3-14 | Cell-specific *egl-1* mRNA concentrations correlate with cell-death phenotypes in the RID and MSpaap lineages. (A–B) The average *egl-1* mRNA concentration is plotted for mother and daughter cells of the (A) RID and (B) MSpaap lineages in the indicated genetic backgrounds (refer to legends for cell identity and genetic background). Cells are arranged by increasing *egl-1* mRNA concentration, for which the mean values are given above. Cells which always survive or die, regardless of the genetic background, are indicated. Figure taken from Sherrard et al. (2017), supplemental material.

3.2 RBP-mediated regulation of programmed cell death

3.2.1 Loss of *puf-8*, but not *puf-9*, produces an abnormal cell-death phenotype in embryos

I explored the role of PUF proteins in cell death by first using two independent alleles of *puf-8*—*q725* and *ok302*. Both are large deletions that eliminate seven of the eight Puf repeats, severely disrupting the Pum-HD (Fig. 3-15). Therefore, *q725* and *ok302* (collectively referred to as “*puf-8(lf)*”) are considered strong loss-of-function alleles of *puf-8* (Subramaniam & Seydoux 2003; Bachorik & Kimble 2005).

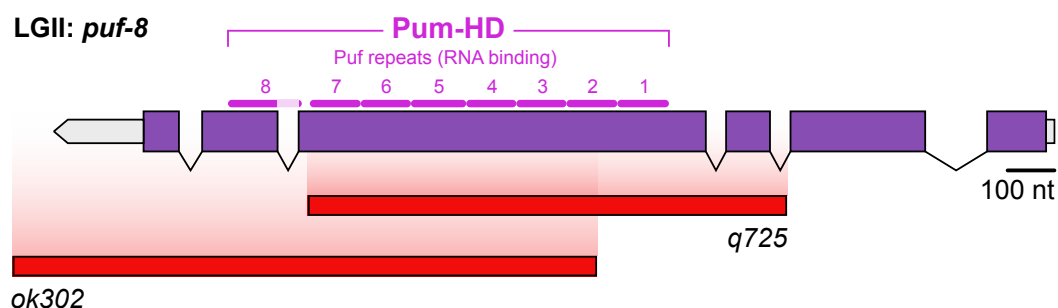


Fig. 3-15 | *q725* and *ok302* are large deletion alleles of *puf-8*. The *puf-8* transcription unit is 2138 nt in length and resides on the negative strand of chromosome II (LGII). Purple boxes represent exons, while connecting lines represent introns; UTRs are coloured in grey. The Pum-HD as well the eight comprising Puf repeats are shown in pink. Regions deleted by the strong loss-of-function alleles *q725* and *ok302* are indicated in red.

Using 4D microscopy, *puf-8(lf)* embryos were screened for abnormal cell-death phenotypes. In both *puf-8(lf)* mutants, normal cell corpses were present during development; however, large cell corpses were also visible in some embryos (Fig. 3-16A). This phenotype resembled the large-cell-corpse phenotype of *mir-35*-family mutants, as described in the previous section. The number of large cell corpses was quantified in *puf-8(lf)* embryos, up until the predetermined morphological endpoint of epidermal ventral enclosure. For both alleles, the number of large corpses per embryo was almost identical— 1.4 ± 0.9 and 1.3 ± 0.9 for *puf-8(q725)* and *puf-8(ok302)* embryos, respectively (Fig. 3-16B). Next, lineage analyses were used to assess all 14 cell deaths of the first wave—13 in the AB lineage and 1 in the MS lineage. All 14 cell corpses were detected in wild-type embryos, whereas both *puf-8(lf)* mutants had slightly fewer than 14 cell corpses on average (13.6 ± 0.2 and 13.3 ± 0.8 for *puf-8(q725)* and *puf-8(ok302)*, respectively) (Fig. 3-16B). There were two reasons for this slight reduction: 1) the inappropriate survival of a

first-wave cell death; and 2) the inappropriate death of a first-wave mother cell. This finding shows that loss of *puf-8* has two contrasting effects, the first suggesting an overactive cell-death pathway and the second suggesting an underactive pathway.

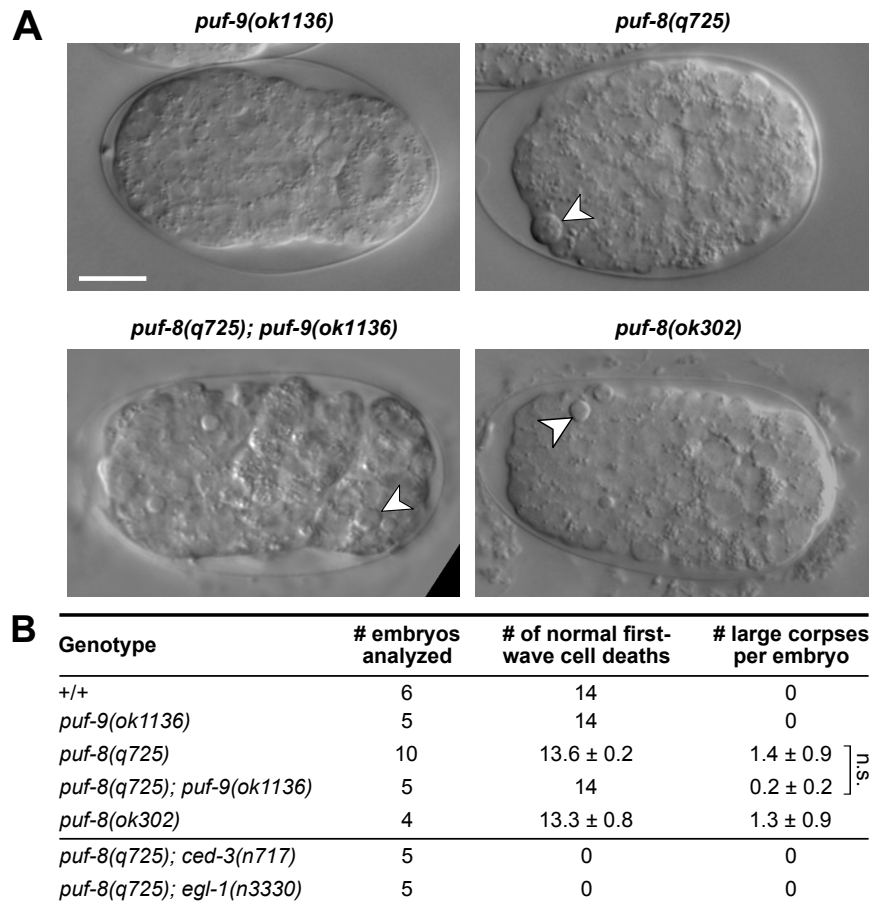


Fig. 3-16 | Abnormally large cell corpses are present in *puf-8(lf)* embryos. (A) DIC images of embryos with genotypes specified. Abnormally large corpses are present in *puf-8(q725)* and *puf-8(ok302)* embryos, as indicated by arrowheads. The identity of the large cell corpse pictured in the *puf-8(q725)* embryo is ABalaappa, the mother of a first-wave cell death. Scale bar: 10 μ m. **(B)** Quantification of large cell corpses arising during embryogenesis, before ventral enclosure. Values are averages \pm SEM, when applicable. (n.s.) not significant.

Considering that PUF-9 is in the same subgroup as PUF-8, embryos lacking *puf-9* were also examined for large cell corpses. The allele *ok1136* was used, which is a large deletion that removes 1581 nt of the *puf-9* transcription unit, including the entire Pum-HD domain (Nolde et al. 2007). A total of five *puf-9(ok1136)* embryos were analyzed by 4D microscopy, and no large corpses were detected prior to ventral enclosure (Fig. 3-16A,B). Although a loss of *puf-9* did not produce a cell-death phenotype on its own, I speculated that it might enhance the large-cell-corpse phenotype of *puf-8* mutants. To test this, K. Ikegami

RESULTS

generated a *puf-8(q725); puf-9(ok1136)* double-mutant strain. These animals were viable, allowing embryonic analyses to be performed. I analyzed a total of five embryos by 4D microscopy, and the average number of large cell corpses per embryo was 0.2 ± 0.2 (Fig. 3-16B). Next, the first-wave of cell death was assayed, and all 14 cell corpses were detected in both *puf-9(ok1136)* and *puf-8(q725); puf-9(ok1136)* embryos (Fig. 3-16B). Taken together, these data suggest that a loss of *puf-9* does not enhance the *puf-8*-dependent large-cell-corpse phenotype; rather, the phenotype may be suppressed in the double mutant.

Finally, it was determined if the formation of large cell corpses in *puf-8(lf)* embryos is dependent on the central cell-death pathway. To this end, strong loss-of-function alleles of *egl-1* and *ced-3* were used for epistatic analyses. Two double-mutant strains were generated and analyzed by K. Ikegami: *puf-8(q725); egl-1(n3330)* and *puf-8(q725); ced-3(n717)*. Embryos derived from these strains did not exhibit normal cell corpses during the first wave of cell death, demonstrating that the central cell-death pathway was indeed blocked (Fig. 3-16B). Moreover, no large cell corpses were detected in either double mutant (Fig. 3-16B). Thus, the formation of large cell corpses in *puf-8(lf)* embryos requires a fully active cell-death pathway.

3.2.2 Large cell corpses in *puf-8(lf)* animals belong to both cell-death and non-cell-death lineages

To identify the large cell corpses present in *puf-8(lf)* embryos, I performed lineage analyses on 4D recordings. For *puf-8(q725)*, a total of 14 large cell corpses were identified across 10 embryos, of which 8 were mothers of a cell death and 6 were not closely related to a cell death (i.e. not a mother, sister, or grandmother) (Fig. 3-17). Of the eight mother cells, one belonged to the first wave of cell death—the largest cell corpse observed with a diameter of $\sim 4.5 \mu\text{m}$ (Fig. 3-16A)—five belonged to the second wave and two to the third wave. For *puf-8(ok302)*, a total of five large cell corpses were identified across four embryos, of which two were related to a cell death and three were not (Fig. 3-17). Finally in *puf-8(q725); puf-9(ok1136)* embryos, only one large cell was identified from five embryos, and it was the sister of a dying cell (Fig. 3-17). Hence, abnormally large cell corpses in *puf-8* mutants arise from both cell-death and non-cell-death lineages, suggesting that the underlying misregulation differs from that observed in *mir-35*-family mutants.

Unlike the large cell corpses in *mir-35*-family mutants, no individual cell died inappropriately in more than one embryo of a given *puf-8(lf)* genotype (Fig. 3-17). Interestingly, the RIDnb (ABalappaap) died precociously in one out of ten *puf-8(q725)* embryos, as this cell was also susceptible to precocious death in *mir-35*-family and *mir-35 mir-58* double-family mutants. The only other cell common to both analyses was ABpraapapp—precursor of the ASIR neuron and mother of a third-wave cell death—which died precociously in 60% of *mir-35*-family mutants. This further demonstrates that the cause of inappropriate cell death in *puf-8(lf)* embryos differs from that of *mir-35*-family mutants.

	Cell	% inappropriate death	Closest relation to cell death	Mother of n th wave AB cell death
<i>puf-8(q725)</i>	ABalaappa	10	mother	1st
	ABalaappa	10	mother	2nd
	ABalapaapa	10	mother	2nd
	ABalappaap	10	mother	2nd
	ABarapaapa	10	mother	2nd
	ABarapapaa	10	mother	2nd
	ABaraapapaa	10	mother	3rd
	ABpraapapp	10	mother	3rd
	ABalapapp	10	-	-
	ABprpapp	10	-	-
	ABalaappapp	10	-	-
	ABalapppaaa	10	-	-
	ABaraappaaa	10	-	-
	MSpaaapa	10	-	-
<i>puf-8(q725); puf-9(ok1136)</i>	ABalapapa	25	mother	1st
	ABalpappa	25	grandmother	-
	ABalpapaap	25	-	-
	ABarpapppaa	25	-	-
	ABarppapaa	25	-	-
	ABplppaapap	20	sister	-

Fig. 3-17 | Identities of abnormally large cell corpses present in *puf-8(lf)* embryos. Embryos of three different genotypes were examined: *puf-8(q725)* ($n = 10$ embryos); *puf-8(ok302)* ($n = 4$); and *puf-8(q725); puf-9(ok1136)* ($n = 5$). Only direct relationships to a cell death (i.e. mother, sister, or grandmother) were considered.

3.2.3 The time required to form a refractile cell corpse is prolonged in *puf-8* mutants

Quantification of large cell corpses in *puf-8(lf)* embryos revealed that some cells fail to die during the first wave of cell death (Fig. 3-16B); therefore, I wanted to determine if first-

RESULTS

wave cells take longer to die in general upon loss of *puf-8*. To this end, I measured the time required for a cell to form a round, refractile corpse by 4D recording and lineage analysis (Fig. 3-18A). The time to die for first-wave cell deaths in wild-type embryos was 21.8 ± 0.6 min, and the time in *puf-9(ok1136)* mutants (21.7 ± 0.5 min) did not differ significantly from this (Fig. 3-18B). However, the time to die was significantly longer in both *puf-8(lf)* backgrounds— 25.0 ± 0.6 min in *puf-8(q725)* and 29.9 ± 1.3 min in *puf-8(ok302)* (Fig. 3-18B). Moreover, three first-wave cells failed to die in *puf-8(q725)* embryos and two in *puf-8(ok302)*. The additional loss of *puf-9* did not alter the time-to-die phenotype in a *puf-8(q725)* background, with an average of 24.4 ± 0.8 min in double-mutant embryos (Fig. 3-18B). Thus, loss of *puf-8* results in the inappropriate survival of some first-wave cell deaths, as well as a delay in the formation of cell corpses.

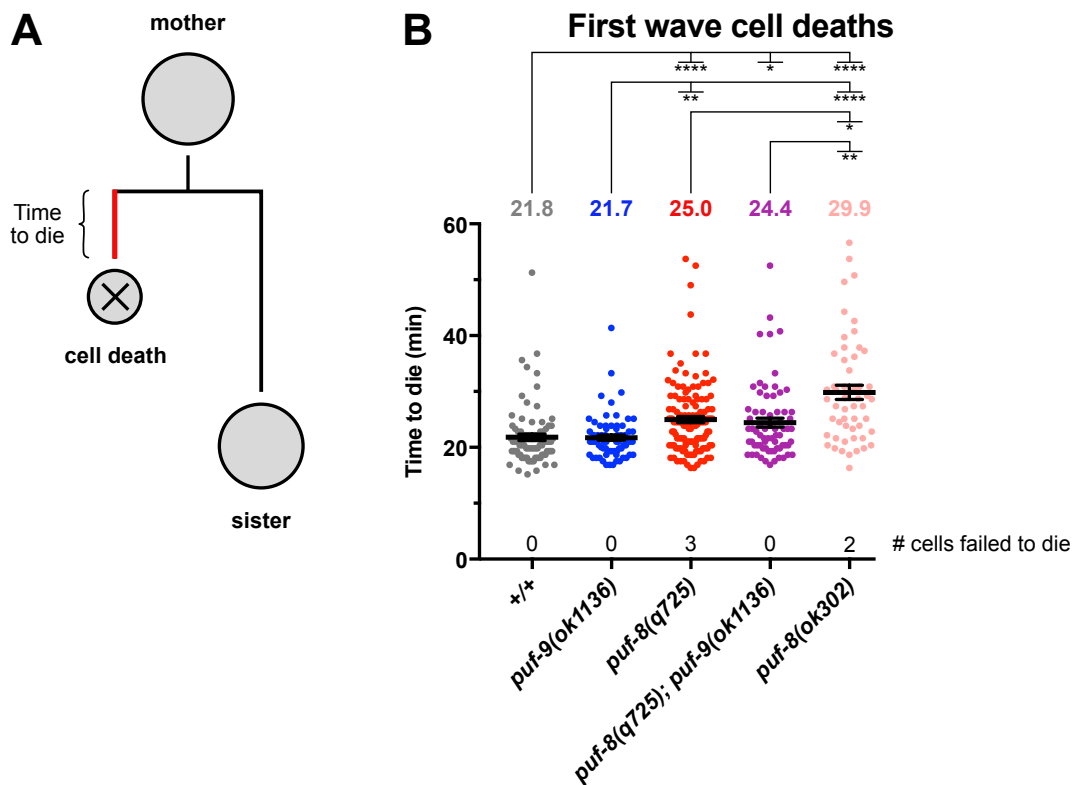


Fig. 3-18 | First-wave cell-corpse formation is delayed in *puf-8(lf)* embryos. (A) The time required for a dying cell to form a refractile cell corpse, post-birth, is represented by the red line in the schematic of a cell-death lineage. (B) The time to die was measured for cell deaths of the first wave in the genotypes indicated. Average values are given above each data set, and the number of instances where a cell failed to die is given below. Bars indicate the average \pm SEM. (*) $P \leq 0.05$; (**) $P \leq 0.01$; (****) $P \leq 0.0001$ by Kruskal-Wallis test.

I next analyzed the time to die for individual cells of the first wave to determine if the delayed cell-death phenotype is general, or if it affects certain lineages more than others. The formation of first-wave cell corpses was delayed for all lineages in *puf-8(ok302)* mutants, with six lineages exhibiting significant delays over wild type, ranging from 1.6- to 1.9-fold (Fig. 3-19). Furthermore, a 2-way ANOVA revealed that both the genotype and cell-death lineage are significant sources of variance in the data, accounting for 16.5% and 10.8% of the total variation, respectively ($P \leq 0.0001$ for each). Therefore, loss of *puf-8* causes lineage-specific delays in cell-corpse formation during the first wave, and this is most prevalent in *puf-8(ok302)* embryos.

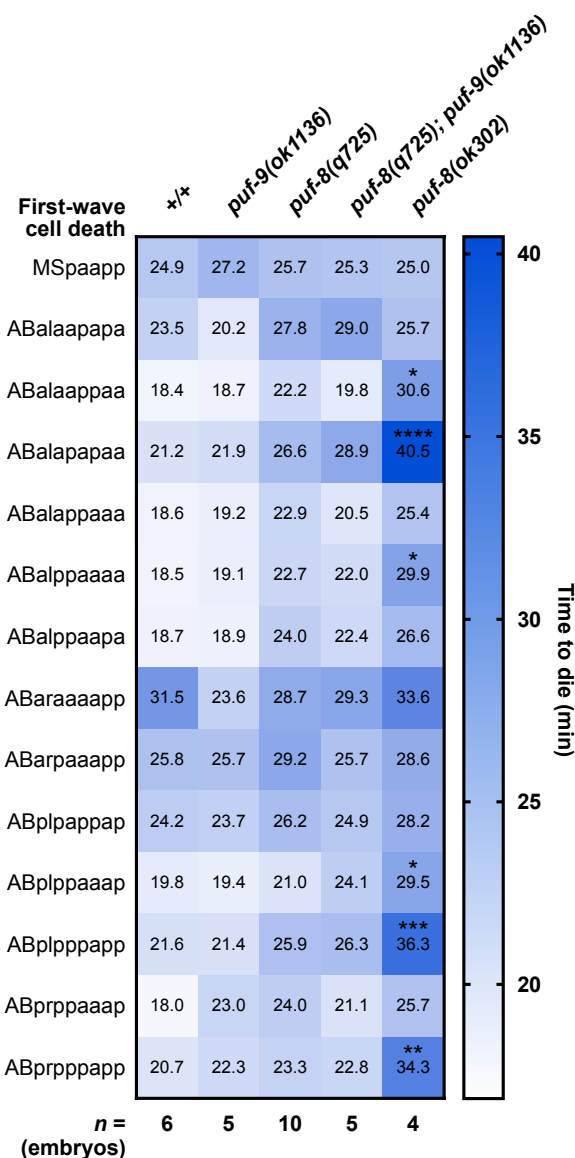


Fig. 3-19 | A lineage-specific effect of *puf-8(lf)* alleles on first-wave cell deaths. Each of the fourteen cell deaths of the first wave are listed on the right, and their average time to die is given for each genotype. Values are coloured according to the scale on the right. The number of embryos examined for each genotype (n) is given at the bottom. (*) $P \leq 0.05$; (**) $P \leq 0.01$; (***) $P \leq 0.001$; (****) $P \leq 0.0001$ by 2-way ANOVA with multiple comparison to wild type.

3.2.4 Knockdown of *fbf* partially suppresses the large-cell-corpse phenotype in *mir-35*-family mutants

The function of FBF is partially redundant with PUF-8 (Bachorik & Kimble 2005). Therefore, to determine if loss of *fbf* also produces an abnormal cell-death phenotype, I analyzed *fbf-1(ok91); fbf-2(q704)* double mutants. Animals lacking *fbf* are not viable due to sterility; therefore, the *mIn1* LGII balancer is used for maintenance, as it contains a wild-type copy of the *fbf-1* and *fbf-2* loci (Edgley & Riddle 2001). Double-mutant embryos that had lost the balancer chromosome were analyzed, and no abnormal cell-corpse phenotype was observed—only normal cell corpses were present (Fig. 3-20A). Although embryos themselves lacked the balancer, it is possible that residual FBF was inherited by the embryo from the mother's germline, thereby minimizing any *fbf*-null phenotypes. Therefore, *fbf* was systemically knocked down by RNAi. Since *fbf-1* and *fbf-2* share more than 90% identity at the nucleotide level, RNAi results in depletion of both targets (Zhang et al. 1997); to be certain, *fbf-1(RNAi)* was conducted in an *fbf-2(q738)* loss-of-function background. Efficient knockdown of *fbf* was confirmed by phenotypic analysis of treated animals at the adult stage, which exhibited improper germline development and a failure to switch from oogenesis to spermatogenesis (Fig. 3-20B), as previously described (Zhang et al. 1997). During embryonic development, no abnormalities in cell death were evident; that is, only normal cell corpses were seen (Fig. 3-20A). However, cells programmed to die during the first wave were slightly delayed in corpse formation relative to wild type (23.1 ± 0.8 min; $P = 0.0256$ by Mann-Whitney test). These data show that *fbf* knockdown does not produce a large-cell-corpse phenotype like that seen in *puf-8(lf)* animals, but delayed first-wave cell death is common to both. Thus, FBF activity may promote the cell-death pathway in cells programmed to die.

To further examine the role of *fbf* in cell death, *mir-35*-family mutants were subjected to *fbf-1(RNAi)* and the large-cell-corpse phenotype was evaluated. Knockdown of *fbf* resulted in a slight but significant decrease in the number of large cell corpses per embryo, from 4.6 to 2.4 (Fig. 3-20B). This result demonstrates that *fbf* interacts genetically with the *mir-35* family, and supports the notion that FBF activity promotes the cell-death pathway during embryogenesis.

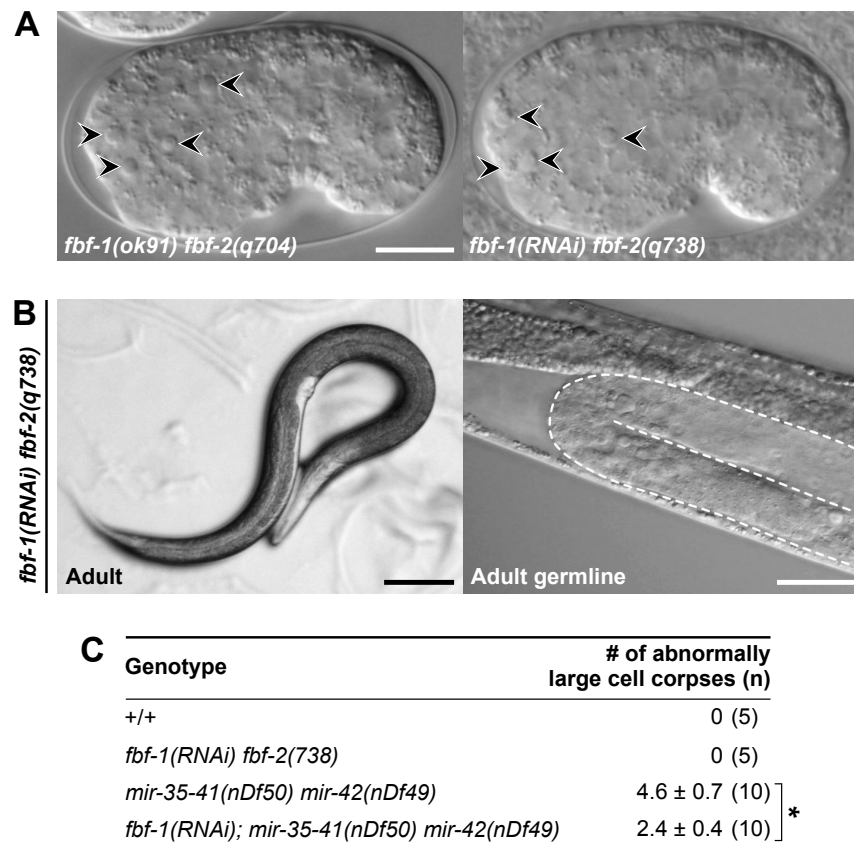


Fig. 3-20 | Knockdown of *fbf* suppresses the large-cell-corpse phenotype in *mir-35*-family mutants. (A) Only normal cell corpses (black arrowheads) were observed in *fbf-1(ok91); fbf-2(q704)* double-mutant embryos and *fbf-1(RNAi) fbf-2(q738)* embryos. Scale bar: 10 μ m. **(B)** *fbf-1(RNAi) fbf-2(q738)* animals grew to be adults with underdeveloped germlines, exhibiting an excess of sperm and lacking oocytes. Scale bars: black, 0.1 mm; white, 25 μ m. **(C)** Quantification of large cell corpses in embryos of the indicated genotypes, prior to ventral enclosure. Values are averages \pm SEM. (*) $P \leq 0.05$ by Student's *t*-test.

3.2.5 The 3'UTRs of *egl-1*, *ced-9*, *ced-4*, and *ced-3* harbor predicted PBEs and FBEs

To identify potential targets of PUF-8 and FBF, the 3'UTRs of *egl-1*, *ced-9*, *ced-4*, and *ced-3* were analyzed for the presence of PBEs and FBEs. The MEME suite of analysis tools was used for this purpose (<http://www.meme-suite.org>, v4.12.0; Bailey et al. 2009). Briefly, RNA sequences known to be targeted by either PUF-8 or FBF were compiled from a previous study, in which a yeast three-hybrid system was used to determine the relative binding specificities of both RBPs (Opperman et al. 2005). A total of 11 and 17 RNA sequences were identified as PUF-8 and FBF targets, respectively, which I then subjected to MEME analysis to yield a position-specific scoring matrix (PSSM) for each RBP (Fig.

RESULTS

3-21). Finally, the 3'UTR sequences of *egl-1*, *ced-9*, *ced-4*, and *ced-3* were screened for occurrences of each motif using FIMO.

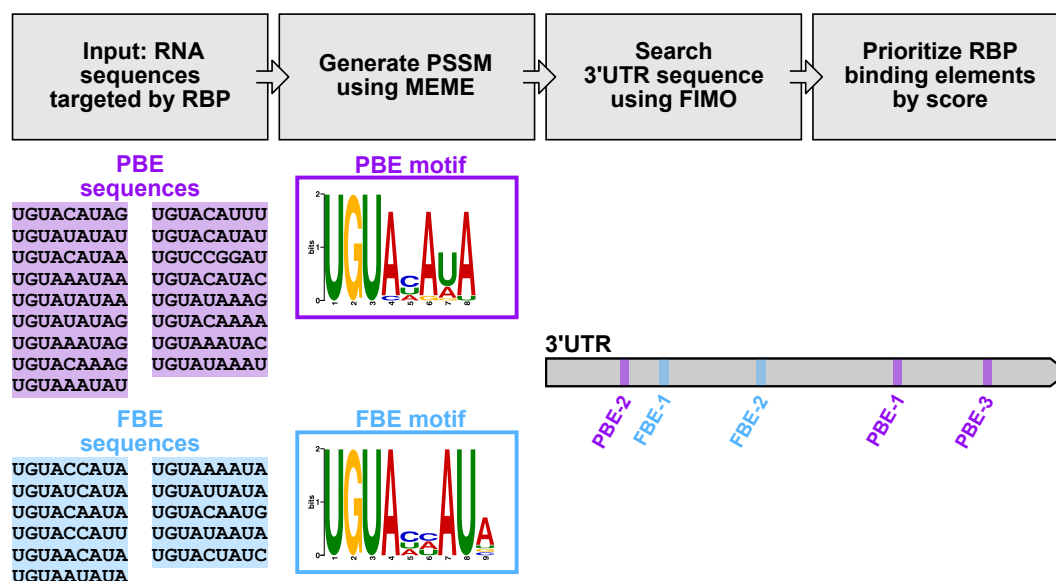


Fig. 3-21 | Pipeline for the identification of RBP motifs in 3'UTR sequences. RNA sequences bound by PUF-8 or FBE, as determined by Opperman et al. (2005), were used to generate PSSMs using MEME. These matrices were subsequently used by FIMO to search 3'UTR sequences for potential elements, which were ranked according to the log-odds score output by FIMO.

The *egl-1* 3'UTR harbors two FBEs that are conserved in at least one other *Caenorhabditis* species (Fig. 3-22). The top-scoring FBE, as determined by FIMO analysis, is referred to as e1-FBE-1 (*egl-1* FBE rank 1) and the second is referred to as e1-FBE-2. Sequence alignment shows that e1-FBE-1 is conserved in both *C. brenneri* and *C. briggsae*, whereas e1-FBE-2 is only conserved in *C. briggsae*. Two previous studies identified both of these elements, and also reported *egl-1* mRNA as a direct target of FBF in the germline, using RIP-Chip (Kershner & Kimble 2010) and iCLIP (Prasad et al. 2016); the functionality of these two FBEs was not investigated. Interestingly, these FBEs flank a reported ALG-1 Argonaute site (Grosswendt et al. 2014). The *egl-1* 3'UTR is not predicted to be a target of PUF-8, as no PBEs were identified.

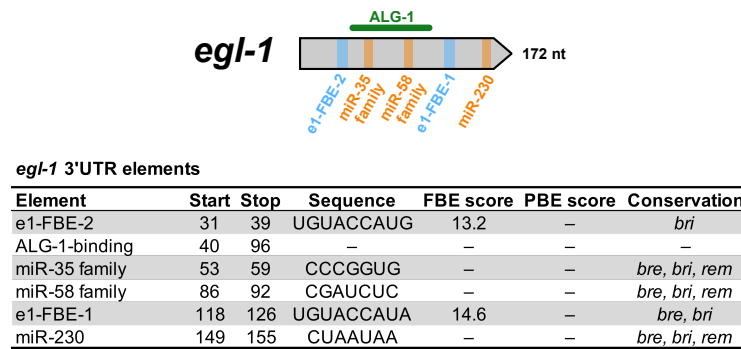


Fig. 3-22 | Predicted *cis*-acting elements in the 3'UTR of *egl-1*. Predicted motifs in the *egl-1* 3'UTR are annotated, when present, with PBEs shown in purple and FBEs shown in blue. Predicted conserved miRNA binding sites for conserved miRNA families are shown in orange, as published on TargetScanWorm (<http://www.targetscan.org>, release 6.2; Jan et al. 2011). Reported ALG-1 Argonaute interaction sites are shown in green, as reported in Grosswendt et al. (2014). PBEs and FBEs are named according to their respective gene and score, as determined by MEME and FIMO analyses (i.e. the top-scoring FBE in the *egl-1* 3'UTR is named 'e1-FBE-1'). Log-likelihood ratio scores output by FIMO are given in the table. Conservation of elements in other *Caenorhabditis* species is indicated as follows: *C. brenneri* (*bre*); *C. briggsae* (*bri*); *C. remanei* (*rem*); *C. japonica* (*jap*). Conservation of ALG-1 interaction sites were not determined.

The *ced-9* 3'UTR contains several elements—five PBEs and two FBEs (Fig. 3-23). c9-PBE-1 is conserved in at least four other nematodes, and partially overlaps with the lower-scoring c9-PBE-5. Two additional pairs of coincident elements are present: 1) c9-PBE-3 and c9-FBE-1, both conserved in *C. brenneri* and *C. remanei*; and 2) c9-PBE-2 and c9-FBE-2, which are not conserved. Furthermore, the only conserved binding site for a conserved miRNA belongs to miR-85 and overlaps with c9-PBE-4.

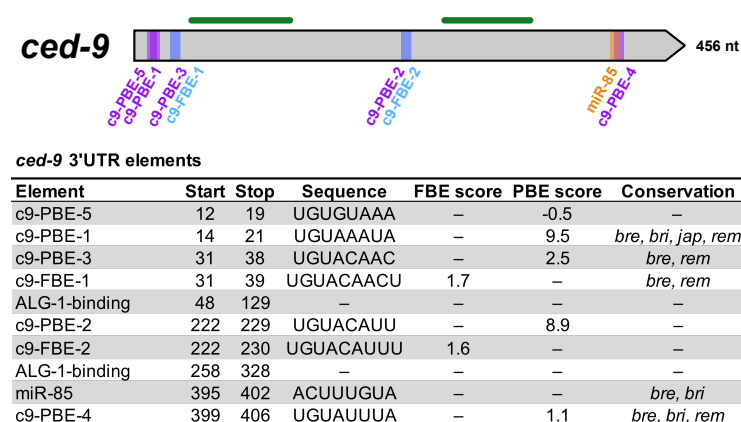


Fig. 3-23 | Predicted *cis*-acting elements in the 3'UTR of *ced-9*. See Figure 3-22 for details.

RESULTS

The *ced-4* 3'UTR also has several elements—two PBEs and three FBEs (Fig. 3-24). The top-scoring element for each RBP, c4-PBE-1 and c4-FBE-1, are coincident with each other and conserved in at least three other nematodes. Two other elements overlap—c4-PBE-2 and c4-FBE-3—however neither are conserved.

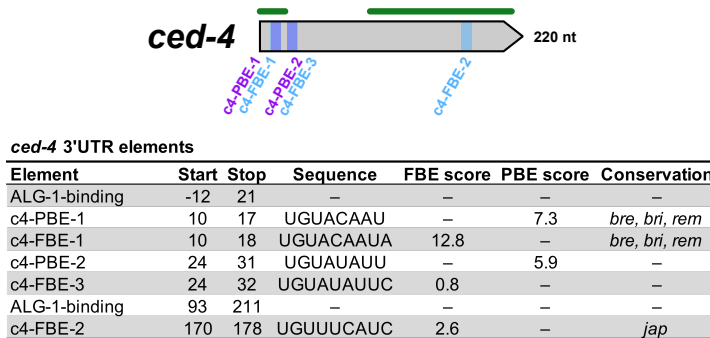


Fig. 3-24 | Predicted *cis*-acting elements in the 3'UTR of *ced-4*. See Figure 3-22 for details.

At 858 nt, the *ced-3* 3'UTR is the longest among the central cell-death genes and harbors many elements—six PBEs and four FBEs (Fig. 3-25). All exhibit some degree of conservation, with the exception of c3-FBE-1 and c3-PBE-5. Similar to elements in the *ced-9* and *ced-4* 3'UTRs, there are several overlaps: 1) c3-PBE-5 and c3-FBE-2; 2) c3-PBE-2 and c3-FBE-1; and 3) c3-PBE-1 and c3-FBE-3. Moreover, there is a triple overlap between the three elements c3-PBE-6, c3-PBE-4, and c3-FBE-4—a feature that was not identified in the 3'UTR of any other cell-death gene. In summary, this analysis identified *egl-1*, *ced-9*, *ced-4*, and *ced-3* as potential post-transcriptional targets of FBF, and the latter three genes as potential targets of PUF-8.

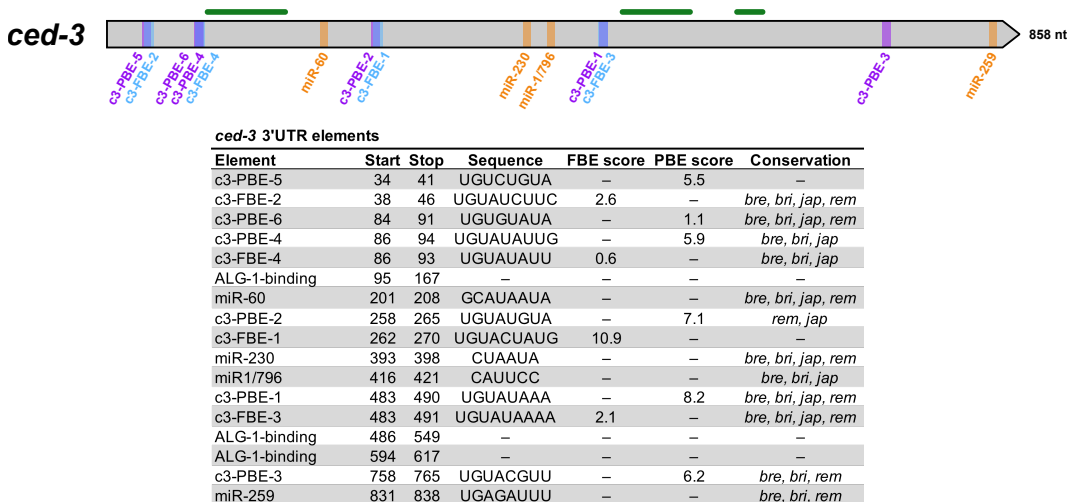


Fig. 3-25 | Predicted *cis*-acting elements in the 3'UTR of *ced-3*. See Figure 3-22 for details.

3.2.6 Embryonic *ced-3* mRNA copy numbers are not elevated in *puf-8(lf)* embryos

K. Ikegami quantified *ced-3* mRNA in whole embryos lacking *puf-8* and/or *puf-9* to determine if *ced-3* is post-transcriptionally degraded by PUF activity. Embryos of three different stages were examined (~50, ~180, and ~360 cells), and smRNA FISH was used to stain endogenous *ced-3* mRNA. At all stages, embryo-wide *ced-3* mRNA copy numbers were not significantly different between wild type and *puf-8(q725)*, *puf-9(ok1136)*, and *puf-8; puf-9* double mutants (Fig. 3-26). These data suggest that PUF-8 and PUF-9 do not mediate an embryo-wide degradation of *ced-3* mRNA, although other regulatory mechanisms (i.e. translational repression) cannot be ruled out.

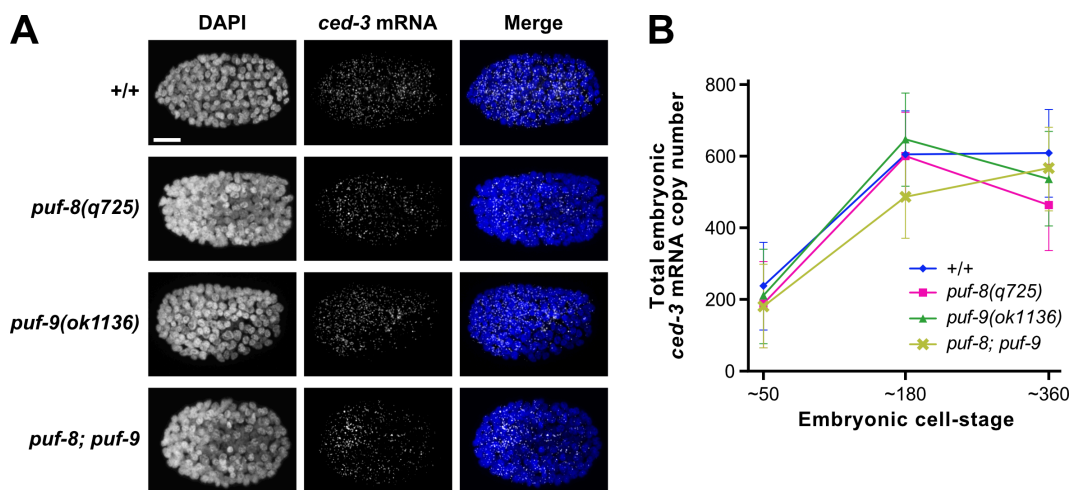


Fig. 3-26 | Total embryo *ced-3* mRNA amounts are not affected by loss of *puf-8*. (A) Confocal microscopy image stacks of whole embryos of the indicated genotypes, showing DAPI and *ced-3* mRNA staining. Images are maximum-intensity projections. (B) Quantification of whole-embryo *ced-3* mRNA copy numbers at three different stages. Average values are plotted \pm SEM.

3.2.7 Two FBEs in the 3'UTR of *egl-1* mediate repression of a transgenic reporter

Evidence already presented from this study showed that *egl-1* is post-transcriptionally regulated by miR-35- and miR-58-family miRNAs. The presence of two FBEs in the *egl-1* 3'UTR could signify an additional level of regulation. Although *egl-1* was previously identified as a target of FBF, these studies were largely germline centric and functionality of the two FBEs was not directly assessed (Kershner & Kimble 2010; Prasad et al. 2016).

RESULTS

Therefore, reporter constructs were generated to assay e1-FBE-1 and e1-FBE-2, based on the $P_{mai-2}gfp::h2b$ constructs presented previously (Fig. 3-27A). These reporters were under the post-transcriptional control of three *egl-1* 3'UTR variants (Fig. 3-27C):

- 1) *egl-1^{wt}* 3'UTR, the wild-type variant with both FBEs intact;
- 2) *egl-1^{mut FBE-1}* 3'UTR, with a point-mutation that disrupts e1-FBE-1;
- 3) *egl-1^{mut FBE-1 FBE-2}* 3'UTR, with point-mutations that disrupt both e1-FBE-1 and e1-FBE-2.

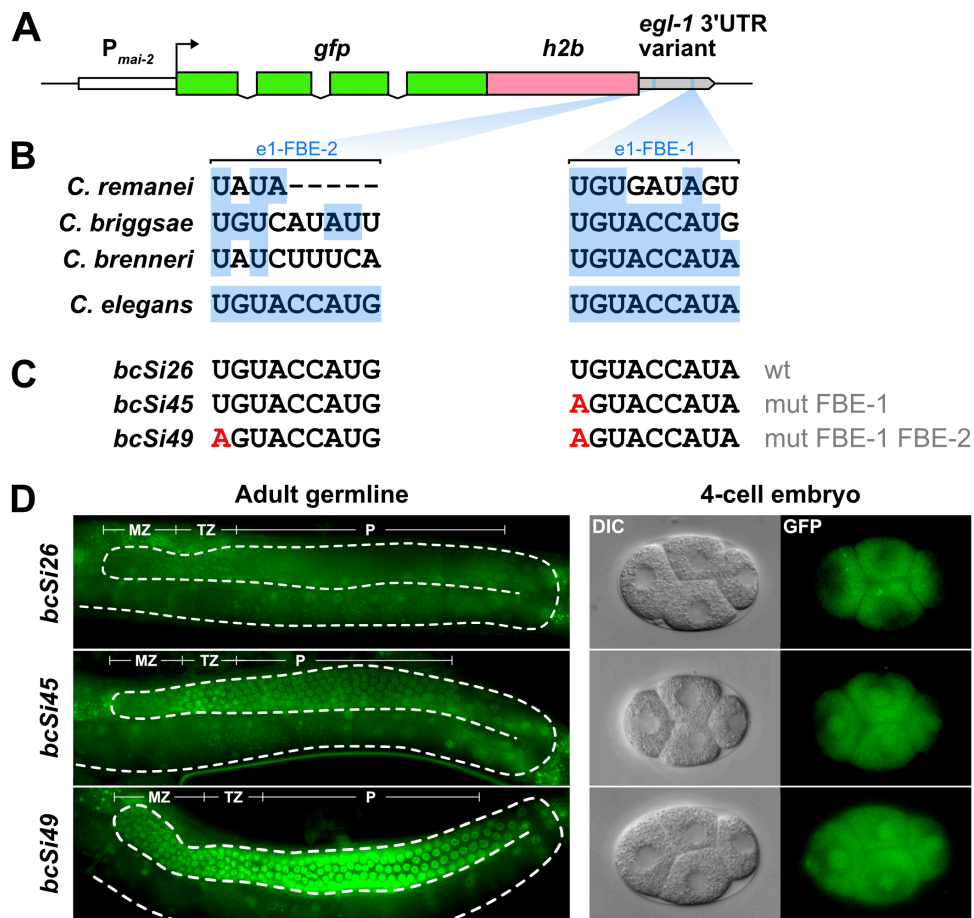


Fig. 3-27 | Mutation of FBEs causes derepression of an *egl-1* 3'UTR reporter in the adult germline and early embryos. (A) A schematic of the 3'UTR reporter used to assay functionality of the FBEs. **(B)** A sequence alignment of e1-FBE-2 and e1-FBE-1 is shown for three other *Caenorhabditis* nematodes. **(C)** Sequence of FBEs in the three *egl-1* 3'UTR variants. Point mutations the in *bcSi45* and *bcSi49* alleles are indicated in red. **(D)** Fluorescence images of nuclear-localized GFP::H2B from the single-copy transgenes *bcSi26*, *bcSi45*, and *bcSi49* in the adult germline and a 4-cell embryo. Regions of the germline are indicated: MZ, mitotic zone; TZ, transition zone; P, pachytene.

The primary site of FBF activity is the distal, mitotic region of the germline; therefore, expression of each 3'UTR transgene was considered in the adult germline in addition to 4-cell embryos. First, the *egl-1^{wt}* 3'UTR transgene was largely repressed in the germline, although weak signal was visible in the transition zone, likely due the condensation of nuclei in this region (Fig. 3-27D). In the 4-cell embryo, nuclear signal of GFP::H2B was very low. Second, the *egl-1^{mut} FBE-1* 3'UTR transgene was visibly derepressed in a general manner in the germline, again with a peak in the transition zone (Fig. 3-27D). In the 4-cell embryo, nuclear-localized signal was also visibly greater than that of the *egl-1^{wt}* 3'UTR transgene. Finally, the *egl-1^{mut} FBE-1 FBE-2* 3'UTR transgene was strongly derepressed in the germline, most considerably in the pachytene region (Fig. 3-27D). In the 4-cell embryo, GFP::H2B signal was also visible but not noticeably stronger than that of the *egl-1^{mut} FBE-1* 3'UTR transgene. Taken together, this assay demonstrates that both FBEs in the *egl-1* 3'UTR are capable of mediating repression in the germline and early embryos, suggesting that *fbf* negatively regulates the cell-death pathway during the first stages of development. Considering my previous finding that *fbf* may promote the cell-death pathway during embryogenesis (Fig. 3-20C), this could indicate a dual role for *fbf* in regulating cell-death with spatiotemporal control.

At least four elements in the 3'UTR of *egl-1* have demonstrated functionality *in vivo*—two miRNA binding sites and two FBEs. Considering that the *egl-1* 3'UTR is only 172 nt long, these four elements are in close proximity to each other and may form secondary interactions. Therefore, a secondary structure prediction of the *egl-1* 3'UTR was generated using RNAfold from the ViennaRNA Package (v2.4.6, <http://rna.tbi.univie.ac.at>; Lorenz et al. 2011). The minimum free energy structure prediction at 20°C revealed potential for the miR-35-family binding site to partially base pair with e1-FBE-2 (Fig. 3-28A). This interaction occurs with ~40% probability and could have functional relevance by obstructing access of miR-35-family miRNAs and/or FBF to their respective binding sites. The miR-58-family binding site and e1-FBE-1 are not predicted to interact with each other; however, they may form moderately-stable base pairs with other regions of the *egl-1* 3'UTR (Fig. 3-28B). Notably, a very stable hairpin is predicted to occur at the 3'-most end with near 100% certainty (Fig. 3-28C). This hairpin is also highly conserved in other nematodes, indicating that it might be functionally important.

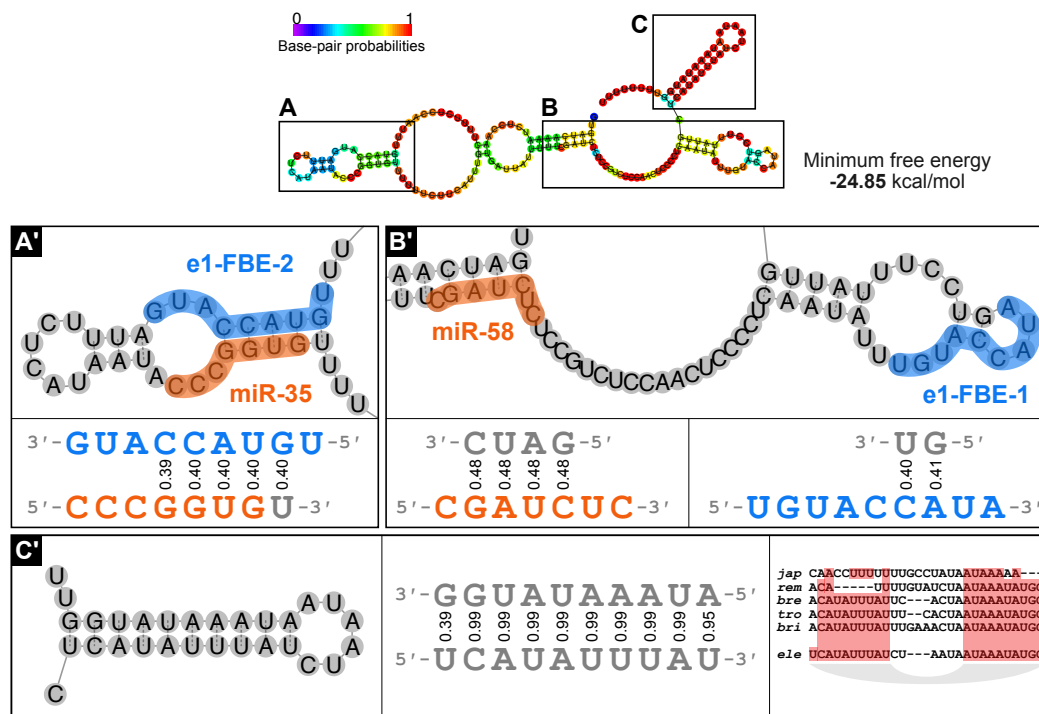


Fig. 3-28 | Secondary structure prediction for the *egl-1* 3'UTR. The structure prediction for the 3'UTR of *egl-1* is shown in its entirety (top), coloured according to base-pair probabilities. Two insets (A and B) highlight the regions containing FBEs and miRNA-family binding sites. Inset C highlights the stable hairpin near the 3' end. These three insets are shown in greater detail below (A', B', and C'), and the probability of each base pair occurring at 20°C is given. Conservation of the hairpin-forming sequence in other *Caenorhabditis* species is also shown in panel C', with abbreviations as follows: *C. japonica* (*jap*); *C. remanei* (*rem*); *C. brenneri* (*bre*); *C. tropicalis* (*tro*); *C. briggsae* (*bri*); *C. elegans* (*ele*). Secondary structure prediction at 20°C was produced by the RNAfold web server (v2.4.6, <http://rna.tbi.univie.ac.at>; Lorenz et al. 2011).

4

DISCUSSION

4.1 miRNA-mediated regulation of programmed cell death

4.1.1 miR-35 and miR-58 family miRNAs cooperatively repress *egl-1* *in vivo*

The collective data generated by S. Lühr, N. Memar, and me, demonstrate that the miR-35 and miR-58 families of miRNAs directly target *egl-1* mRNA and act cooperatively to suppress its expression (Fig. 4-1). This suppression prevents the copy number of *egl-1* mRNA, and consequently EGL-1 activity, from crossing a critical cellular threshold. Without this suppression, precocious and collateral death can occur in cell-death lineages. This was revealed by in-depth analyses of the RID lineage, using smRNA FISH to quantify *egl-1* mRNA at the single-cell level.

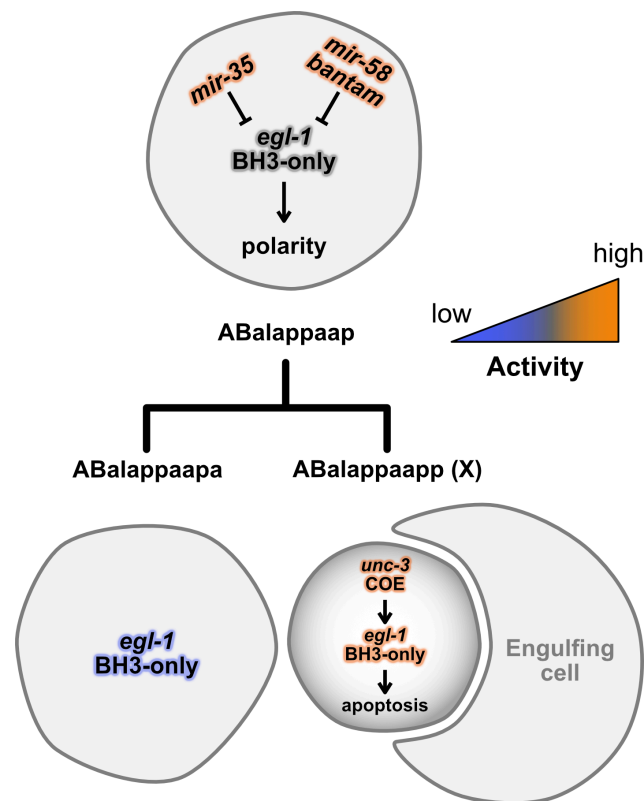


Fig. 4-1 | Genetic model of miRNA-mediated regulation of *egl-1* in the RID lineage. In the mother cell, RIDnb (ABalappaap), *egl-1* is repressed by the cooperative activity of miR-35- and miR-58-family miRNAs, thus preventing its precocious death. Following division, *egl-1* expression quickly declines in the surviving sister cell, the RID neuron (ABalappaapa), while its expression is boosted in the dying daughter, ABalappaapp, by the UNC-3/COE transcription factor. Figure adapted from Sherrard et al. (2017).

miRNA cooperativity is a phenomenon wherein the binding of two miRNAs has a synergistic (i.e. greater-than-additive) effect, resulting in amplified repression of the target (Doench et al. 2003; Broderick et al. 2011). It can occur when two miRNA-binding sites are in close proximity, and is most effective when the two sites are separated by a distance of 13–35 nt (Grimson et al. 2007; Sætrom et al. 2007). In fact, miRNA-binding sites within cooperative distance of each other are enriched in the human transcriptome, suggesting that miRNA cooperativity is an important mechanism to repress gene activity (Rinck et al. 2013). The miR-35- and miR-58-family binding sites in the *egl-1* 3'UTR are separated by 33 nt and within the permissive distance. Furthermore, I reported three lines of evidence in support of miRNA cooperativity. First, the abnormally large-cell-corpse phenotype in *mir-35*-family mutants was enhanced in *mir-35 mir-58* double-family mutants, despite an absence of the phenotype in *mir-58*-family mutants alone. Second, derepression of the $P_{mai-2gfp::h2b::egl-1}$ 3'UTR reporter was greatest when both miR-35- and miR-58-family binding sites were mutated and also more than their predicted combination, based on single-site mutations. Third, single-cell amounts of *egl-1* mRNA were significantly higher in the absence of both miRNA families, and again, more than expected based on individual-family mutants. The concept that miRNAs can regulate their targets in a cooperative manner was already considered in *C. elegans* when the 3'UTR of the TRIM-NHL gene *lin-41* was found to contain multiple targets sites for the miRNA *lin-4* (Lee et al. 1993). However, to my knowledge, the work presented in this study is the first *in vivo* demonstration of cooperative activity between two miRNA families in *C. elegans*. Given that the transcription of *egl-1* is under precise spatial and temporal control, the cooperative post-transcriptional regulation by miRNAs only emphasizes the importance of controlling EGL-1 activity during development.

4.1.2 miR-35- and miR-58-family miRNAs mediate both translational repression and degradation of *egl-1* mRNA

smRNA FISH analysis of *egl-1* in the MSpaap and RID lineages revealed that miR-35- and miR-58-family miRNAs trigger mRNA degradation, while 3'UTR assays also suggested that translational repression is mediated by miRNA activity. A common step in both of these processes is deadenylation of the mRNA which, depending on the extent of poly(A)-tail shortening, can affect translatability and stability of the mRNA (Eulalio et al. 2009; Subtelny et al. 2014; reviewed in Jonas & Izaurralde 2015). Deadenylation can be mediated by the *egl-1* 3'UTR *in vitro* (Wu et al. 2010), leading to a translationally repressed

state, after which the mRNA might be readenylated or undergo degradation. Readenylation and subsequent translation was shown to awaken so-called dormant mRNAs in mouse oocytes (Stutz et al. 1998; reviewed in Goldstrohm & Wickens 2008), and this process might also affect *egl-1* mRNA in certain lineages. One could speculate that the rapid death of cells programmed to die in *C. elegans* may be due to the readenylation and translation of *egl-1* mRNA inherited from the mother cell, which were passed down in a deadenylated, translationally repressed state. Evidence from the MSpaap lineage supports the transfer of *egl-1* mRNA from mother to daughter cells, and it would be interesting to determine if and when this mRNA is translated.

4.1.3 Lineage-specific differences in *egl-1* transcription are buffered by miRNA activity

Transcription of *egl-1* is not governed by the same factors in all cells that undergo programmed death during *C. elegans* development. Rather, cell-death lineages employ their own unique sets of *trans*-acting factors that regulate *egl-1* transcription (reviewed in Conradt et al. 2016). Therefore, the dynamics of *egl-1* upregulation in cells programmed to die can differ from lineage to lineage, and this might explain why only a subset of mother cells die precociously in *mir-35*-family and *mir-35 mir-58* double-family mutants. The likelihood of precocious death may rely on: 1) the timing and degree to which *egl-1* is upregulated in a lineage; and 2) the cooperative activity of miR-35- and miR-58-family miRNAs. In support of this notion, I found that pairs of bilaterally symmetric cells exhibited similar frequencies of inappropriate death in *mir-35*-family mutants, reflecting similar cell-death programs in these cells and a similar reliance on miRNAs to prevent inappropriate death.

The transcription factors that are responsible for upregulating *egl-1* in daughters programmed to die may have non-apoptotic roles in the mother and surviving daughter. In the RID lineage, for example, UNC-3 not only promotes *egl-1* transcription but also plays a role in neuronal terminal differentiation (Wang et al. 2015). The *egl-1* gene itself has a non-apoptotic role in the NSM lineage. In the NSM neuroblast (NSMnb), a dorsal-ventral gradient of CED-3 activity is established that ensures more apoptotic potential is inherited by the daughter programmed to die; in *egl-1(lf)* animals, this gradient is disrupted (Chakraborty et al. 2015). In such cases where *egl-1* has a non-apoptotic role, its activity must be kept below the cell-death threshold. Thus, the buffering activity of

miR-35- and miR-58-family miRNAs is likely a protective mechanism in these cells to prevent their inappropriate death (Fig. 4-2).

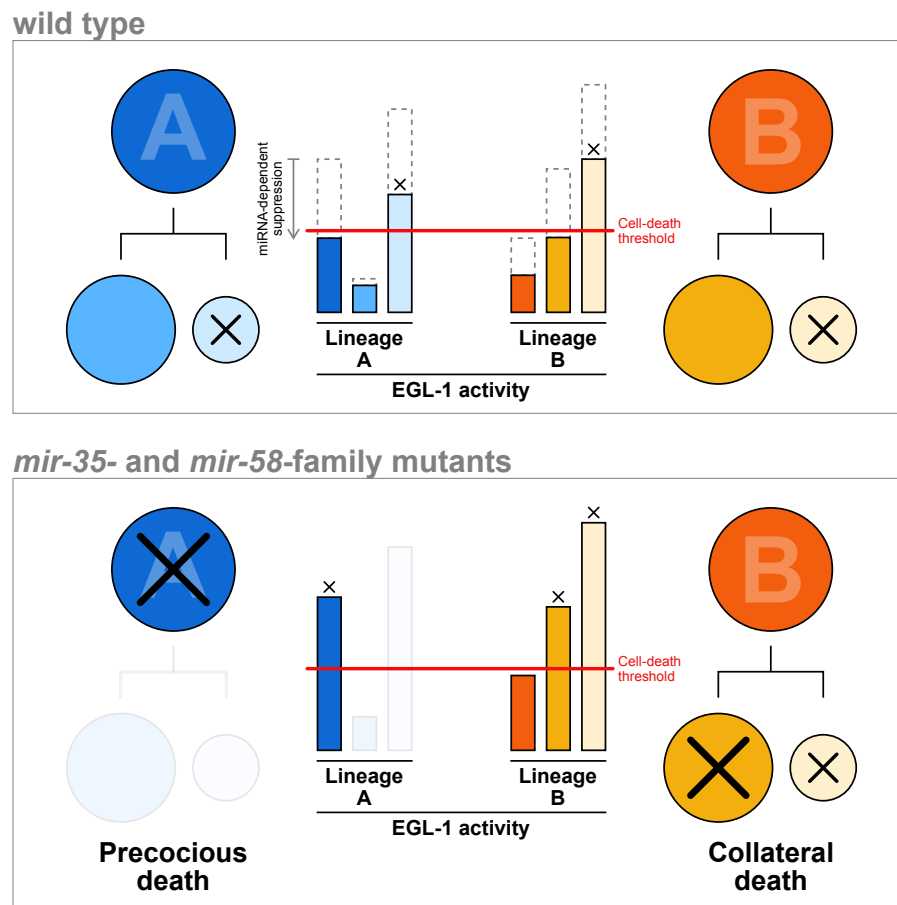


Fig. 4-2 | miRNA-mediated repression fine-tunes EGL-1 activity across cell-death lineages. Two hypothetical cell-death lineages 'A' (blue) and 'B' (orange) are illustrated. In wild-type animals (top panel), EGL-1 activity only crosses the threshold to trigger apoptosis in the daughter cell programmed to die in both lineages. In *mir-35*- and *mir-58*-family mutants (bottom panel), EGL-1 activity is derepressed and climbs above the cell-death threshold in some cells not programmed to die; specifically, in those cells where wild-type levels of EGL-1 activity were already considerable due to transcription factor activity or the need for EGL-1 activity in a non-apoptotic role. Ultimately, this derepression triggers precocious death in lineage 'A' and collateral death in lineage 'B'.

A cellular threshold of *egl-1* mRNA in the RIDnb was found to be 2–3 copies (0.05 to 0.08 copies per μm^3), above which precocious death can be triggered. The view that even a single mRNA molecule in a cell represents above-threshold expression is supported by data from metazoans (Hebenstreit et al. 2011) and fission yeast (Marguerat et al. 2012). Moreover, recent measurements in single mammalian cells showed that a single mRNA

molecule can undergo ~1000 rounds of translation (Albayrak et al. 2016). The threshold likely varies from cell to cell, as demonstrated by the finding that the MSpaap cell can withstand more than double the *egl-1* mRNA concentration of the RIDnb without succumbing to precocious death. Often, mRNA levels are not indicative of protein levels (reviewed in Liu et al. 2016), so it is possible that different cellular concentrations of *egl-1* mRNA can lead to the same protein concentration. Although I did not measure single-cell concentrations of EGL-1 protein and cell-specific thresholds for its activity, the advent of CRISPR/Cas-9 and ability to tag the endogenous *egl-1* locus would aid such a study.

4.1.4 miR-35- and miR-58-family miRNAs ensure the continuous regulation of *egl-1* during development

The partial overlap of miR-35- and miR-58-family activity during development allows for the continuous post-transcriptional regulation of common targets, such as *egl-1*. However, the relative contribution of each family might not always be equal. The phenotypic, 3'UTR-reporter and smRNA-FISH evidence presented in this study shows that miR-35-family miRNAs mediate a stronger repression of *egl-1*. This corroborates data from an *in vitro*, luciferase-based *egl-1* 3'UTR assay, where mutation of the miR-35-family binding site resulted in complete derepression of the reporter (Wu et al. 2010); the same assay only produced mild effects when the miR-58-family binding site was mutated. Considering that the miR-35 family is most abundant in early embryos, it suggests that *egl-1* repression is especially crucial during this phase of development. Presumably, the inappropriate death of early, naïve precursor cells is more detrimental to an animal's fitness than that of terminally differentiated cells in the adult stage. This may explain the need for strong, miR-35-mediated repression of *egl-1* during embryogenesis, and why a weaker miR-58-mediated repression can be tolerated at later stages of development.

I found that only a small percentage of mother cells die precociously in *mir-35*-family and *mir-35 mir-58* double-family mutants, and that precocious death is more likely to occur in later cell-death waves. Specifically, 0%, 1.8%, and 8.0% of first-, second-, and third-wave mothers, respectively, die precociously in the AB lineage. It may be that mother cells are less affected in earlier cell-death waves because other factors may be limiting at this time of development, such as CED-4 and/or CED-3 activity. Another factor might be cell size, with the relatively large cytoplasmic volume of early mother cells conferring some

resistance to fluctuating *egl-1* expression. It is also possible that EGL-1 is post-translationally inhibited in early mother cells, however this has not yet been investigated.

The overall weak penetrance of precocious cell death could mean that not all mothers rely on the cooperative repression of *egl-1* by miRNAs of the the miR-35 and miR-58 families, and that transcriptional regulation of *egl-1* is adequate for the majority of cell-death lineages. Alternatively, it could mean that there are other regulatory mechanisms controlling *egl-1* expression. The 3'UTR of *egl-1* does harbor a third conserved miRNA binding site for miR-230, which is predicted to bind as a 7mer-A1 near the 3' end of the transcript. Nevertheless, miR-230 is unlikely to regulate embryonic cell death to the extent seen with miR-35- and miR-58-family miRNAs, since both a $P_{mir-230}gfp$ transcriptional reporter and Northern blot analysis showed onset of *mir-230* expression at the L1-larval stage (Martinez et al. 2008). Supporting this, I conducted a brief analysis of *mir-230(n3545)* null mutants, and this did not reveal an obvious cell-death phenotype in embryos (data not shown). Another point of *egl-1* regulation could be the accessibility of its genomic locus to *trans*-acting factors (i.e. heterochromatic versus euchromatic states). One hypothesis is that the *egl-1* locus is in a closed heterochromatic state by default, and only becomes accessible in the mothers of cells programmed to die; however, this still remains to be determined. Finally, *egl-1* might be post-transcriptionally regulated by RBPs—I discuss this in the next section.

4.2 RBP-mediated regulation of programmed cell death

4.2.1 *puf-8* possesses a novel activity required for cell-death specification and timing

I reported a novel cell-death phenotype associated with the loss of *puf-8*. To my knowledge, this is only the second non-germline role described for *puf-8*, the other being as a regulator of vulval differentiation (Walser et al. 2006). This cell-death phenotype is not enhanced by the subsequent loss of *puf-9*, despite its potential redundancy with *puf-8*, nor is it present upon knockdown of *fbf*. Both deletion alleles of *puf-8*—*q725* and *ok302*—produced similar cell-death phenotypes, although *ok302* resulted in a significantly longer delay in the time to die for first-wave cell deaths. Both alleles are large deletions that abolish the Pum-HD, hence it is unclear why *ok302* is more severe; one possibility is that it disrupts more crucial *cis*-regulatory elements, such as those in the 3'UTR of *puf-8*.

The *puf-8(lf)* cell-death phenotype has of two contrasting defects. The first, inappropriate death, implies an overactive cell-death pathway, whereas the second, delayed corpse formation, implies an underactive pathway. Dual activity of PUF proteins is not unheard of; for example, FBF can recruit both deadenylases and poly(A) polymerases to at least one of its germline targets, *gld-1* (Suh et al. 2009). Such regulation of the cell-death pathway by *puf-8*—negative and positive regulation of a single target—could explain the two contrasting effects in *puf-8(lf)* mutants. It would suggest that the activity of *puf-8* is temporally and/or spatially dynamic, such that it prevents inappropriate death in mother cells but promotes cell death in daughters programmed to die. Alternatively, PUF-8 may target two or more cell-death genes with opposing activities, or the *puf-8(lf)* phenotype may be due to an indirect effect on the cell-death pathway. A comprehensive list of PUF-8 targets would help narrow the list of candidate genes whose misregulation could underlie the *puf-8(lf)* phenotype; however, such a study—using either RIP-Chip or iCLIP—has not yet been published.

At least two studies have found a connection between *puf-8* and germline cell death. The first found that a *ced-3* 3'UTR reporter is repressed by PUF-8 in the distal region of the germline; however, no increase in germ-cell corpses was found in *puf-8(ok302)* animals, which was attributed to other limiting factors in this region of the germline (Subasic et al. 2016). The second study found that *puf-8* facilitates the pairing of homologous chromosomes by promoting proteasome activity during meiotic entry, and the

accumulation of unpaired chromosomes in *puf-8(ok302)* animals triggered the *ced-3*-dependent death of oocytes (Kumar & Subramaniam 2018). In this study, a direct target of PUF-8 was not identified, leaving the underlying mechanism unclear. It is not known if either of these reported functions of *puf-8* extend to the soma, but the link between *puf-8* and proteasome activity could be relevant to somatic cell death. Regulation of apoptosis by the ubiquitin–proteasome system has been described in *Drosophila* and mammals, where the levels of several pro- and anti-apoptotic proteins—including caspases and BH3-only proteins—are controlled by ubiquitin-dependent degradation (reviewed in Broemer & Meier 2009). BIM, for example, is ubiquitinated under non-apoptotic conditions and subsequently degraded by the proteasome (Akiyama et al. 2003; Ley et al. 2003). Anti-apoptotic Bcl-2-family member MCL-1 is also regulated post-translationally by ubiquitination as one of the first steps in DNA damage-induced apoptosis (Zhong et al. 2005). In *C. elegans*, ubiquitination of EGL-1 has been proposed as a step in DNA damage-induced germ-cell apoptosis (Ross et al. 2011), and the ubiquitin-proteasome system is required for linker cell-type death (Kinet et al. 2016). It would therefore be interesting to see if one or both aspects of the *puf-8(lf)* cell-death phenotype are related to impaired proteasome activity.

4.2.2 PUF-8 activity prevents inappropriate death in both cell-death and non-cell-death lineages

The large cell corpses found in *puf-8* mutants belong to both cell-death and non-cell-death lineages, which differs from the phenotype observed in *mir-35*-family mutants and hints at potential targets of PUF-8 activity. Since *egl-1* expression is largely restricted to cell-death lineages and a PBE is not predicted to occur in its 3'UTR, it is unlikely that *egl-1* misregulation is the cause of ectopic death in *puf-8* mutants. On the other hand, *ced-9*, *ced-4*, and *ced-3* all exhibit broader expression patterns in the embryo (Tzur et al. 2006; Maurer et al. 2007), and all have predicted PBEs in their 3'UTRs.

A recent study found that *ced-3* is post-transcriptionally repressed by PUF-8 in the mitotic and early meiotic zones of the germline (Subasic et al. 2016); however, the authors could not identify a functional PBE in the 3'UTR. They assayed four elements, all of which were among the six I identified in this study by MEME and FIMO analysis—c3-PBE-1, -2, -3, and -5—and found that mutation of all four sites did not alter expression of a *ced-3* 3'UTR reporter. It is possible that all six PBEs operate in combination, with other *cis*-acting

elements, or in tissues and at developmental stages that were not examined. A total of five and two PBEs in the 3'UTRs of *ced-9* and *ced-4*, respectively, remain to be assayed, with c9-PBE-1 being the most attractive candidate due to its strong conservation and overlap with another element, c9-PBE-5.

4.2.3 Regulation via conserved secondary structure elements

RNA function depends on its secondary structure, and those formed by the 3'UTR are particularly crucial. Binding motifs within the 3'UTR of *egl-1*—or any other mRNA—may be accessible only under certain cellular conditions. Alternatively, the binding of RBPs to the mRNA may alter local structure elements and change the accessibility of nearby motifs, as shown previously for the mRNA of human *p27* (Kedde et al. 2010). Interestingly, a stable and conserved hairpin structure is predicted to form at the 3'-most end of *egl-1* mRNA, and elements such as this are known to be targeted by RBPs; Staufén, for example, is known to bind to the dsRNA region of hairpins. A RIP-Chip-based study of *C. elegans* STAU-1 did not identify *egl-1* mRNA as a target (LeGendre et al. 2013), however this study used young adults and may have missed embryo-specific targets. It should be tested whether this hairpin can fold under physiological conditions, and it would be interesting to analyze the 3'UTRs of *ced-9*, *ced-4*, and *ced-3* to determine if they also harbor conserved structural elements.

4.3 Complex regulation of programmed cell death by PUF proteins and miRNAs

I demonstrated that two FBEs in the 3'UTR of *egl-1* can mediate repression of a reporter *in vivo*, in agreement with two previous studies that identified *egl-1* as a target of FBF (Kershner & Kimble 2010; Prasad et al. 2016). Targeting of BH3-only genes by PUF proteins has also been described in higher animals. For example, mammalian Bim mRNA harbors five predicted binding sites in its 3'UTR for PUM1 and PUM2, and Bim was identified as a direct target of both PUM1 and PUM2 by RIP-Chip (Galgano et al. 2008). A more recent study using iCLIP found that Bim is targeted by PUM1 but not PUM2 (Zhang et al. 2017). At least three other mammalian BH3-only genes are potential targets of PUF proteins, with three predicted binding sites in the 3'UTR of Hrk and one in each of Bmf and Puma.

I also found that knockdown of *fbf* by RNAi partially suppresses the formation of large cell corpses in *mir-35*-family mutants. It would be interesting to see if knockdown of *fbf* in *mir-35 mir-58* double-family mutants also suppresses the large-cell-corpse phenotype in these animals. If so, then this would strengthen the argument that *fbf*, like *puf-8*, acts as both a suppressor and activator of the cell-death pathway. The prevailing activity of FBF could be regulated in a spatiotemporal manner, dependent on cell lineage, developmental stage, and other cofactors. Alternatively, suppression of the large-cell-corpse phenotype in *mir-35*-family mutants might be an indirect effect of *fbf* knockdown. More than 1400 RNAs are germline targets of FBF, with many involved in cell-cycle regulation (Prasad et al. 2016). FBF also targets *puf-8* and other RNA-binding proteins; notably, *ced-4* and *ced-3* are also targets (Prasad et al. 2016). The regulation of caspases by PUF proteins may extend to mammals, since caspase-3 has a PBE in its 3'UTR and was experimentally shown to be targeted by PUM1 and PUM2 (Galgano et al. 2008).

The post-transcriptional regulation of cell-death genes by miRNAs and PUF proteins is likely complex, and mounting evidence shows that these two mechanisms may cooperate. This could be the case with *egl-1* and its regulation by *fbf* and the *mir-35* and *mir-58* families. The somatic expression pattern of *fbf* has not been investigated in depth, but both *fbf-1* and *fbf-2* transcripts have been detected in the AB lineage of embryos (Hashimshony et al. 2015). Cooperative regulation might also affect *ced-9* and *ced-3*, as both have predicted miRNA binding sites, PBEs, and FBE in their 3'UTRs. Together,

DISCUSSION

these layers of post-transcriptional regulation could further fine-tune activity of the cell-death pathway, preserving the invariant pattern of cell death during *C. elegans* development.

4.4 Conclusion and future perspectives

4.4.1 Summary and open questions

Here, my colleagues S. Lühr, N. Memar and I show that *egl-1* is post-transcriptionally repressed by miRNAs of the miR-35 and miR-58 families during *C. elegans* embryogenesis, as that the activity of these two miRNA families is cooperative (Fig. 4-3A). The overlapping expression patterns of *mir-35*- and *mir-58*-family genes allow for the continuous regulation of *egl-1*, thereby preventing precocious and collateral death in cell-death lineages. Furthermore, my colleague K. Ikegami and I demonstrate that *puf-8* activity is also needed to prevent inappropriate death during embryogenesis, while also being required for the proper timing of apoptosis in cells programmed to die (Fig. 4-3B). I also presented evidence for a genetic interaction between *fbf* and the *mir-35* family in the regulation of cell death, and identified the *egl-1* 3'UTR as a target of FBF.

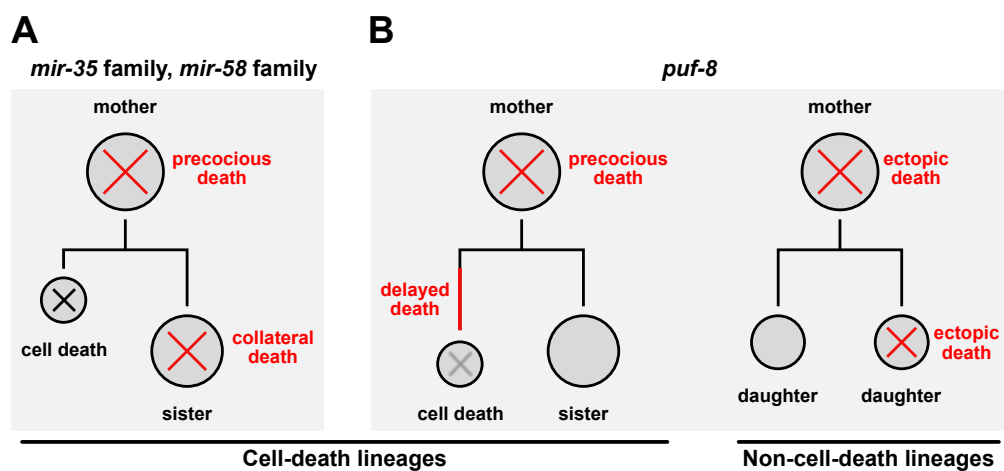


Fig. 4-3 | Cell-death phenotypes associated with post-transcriptional regulation of the apoptotic pathway. (A) Loss of the *mir-35* family affects cell death lineages, leading to precocious and collateral death. This is enhanced by loss of the *mir-58* family. **(B)** Loss of *puf-8* affects cell-death lineages, leading to precocious death and a delay in the death of first-wave cell deaths, but it also affects non-cell-death lineages, leading to ectopic death.

Several questions still remain to be answered. Among them, do other miRNAs and RBPs regulate the cell-death pathway, and to what extent? Currently, there are methods to isolate and identify *trans*-acting factors of a specific mRNA species—I discuss these in the next section. What target(s) of PUF-8 connects it to programmed cell death, and what is the mechanism of regulation? The identification of PUF-8 targets via iCLIP and/or RIP-Chip would provide candidates in this regard. Finally, what is the nature of *fbf*-mediated

regulation of cell death, and is there a direct interaction with the miRNA silencing pathway? It could be that *fbf* activity is directly responsible for its perceived dual regulation of the cell-death pathway—via targets such as *egl-1*, *ced-4*, and *ced-3*—but it could also occur indirectly via other FBF targets. Future genetic studies should provide the answer, and the precise mutation of candidate FBEs using CRISPR/Cas-9 should pinpoint the target gene(s) and binding element(s) that ties *fbf* activity to cell death.

4.4.2 Emerging fields of post-transcriptional gene regulation

New mechanisms of post-transcriptional regulation continue to be discovered. In particular, investigations into the chemical modification of RNA bases have given rise to the term “epitranscriptome”, which describes the biochemical features of a collective mRNA pool. These features include *N*⁶-methyladenosine (m⁶A), *N*¹-methyladenosine (m¹A), 5-methylcytosine (m⁵C), 2'-O-methylation (2'OMe), and pseudouridine (reviewed in Zhao et al. 2017). m⁶A is the most abundant internal mRNA modification in eukaryotes and, importantly, it can be reversed by demethylases (Jia et al. 2011). Moreover, mRNA modifications can impact the binding of RBPs. For example, pseudouridine and *N*⁶-methyladenosine modifications can weaken the interaction between PUF proteins and their target mRNAs (Vaidyanathan et al. 2017). m⁶A-specific binding proteins also exist and can affect mRNA splicing, stability, translation (Wang et al. 2014, 2015; Xiao et al. 2016).

Another emerging area in post-transcriptional regulation describes competitive endogenous RNAs (ceRNAs) as antagonists of miRNA function (Salmena et al. 2011). These ceRNAs are often non-coding and described as “miRNA sponges”, effectively sequestering the activity of miRNAs to prevent them from targeting coding mRNA, and they come in several forms (reviewed in Thomson & Dinger 2016). The first, long non-coding RNAs (lncRNAs), are defined as transcripts that are over 200 nucleotides in length with low-to-zero protein-coding potential. The second, pseudogenes, resemble functional genes in their structure, but have lost the ability to be properly transcribed or code for a functional protein. The third, circular RNAs (circRNAs), are formed by the covalent head-to-tail linkage of spliced introns or exons. As they lack free ends, circRNAs are resistant to exonuclease-mediated degradation and are generally more stable than linear RNAs *in vivo* (Jeck et al. 2013; Enuka et al. 2016).

Finally, guanylation of the poly(A) tail is a recently discovered phenomenon, whereby non-canonical poly(A) polymerases generate a poly(A) tail with intermittent guanosine residues that impede deadenylation (Lim et al. 2018). This prolongs mRNA half-life *in vivo*, and invites further investigation into poly(A) tail composition as a mechanism of post-transcriptional regulation.

4.4.3 Purification of transcript-specific mRNP complexes

There are established methods to identify the targets of a specific RBP (e.g. iCLIP and RIP-Chip), but the inverse is also possible—to identify the factors associated with a single mRNA population. In these approaches, UV- or chemically induced crosslinking is used to trap native mRNP complexes *in vivo*, then a specific population is purified and the associated proteins or miRNAs are identified by downstream methods.

One approach uses a biotinylated antisense capture oligonucleotide specific to the mRNA of interest and purification using streptavidin beads to identify bound miRNAs (Hassan et al. 2013). A similar method, termed comprehensive identification of RNA binding proteins by mass spectrometry (ChIRP-MS), can be used to identify RBPs (Chu et al. 2015). mRNP complexes can also be pulled down by hybridization with a bead-coupled antisense locked nucleic acid (LNA) oligonucleotide—a high-affinity RNA analog with increased affinity for its complement (Rogell et al. 2017). Finally, rather than capturing the mRNA of interest using oligonucleotides, one can express a variant of the mRNA tagged with MS2-binding stem-loops. This method, termed MS2-Tagged RNA affinity purification (MS2-TRAP), captures the mRNA and its associated factors via coexpression and affinity purification of a GST-tagged MS2 protein, and it can be used to identify associated miRNAs and proteins (Yoon et al. 2012, 2016).

These methods could be used to find miRNAs and RBPs that directly regulate genes of the central cell-death pathway in *C. elegans*. Not only would these approaches identify novel regulators, but they could also verify known interactors such as miRNAs of the miR-35 and miR-58 families.

4.4.4 Medical implications of cell-death regulation

The discovery of homologous cell-death genes in mammals and *C. elegans* showed that the underlying mechanisms of programmed cell death are evolutionarily conserved, and that investigations carried out in the small nematode could have direct implications for human health and disease. Already, basic research in the cell-death field has led to the development of promising cancer drugs. Since the BCL-2 family has an essential role in apoptosis and cancer cell survival, the past decade has seen the development of drugs whose structure mimics that of the pro-apoptotic BH3 domain as a way to induce apoptosis in cancer cells. Recent clinical trials of the BH3 mimetic venetoclax/ABT-199, which inhibits BCL-2, have led to its approval by the U.S. Food and Drug Administration for patients with chronic lymphocytic leukemia or small lymphocytic lymphoma, and further applications are being explored (Souers et al. 2013; Green 2016). In the meantime, drug development continues to target BCL-2 family members with promising results (reviewed in Ashkenazi et al. 2017).

It is an exciting era when knowledge of the pathways that control programmed cell death is used for the development of successful disease treatments. However, pharmacological manipulation of programmed cell death will be limited until we have a clear understanding of the regulatory network that controls apoptosis. Knowledge gained directly from studies in model organisms, such as *C. elegans*, will continue to be the source of remarkable discoveries on this front. This study now places two miRNA families and PUF RBPs in that regulatory network, and we can anticipate that further studies will provide the medical community with novel drug targets in the fight against diseases linked to defects in cell death.

REFERENCES

REFERENCES

- Abraham MC, Lu Y & Shaham S (2007). A morphologically conserved nonapoptotic program promotes linker cell death in *Caenorhabditis elegans*. *Dev Cell* 12, 73–86.
- Adlakha YK & Saini N (2011). MicroRNA-128 downregulates Bax and induces apoptosis in human embryonic kidney cells. *Cell Mol Life Sci* 68, 1415–1428.
- Agarwal V, Bell GW, Nam J-W & Bartel DP (2015). Predicting effective microRNA target sites in mammalian mRNAs. *eLife* 4, 101.
- Akiyama T, Bouillet P, Miyazaki T, Kadono Y, Chikuda H, Chung U-I, Fukuda A, Hikita A, Seto H, Okada T, Inaba T, Sanjay A, Baron R, Kawaguchi H, Oda H, Nakamura K, Strasser A & Tanaka S (2003). Regulation of osteoclast apoptosis by ubiquitylation of proapoptotic BH3-only Bcl-2 family member Bim. *EMBO J* 22, 6653–6664.
- Albayrak C, Jordi CA, Zechner C, Lin J, Bichsel CA, Khammash M & Tay S (2016). Digital quantification of proteins and mRNA in single mammalian cells. *Mol Cell* 61, 914–924.
- Alberti C & Cochella L (2017). A framework for understanding the roles of miRNAs in animal development. *Development* 144, 2548–2559.
- Alvarez-Saavedra E & Horvitz HR (2010). Many families of *C. elegans* microRNAs are not essential for development or viability. *Curr Biol* 20, 367–373.
- Ambros V (2004). The functions of animal microRNAs. *Nature* 431, 350–355.
- Ambros V & Ruvkun G (2018). Recent molecular genetic explorations of *Caenorhabditis elegans* microRNAs. *Genetics* 209, 651–673.
- Archer SK, Luu V-D, de Queiroz RA, Brems S & Clayton C (2009). *Trypanosoma brucei* PUF9 regulates mRNAs for proteins involved in replicative processes over the cell cycle. *PLoS Pathog* 5, e1000565.
- Ariz M, Mainpal R & Subramaniam K (2009). *C. elegans* RNA-binding proteins PUF-8 and MEX-3 function redundantly to promote germline stem cell mitosis. *Dev Biol* 326, 295–304.

- Ashkenazi A, Fairbrother WJ, Levenson JD & Souers AJ (2017). From basic apoptosis discoveries to advanced selective BCL-2 family inhibitors. *Nat Rev Drug Discov* 16, 273–284.
- Bachorik JL & Kimble J (2005). Redundant control of the *Caenorhabditis elegans* sperm/oocyte switch by PUF-8 and FBF-1, two distinct PUF RNA-binding proteins. *Proc Natl Acad Sci USA* 102, 10893–10897.
- Bae J, Leo CP, Hsu SY & Hsueh AJ (2000). MCL-1S, a splicing variant of the antiapoptotic BCL-2 family member MCL-1, encodes a proapoptotic protein possessing only the BH3 domain. *J Biol Chem* 275, 25255–25261.
- Bagga S, Bracht J, Hunter S, Massirer K, Holtz J, Eachus R & Pasquinelli AE (2005). Regulation by *let-7* and *lin-4* miRNAs results in target mRNA degradation. *Cell* 122, 553–563.
- Bailey TL, Boden M, Buske FA, Frith M, Grant CE, Clementi L, Ren J, Li WW & Noble WS (2009). MEME SUITE: tools for motif discovery and searching. *Nucleic Acids Res* 37, W202–W208.
- Bartel DP (2009). MicroRNAs: target recognition and regulatory functions. *Cell* 136, 215–233.
- Bazzini AA, Lee MT & Giraldez AJ (2012). Ribosome profiling shows that miR-430 reduces translation before causing mRNA decay in zebrafish. *Science* 336, 233–237.
- Behm-Ansmant I, Rehwinkel J, Doerks T, Stark A, Bork P & Izaurralde E (2006). mRNA degradation by miRNAs and GW182 requires both CCR4:NOT deadenylase and DCP1:DCP2 decapping complexes. *Genes Dev* 20, 1885–1898.
- Bernstein E, Caudy AA, Hammond SM & Hannon GJ (2001). Role for a bidentate ribonuclease in the initiation step of RNA interference. *Nature* 409, 363–366.
- Bevilacqua PC, Ritchey LE, Su Z & Assmann SM (2016). Genome-wide analysis of RNA secondary structure. *Annu Rev Genet* 50, 235–266.

REFERENCES

- Bhattacharyya SN, Habermacher R, Martine U, Closs EI & Filipowicz W (2006). Relief of microRNA-mediated translational repression in human cells subjected to stress. *Cell* 125, 1111–1124.
- Blum ES, Abraham MC, Yoshimura S, Lu Y & Shaham S (2012). Control of nonapoptotic developmental cell death in *Caenorhabditis elegans* by a polyglutamine-repeat protein. *Science* 335, 970–973.
- Boise LH, González-García M, Postema CE, Ding L, Lindsten T, Turka LA, Mao X, Núñez G & Thompson CB (1993). *bcl-x*, a *bcl-2*-related gene that functions as a dominant regulator of apoptotic cell death. *Cell* 74, 597–608.
- Brancati G & Großhans H (2018). An interplay of miRNA abundance and target site architecture determines miRNA activity and specificity. *Nucleic Acids Res* 46, 3259–3269.
- Brennecke J, Hipfner DR, Stark A, Russell RB & Cohen SM (2003). *bantam* encodes a developmentally regulated microRNA that controls cell proliferation and regulates the proapoptotic gene *hid* in *Drosophila*. *Cell* 113, 25–36.
- Brenner S (1974). The genetics of *Caenorhabditis elegans*. *Genetics* 77, 71–94.
- Broderick JA, Salomon WE, Ryder SP, Aronin N & Zamore PD (2011). Argonaute protein identity and pairing geometry determine cooperativity in mammalian RNA silencing. *RNA* 17, 1858–1869.
- Broemer M & Meier P (2009). Ubiquitin-mediated regulation of apoptosis. *Trends Cell Biol* 19, 130–140.
- Brümmer A, Kishore S, Subasic D, Hengartner M & Zavolan M (2013). Modeling the binding specificity of the RNA-binding protein GLD-1 suggests a function of coding region-located sites in translational repression. *RNA* 19, 1317–1326.
- C. elegans* Deletion Mutant Consortium (2012). Large-scale screening for targeted knockouts in the *Caenorhabditis elegans* genome. *G3 (Bethesda)* 2, 1415–1425.
- Carmody SR & Wenthe SR (2009). mRNA nuclear export at a glance. *J Cell Sci* 122, 1933–1937.

- Chakraborty S, Lambie EJ, Bindu S, Mikeladze-Dvali T & Conradt B (2015). Engulfment pathways promote programmed cell death by enhancing the unequal segregation of apoptotic potential. *Nat Commun* 6, 10126.
- Chapat C, Jafarnejad SM, Matta-Camacho E, Hesketh GG, Gelbart IA, Attig J, Gkogkas CG, Alain T, Stern-Ginossar N, Fabian MR, Gingras A-C, Duchaine TF & Sonenberg N (2017). Cap-binding protein 4EHP effects translation silencing by microRNAs. *Proc Natl Acad Sci USA* 13, 201701488–6.
- Chen F, Hersh BM, Conradt B, Zhou Z, Riemer D, Gruenbaum Y & Horvitz HR (2000). Translocation of *C. elegans* CED-4 to nuclear membranes during programmed cell death. *Science* 287, 1485–1489.
- Cimmino A, Calin GA, Fabbri M, Iorio MV, Ferracin M, Shimizu M, Wojcik SE, Aqeilan RI, Zupo S, Dono M, Rassenti L, Alder H, Volinia S, Liu C-G, Kipps TJ, Negrini M & Croce CM (2005). miR-15 and miR-16 induce apoptosis by targeting BCL2. *Proc Natl Acad Sci USA* 102, 13944–13949.
- Clybourn C, Merino D, Nebl T, Masson F, Robati M, O'Reilly L, Hübner A, Davis RJ, Strasser A & Bouillet P (2012). Alternative splicing of Bim and Erk-mediated Bim(EL) phosphorylation are dispensable for hematopoietic homeostasis in vivo. *Cell Death Differ* 19, 1060–1068.
- Conradt B & Horvitz HR (1998). The *C. elegans* protein EGL-1 is required for programmed cell death and interacts with the Bcl-2-like protein CED-9. *Cell* 93: 519–529.
- Conradt B & Horvitz HR (1999). The TRA-1A sex determination protein of *C. elegans* regulates sexually dimorphic cell deaths by repressing the *egl-1* cell death activator gene. *Cell* 98, 317–327.
- Conradt B (2009). Genetic control of programmed cell death during animal development. *Annu Rev Genet* 43, 493–523.
- Conradt B, Wu Y-C & Xue D (2016). Programmed cell death during *Caenorhabditis elegans* development. *Genetics* 203, 1533–1562.
- Crittenden SL, Bernstein DS, Bachorik JL, Thompson BE, Gallegos M, Petcherski AG, Moulder G, Barstead R, Wickens M & Kimble J (2002). A conserved RNA-binding protein controls germline stem cells in *Caenorhabditis elegans*. *Nature* 417, 660–663.

REFERENCES

- Cui J & Placzek WJ (2018). Post-transcriptional regulation of anti-apoptotic BCL2 family members. *Int J Mol Sci* 19, e308.
- Dekkers MPJ, Nikolettou V & Barde Y-A (2013). Cell biology in neuroscience: death of developing neurons: new insights and implications for connectivity. *J Cell Bio* 203, 385–393.
- del Peso L, González VM & Núñez G (1998). *Caenorhabditis elegans* EGL-1 disrupts the interaction of CED-9 with CED-4 and promotes CED-3 activation. *J Biol Chem* 273, 33495–33500.
- del Peso L, González VM, Inohara N, Ellis RE & Núñez G (2000). Disruption of the CED-9.CED-4 complex by EGL-1 is a critical step for programmed cell death in *Caenorhabditis elegans*. *J Biol Chem* 275, 27205–27211.
- Delbridge ARD, Grabow S, Strasser A & Vaux DL (2016). Thirty years of BCL-2: translating cell death discoveries into novel cancer therapies. *Nat Rev Cancer* 16, 99–109.
- Deng Y, Singer RH & Gu W (2008). Translation of ASH1 mRNA is repressed by Puf6p-Fun12p/eIF5B interaction and released by CK2 phosphorylation. *Genes Dev* 22, 1037–1050.
- Desai C, Garriga G, McIntire SL & Horvitz HR (1988). A genetic pathway for the development of the *Caenorhabditis elegans* HSN motor neurons. *Nature* 336, 638–646.
- Dijkers PF, Medema RH, Lammers JW, Koenderman L & Coffey PJ (2000). Expression of the pro-apoptotic Bcl-2 family member Bim is regulated by the forkhead transcription factor FKHR-L1. *Curr Biol* 10, 1201–1204.
- Djuranovic S, Nahvi A & Green R (2012). miRNA-mediated gene silencing by translational repression followed by mRNA deadenylation and decay. *Science* 336, 237–240.
- Doench JG, Petersen CP & Sharp PA (2003). siRNAs can function as miRNAs. *Genes Dev* 17, 438–442.

- Dominguez D, Freese P, Alexis MS, Su A, Hochman M, Palden T, Bazile C, Lambert NJ, Van Nostrand EL, Pratt GA, Yeo GW, Graveley BR & Burge CB (2018). Sequence, structure, and context preferences of human RNA binding proteins. *Mol Cell* 70, 854–867.e859.
- Eckmann CR, Crittenden SL, Suh N & Kimble J (2004). GLD-3 and control of the mitosis/meiosis decision in the germline of *Caenorhabditis elegans*. *Genetics* 168, 147–160.
- Edgley ML & Riddle DL (2001). LG II balancer chromosomes in *Caenorhabditis elegans*: *mT1(II;III)* and the *mIn1* set of dominantly and recessively marked inversions. *Mol Genet Genomics* 266, 385–395.
- Eichhorn SW, Guo H, McGearry SE, Rodriguez-Mias RA, Shin C, Baek D, Hsu S-H, Ghoshal K, Villén J & Bartel DP (2014). mRNA destabilization is the dominant effect of mammalian microRNAs by the time substantial repression ensues. *Mol Cell* 56, 104–115.
- Ellis HM & Horvitz HR. (1986). Genetic control of programmed cell death in the nematode *C. elegans*. *Cell* 44: 817–829.
- Enuka Y, Lauriola M, Feldman ME, Sas-Chen A, Ulitsky I & Yarden Y (2016). Circular RNAs are long-lived and display only minimal early alterations in response to a growth factor. *Nucleic Acids Res* 44, 1370–1383.
- Eulalio A, Huntzinger E, Nishihara T, Rehwinkel J, Fauser M & Izaurralde E (2009). Deadenylation is a widespread effect of miRNA regulation. *RNA* 15, 21–32.
- Fire A, Xu S, Montgomery MK, Kostas SA, Driver SE & Mello CC (1998). Potent and specific genetic interference by double-stranded RNA in *Caenorhabditis elegans*. *Nature* 391, 806–811.
- Frank CA, Hawkins NC, Guenther C, Horvitz HR & Garriga G (2005). *C. elegans* HAM-1 positions the cleavage plane and regulates apoptosis in asymmetric neuroblast divisions. *Dev Biol* 284, 301–310.
- Friedländer MR, Chen W, Adamidi C, Maaskola J, Einspanier R, Knespel S & Rajewsky N (2008). Discovering microRNAs from deep sequencing data using miRDeep. *Nature Biotechnol* 26, 407–415.

REFERENCES

- Friend K, Campbell ZT, Cooke A, Kroll-Conner P, Wickens MP & Kimble J (2012). A conserved PUF-Ago-eEF1A complex attenuates translation elongation. *Nat Struct Mol Biol* 19, 176–183.
- Frøkjær-Jensen C, Davis MW, Hopkins CE, Newman BJ, Thummel JM, Olesen S-P, Grunnet M, Jorgensen EM. (2008). Single-copy insertion of transgenes in *Caenorhabditis elegans*. *Nat Genet* 40: 1375–1383.
- Frøkjær-Jensen C, Davis MW, Ailion M. (2012). Improved *Mos1*-mediated transgenesis in *C. elegans*. *Nat Meth* 9: 117–118.
- Frøkjær-Jensen C, Davis MW, Sarov M, Taylor J, Flibotte S, LaBella M, Pozniakovsky A, Moerman DG & Jorgensen EM (2014). Random and targeted transgene insertion in *Caenorhabditis elegans* using a modified *Mos1* transposon. *Nat Meth* 11, 529–534.
- Fuchs Y & Steller H (2011). Programmed cell death in animal development and disease. *Cell* 147, 742–758.
- Fuchs Y & Steller H (2015). Live to die another way: modes of programmed cell death and the signals emanating from dying cells. *Nat Rev Mol Cell Biol* 16, 329–344.
- Galgano A, Forrer M, Jaskiewicz L, Kanitz A, Zavolan M & Gerber AP (2008). Comparative analysis of mRNA targets for human PUF-family proteins suggests extensive interaction with the miRNA regulatory system. *PLoS ONE* 3, e3164.
- Galindo KA, Lu W-J, Park JH & Abrams JM (2009). The Bax/Bak ortholog in *Drosophila*, Debcl, exerts limited control over programmed cell death. *Development* 136, 275–283.
- Ge W, Chen Y-W, Weng R, Lim SF, Buescher M, Zhang R & Cohen SM (2012). Overlapping functions of microRNAs in control of apoptosis during *Drosophila* embryogenesis. *Cell Death Differ* 19, 839–846.
- Gerber AP, Herschlag D & Brown PO (2004). Extensive association of functionally and cytologically related mRNAs with Puf family RNA-binding proteins in yeast. *Plos Biol* 2, E79.

- Gerber AP, Luschnig S, Krasnow MA, Brown PO & Herschlag D (2006). Genome-wide identification of mRNAs associated with the translational regulator PUMILIO in *Drosophila melanogaster*. *Proc Natl Acad Sci USA* 103, 4487–4492.
- Gibson DG, Young L, Chuang R-Y, Venter JC, Hutchison CA & Smith HO (2009). Enzymatic assembly of DNA molecules up to several hundred kilobases. *Nat Meth* 6, 343–345.
- Giraldez AJ, Mishima Y, Rihel J, Grocock RJ, Van Dongen S, Inoue K, Enright AJ & Schier AF (2006). Zebrafish MiR-430 promotes deadenylation and clearance of maternal mRNAs. *Science* 312, 75–79.
- Glisovic T, Bachorik JL, Yong J & Dreyfuss G (2008). RNA-binding proteins and post-transcriptional gene regulation. *FEBS Lett* 582, 1977–1986.
- Goldstrohm AC, Seay DJ, Hook BA & Wickens M (2007). PUF protein-mediated deadenylation is catalyzed by Ccr4p. *J Biol Chem* 282, 109–114.
- Goldstrohm AC & Wickens M (2008). Multifunctional deadenylase complexes diversify mRNA control. *Nat Rev Mol Cell Biol* 9, 337–344.
- Gong J, Zhang J-P, Li B, Zeng C, You K, Chen M-X, Yuan Y & Zhuang S-M (2013). MicroRNA-125b promotes apoptosis by regulating the expression of Mcl-1, Bcl-w and IL-6R. *Oncogene* 32, 3071–3079.
- Green DR (2016). A BH3 mimetic for killing cancer cells. *Cell* 165, 1560.
- Grether ME, Abrams JM, Agapite J, White K, Steller H. (1995). The head involution defective gene of *Drosophila melanogaster* functions in programmed cell death. *Genes Dev* 9, 1694–1708.
- Grimson A, Farh KK-H, Johnston WK, Garrett-Engle P, Lim LP & Bartel DP (2007). MicroRNA targeting specificity in mammals: determinants beyond seed pairing. *Mol Cell* 27, 91–105.
- Grosswendt S, Filipchuk A, Manzano M, Klironomos F, Schilling M, Herzog M, Gottwein E & Rajewsky N (2014). Unambiguous identification of miRNA:target site interactions by different types of ligation reactions. *Mol Cell* 54, 1042–1054.

REFERENCES

- Gumienny TL, Lambie E, Hartweg E, Horvitz HR & Hengartner MO (1999). Genetic control of programmed cell death in the *Caenorhabditis elegans* hermaphrodite germline. *Development* 126, 1011–1022.
- Guo H, Ingolia NT, Weissman JS & Bartel DP (2010). Mammalian microRNAs predominantly act to decrease target mRNA levels. *Nature* 466, 835–840.
- Hamada S, Masamune A, Miura S, Satoh K & Shimosegawa T (2014). MiR-365 induces gemcitabine resistance in pancreatic cancer cells by targeting the adaptor protein SHC1 and pro-apoptotic regulator BAX. *Cell Signal* 26, 179–185.
- Happo L, Strasser A & Cory S (2012). BH3-only proteins in apoptosis at a glance. *J Cell Sci* 125, 1081–1087.
- Harvey R, Dezi V, Pizzinga M & Willis AE (2017). Post-transcriptional control of gene expression following stress: the role of RNA-binding proteins. *Biochem Soc Trans* 45, 1007–1014.
- Hashimshony T, Feder M, Levin M, Hall BK & Yanai I (2015). Spatiotemporal transcriptomics reveals the evolutionary history of the endoderm germ layer. *Nature* 519, 219–222.
- Hassan T, Smith SGJ, Gaughan K, Oglesby IK, O'Neill S, McElvaney NG & Greene CM (2013). Isolation and identification of cell-specific microRNAs targeting a messenger RNA using a biotinylated anti-sense oligonucleotide capture affinity technique. *Nucleic Acids Research* 41, e71.
- Hebenstreit D, Fang M, Gu M, Charoensawan V, van Oudenaarden A & Teichmann SA (2011). RNA sequencing reveals two major classes of gene expression levels in metazoan cells. *Mol Syst Biol* 7, 497–497.
- Hengartner MO, Ellis RE & Horvitz HR (1992). *Caenorhabditis elegans* gene *ced-9* protects cells from programmed cell death. *Nature* 356, 494–499.
- Hengartner MO & Horvitz HR (1994). *C. elegans* cell survival gene *ced-9* encodes a functional homolog of the mammalian proto-oncogene *bcl-2*. *Cell* 76, 665–676.
- Hershko T & Ginsberg D (2004). Up-regulation of Bcl-2 homology 3 (BH3)-only proteins by E2F1 mediates apoptosis. *J Biol Chem* 279, 8627–8634.

- Hipfner DR, Weigmann K & Cohen SM (2002). The *bantam* gene regulates *Drosophila* growth. *Genetics* 161, 1527–1537.
- Hirose T, Galvin BD & Horvitz HR (2010). Six and Eya promote apoptosis through direct transcriptional activation of the proapoptotic BH3-only gene *egl-1* in *Caenorhabditis elegans*. *Proc Natl Acad Sci USA* 107, 15479–15484.
- Hirose T & Horvitz HR (2013). An Sp1 transcription factor coordinates caspase-dependent and -independent apoptotic pathways. *Nature* 500, 354–358.
- Horvitz HR (2003). Worms, life, and death (Nobel lecture). *Chembiochem* 4, 697–711.
- Huang W, Jiang T, Choi W, Qi S, Pang Y, Hu Q, Xu Y, Gong X, Jeffrey PD, Wang J & Shi Y (2013). Mechanistic insights into CED-4-mediated activation of CED-3. *Genes Dev* 27, 2039–2048.
- Huppertz I, Attig J, D’Ambrogio A, Easton LE, Sibley CR, Sugimoto Y, Tajnik M, König J & Ule J (2014). iCLIP: protein-RNA interactions at nucleotide resolution. *Methods* 65, 274–287.
- Ichikawa N, Ando C, Fumino M. (2006). *Caenorhabditis elegans* MAI-1 protein, which is similar to mitochondrial ATPase inhibitor (IF1), can inhibit yeast F0F1-ATPase but cannot be transported to yeast mitochondria. *J Bioenerg Biomembr* 38: 93–99.
- Isik M, Korswagen HC & Berezikov E (2010). Expression patterns of intronic microRNAs in *Caenorhabditis elegans*. *Silence* 1, 5.
- Iwakawa H-O & Tomari Y (2015). The functions of microRNAs: mRNA decay and translational repression. *Trends Cell Biol* 25, 651–665.
- Jan CH, Friedman RC, Ruby JG & Bartel DP (2011). Formation, regulation and evolution of *Caenorhabditis elegans* 3’UTRs. *Nature* 469, 97–101.
- Jankowsky E & Harris ME (2015). Specificity and nonspecificity in RNA-protein interactions. *Nat Rev Mol Cell Biol* 16, 533–544.
- Jeck WR, Sorrentino JA, Wang K, Slevin MK, Burd CE, Liu J, Marzluff WF & Sharpless NE (2013). Circular RNAs are abundant, conserved, and associated with ALU repeats. *RNA* 19, 141–157.

REFERENCES

- Jia G, Fu Y, Zhao X, Dai Q, Zheng G, Yang Y, Yi C, Lindahl T, Pan T, Yang Y-G & He C (2011). N6-methyladenosine in nuclear RNA is a major substrate of the obesity-associated FTO. *Nat Chem Biol* 7, 885–887.
- Jiang H-S & Wu Y-C (2014). LIN-3/EGF promotes the programmed cell death of specific cells in *Caenorhabditis elegans* by transcriptional activation of the pro-apoptotic gene *egl-1*. *PLoS Genet* 10, e1004513.
- Jonas S & Izaurralde E (2015). Towards a molecular understanding of microRNA-mediated gene silencing. *Nat Rev Genet* 16, 421–433.
- Kadyrova LY, Habara Y, Lee TH & Wharton RP (2007). Translational control of maternal Cyclin B mRNA by Nanos in the *Drosophila* germline. *Development* 134, 1519–1527.
- Kagias K & Pocock R (2015). microRNA regulation of the embryonic hypoxic response in *Caenorhabditis elegans*. *Sci Rep* 5, 11284.
- Kamath RS, Fraser AG, Dong Y, Poulin G, Durbin R, Gotta M, Kanapin A, Le Bot N, Moreno S, Sohrmann M, Welchman DP, Zipperlen P & Ahringer J (2003). Systematic functional analysis of the *Caenorhabditis elegans* genome using RNAi. *Nature* 421, 231–237.
- Kastenhuber ER & Lowe SW (2017). Putting p53 in context. *Cell* 170, 1062–1078.
- Kato M, de Lencastre A, Pincus Z & Slack FJ (2009). Dynamic expression of small non-coding RNAs, including novel microRNAs and piRNAs/21U-RNAs, during *Caenorhabditis elegans* development. *Genome Biol* 10, R54.
- Kaye JA, Rose NC, Goldsworthy B, Goga A & L'Etoile ND (2009). A 3'UTR pumilio-binding element directs translational activation in olfactory sensory neurons. *Neuron* 61, 57–70.
- Kedde M, Strasser MJ, Boldajipour B, Oude Vrielink JAF, Slanchev K, le Sage C, Nagel R, Voorhoeve PM, van Duijse J, Ørom UA, Lund AH, Perrakis A, Raz E & Agami R (2007). RNA-binding protein Dnd1 inhibits microRNA access to target mRNA. *Cell* 131, 1273–1286.

- Kedde M, van Kouwenhove M, Zwart W, Oude Vrielink JAF, Elkon R & Agami R (2010). A Pumilio-induced RNA structure switch in p27-3' UTR controls miR-221 and miR-222 accessibility. *Nat Cell Biol* 12, 1014–1020.
- Keene JD, Komisarow JM & Friedersdorf MB (2006). RIP-Chip: the isolation and identification of mRNAs, microRNAs and protein components of ribonucleoprotein complexes from cell extracts. *Nat Protoc* 1, 302–307.
- Kerr JF, Wyllie AH & Currie AR (1972). Apoptosis: a basic biological phenomenon with wide-ranging implications in tissue kinetics. *Br J Cancer* 26, 239–257.
- Kershner AM & Kimble J (2010). Genome-wide analysis of mRNA targets for *Caenorhabditis elegans* FBF, a conserved stem cell regulator. *Proc Natl Acad Sci USA* 107, 3936–3941.
- Kim J-H, Sim S-H, Ha H-J, Ko J-J, Lee K & Bae J (2009). MCL-1ES, a novel variant of MCL-1, associates with MCL-1L and induces mitochondrial cell death. *FEBS Lett* 583, 2758–2764.
- Kimble J & Hirsh D (1979). The postembryonic cell lineages of the hermaphrodite and male gonads in *Caenorhabditis elegans*. *Dev Biol* 70, 396–417.
- Kinet MJ, Malin JA, Abraham MC, Blum ES, Silverman MR, Lu Y & Shaham S (2016). HSF-1 activates the ubiquitin proteasome system to promote non-apoptotic developmental cell death in *C. elegans*. *eLife* 5, 73.
- Koh YY, Opperman L, Stumpf C, Mandan A, Keles S & Wickens M (2009). A single *C. elegans* PUF protein binds RNA in multiple modes. *RNA* 15, 1090–1099.
- Kolb JP, Oguin TH, Oberst A & Martinez J (2017). Programmed cell death and inflammation: winter is coming. *Trends Immunol* 38, 705–718.
- Kole AJ, Swahari V, Hammond SM & Deshmukh M (2011). miR-29b is activated during neuronal maturation and targets BH3-only genes to restrict apoptosis. *Genes Dev* 25, 125–130.
- Kumar GA & Subramaniam K (2018). PUF-8 facilitates homologous chromosome pairing by promoting proteasome activity during meiotic entry in *C. elegans*. *Development* 145, dev163949.

REFERENCES

- Kundu P, Fabian MR, Sonenberg N, Bhattacharyya SN & Filipowicz W (2012). HuR protein attenuates miRNA-mediated repression by promoting miRISC dissociation from the target RNA. *Nucleic Acids Res* 40, 5088–5100.
- Lamont LB, Crittenden SL, Bernstein D, Wickens M & Kimble J (2004). FBF-1 and FBF-2 regulate the size of the mitotic region in the *C. elegans* germline. *Dev Cell* 7, 697–707.
- Lau NC, Lim LP, Weinstein EG & Bartel DP (2001). An abundant class of tiny RNAs with probable regulatory roles in *Caenorhabditis elegans*. *Science* 294, 858–862.
- Lebedeva S, Jens M, Theil K, Schwanhäusser B, Selbach M, Landthaler M & Rajewsky N (2011). Transcriptome-wide analysis of regulatory interactions of the RNA-binding protein HuR. *Mol Cell* 43, 340–352.
- Lee RC, Feinbaum RL & Ambros V (1993). The *C. elegans* heterochronic gene *lin-4* encodes small RNAs with antisense complementarity to *lin-14*. *Cell* 75, 843–854.
- Lee RC & Ambros V (2001). An extensive class of small RNAs in *Caenorhabditis elegans*. *Science* 294, 862–864.
- Lee Y, Ahn C, Han J, Choi H, Kim J, Yim J, Lee J, Provost P, Rådmark O, Kim S & Kim VN (2003). The nuclear RNase III Drosha initiates microRNA processing. *Nature* 425, 415–419.
- LeGendre JB, Campbell ZT, Kroll-Conner P, Anderson P, Kimble J & Wickens M (2013). RNA targets and specificity of Staufen, a double-stranded RNA-binding protein in *Caenorhabditis elegans*. *J Biol Chem* 288, 2532–2545.
- Letai A (2017). Apoptosis and cancer. *Annu Rev Cancer Biol* 1, 275–294.
- Ley R, Balmanno K, Hadfield K, Weston C & Cook SJ (2003). Activation of the ERK1/2 signaling pathway promotes phosphorylation and proteasome-dependent degradation of the BH3-only protein, Bim. *J Biol Chem* 278, 18811–18816.
- Li H, Zhu H, Xu CJ & Yuan J (1998). Cleavage of BID by caspase 8 mediates the mitochondrial damage in the Fas pathway of apoptosis. *Cell* 94, 491–501.

- Li XH, Ha CT & Xiao M (2016). MicroRNA-30 inhibits antiapoptotic factor Mcl-1 in mouse and human hematopoietic cells after radiation exposure. *Apoptosis* 21, 708–720.
- Lim J, Kim D, Lee Y-S, Ha M, Lee M, Yeo J, Chang H, Song J, Ahn K & Kim VN (2018). Mixed tailing by TENT4A and TENT4B shields mRNA from rapid deadenylation. *Science* 361, 701–704.
- Lim LP, Lau NC, Weinstein EG, Abdelhakim A, Yekta S, Rhoades MW, Burge CB & Bartel DP (2003). The microRNAs of *Caenorhabditis elegans*. *Genes Dev* 17, 991–1008.
- Lim LP, Lau NC, Garrett-Engle P, Grimson A, Schelter JM, Castle J, Bartel DP, Linsley PS & Johnson JM (2005). Microarray analysis shows that some microRNAs downregulate large numbers of target mRNAs. *Nature* 433, 769–773.
- Liu H, Strauss TJ, Potts MB & Cameron S (2006). Direct regulation of *egl-1* and of programmed cell death by the Hox protein MAB-5 and by CEH-20, a *C. elegans* homolog of Pbx1. *Development* 133, 641–650.
- Liu Q, Stumpf C, Thomas C, Wickens M & Haag ES (2012). Context-dependent function of a conserved translational regulatory module. *Development* 139, 1509–1521.
- Liu Y, Beyer A & Aebersold R (2016). On the dependency of cellular protein levels on mRNA abundance. *Cell* 165, 535–550.
- Lorenz R, Bernhart SH, Höner Zu Siederdisen C, Tafer H, Flamm C, Stadler PF & Hofacker IL (2011). ViennaRNA Package 2.0. *Algorithms Mol Biol* 6, 26.
- Lublin AL & Evans TC (2007). The RNA-binding proteins PUF-5, PUF-6, and PUF-7 reveal multiple systems for maternal mRNA regulation during *C. elegans* oogenesis. *Dev Biol* 303, 635–649.
- Luo X, Budihardjo I, Zou H, Slaughter C & Wang X (1998). Bid, a Bcl2 interacting protein, mediates cytochrome c release from mitochondria in response to activation of cell surface death receptors. *Cell* 94, 481–490.
- Maduro M & Pilgrim D (1995). Identification and cloning of *unc-119*, a gene expressed in the *Caenorhabditis elegans* nervous system. *Genetics* 141, 977–988.

REFERENCES

- Mainpal R, Priti A & Subramaniam K (2011). PUF-8 suppresses the somatic transcription factor PAL-1 expression in *C. elegans* germline stem cells. *Dev Biol* 360, 195–207.
- Malin JA, Kinet MJ, Abraham MC, Blum ES & Shaham S (2016). Transcriptional control of non-apoptotic developmental cell death in *C. elegans*. *Cell Death Differ* 23, 1985–1994.
- Marguerat S, Schmidt A, Codlin S, Chen W, Aebersold R & Bähler J (2012). Quantitative analysis of fission yeast transcriptomes and proteomes in proliferating and quiescent cells. *Cell* 151, 671–683.
- Martinez NJ, Ow MC, Reece-Hoyes JS, Barrasa MI, Ambros VR & Walhout AJM (2008). Genome-scale spatiotemporal analysis of *Caenorhabditis elegans* microRNA promoter activity. *Genome Res* 18, 2005–2015.
- Massirer KB, Perez SG, Mondol V & Pasquinelli AE (2012). The miR-35-41 family of microRNAs regulates RNAi sensitivity in *Caenorhabditis elegans*. *PLoS Genet* 8, e1002536.
- Mathai JP, Germain M, Marcellus RC & Shore GC (2002). Induction and endoplasmic reticulum location of BIK/NBK in response to apoptotic signaling by E1A and p53. *Oncogene* 21, 2534–2544.
- Maurer CW, Chiorazzi M & Shaham S (2007). Timing of the onset of a developmental cell death is controlled by transcriptional induction of the *C. elegans ced-3* caspase-encoding gene. *Development* 134, 1357–1368.
- Mayr C (2017). Regulation by 3'-untranslated regions. *Annu Rev Genet* 51, 171–194.
- McJunkin K & Ambros V (2014). The embryonic *mir-35* family of microRNAs promotes multiple aspects of fecundity in *Caenorhabditis elegans*. *G3 (Bethesda)* 4, 1747–1754.
- McJunkin K & Ambros V (2017). A microRNA family exerts maternal control on sex determination in *C. elegans*. *Genes Dev* 31, 422–437.
- Mello CC, Kramer JM, Stinchcomb D & Ambros V (1991). Efficient gene transfer in *C. elegans*: extrachromosomal maintenance and integration of transforming sequences. *EMBO J* 10, 3959–3970.

- Miska EA, Alvarez-Saavedra E, Abbott AL, Lau NC, Hellman AB, McGonagle SM, Bartel DP, Ambros VR & Horvitz HR (2007). Most *Caenorhabditis elegans* microRNAs are individually not essential for development or viability. *PLoS Genet* 3, e215.
- Moretti F, Kaiser C, Zdanowicz-Specht A & Hentze MW (2012). PABP and the poly(A) tail augment microRNA repression by facilitated miRISC binding. *Nat Struct Mol Biol* 19, 603–608.
- Mott JL, Kobayashi S, Bronk SF & Gores GJ (2007). mir-29 regulates Mcl-1 protein expression and apoptosis. *Oncogene* 26, 6133–6140.
- Müller-McNicoll M & Neugebauer KM (2013). How cells get the message: dynamic assembly and function of mRNA-protein complexes. *Nat Rev Genet* 14, 275–287.
- Murata Y & Wharton RP (1995). Binding of Pumilio to maternal hunchback mRNA is required for posterior patterning in *Drosophila* embryos. *Cell* 80, 747–756.
- Nagata S (2018). Apoptosis and clearance of apoptotic cells. *Annu Rev Immunol* 36, 489–517.
- Nakano H, Miyazawa T, Kinoshita K, Yamada Y & Yoshida T (2010). Functional screening identifies a microRNA, miR-491 that induces apoptosis by targeting Bcl-X(L) in colorectal cancer cells. *Int J Cancer* 127, 1072–1080.
- Nakano K & Vousden KH (2001). *PUMA*, a novel proapoptotic gene, is induced by p53. *Mol Cell* 7, 683–694.
- Nehme R & Conradt B (2008). *egl-1*: a key activator of apoptotic cell death in *C. elegans*. *Oncogene* 27, S30–S40.
- Nejman-Faleńczyk B, Bloch S, Licznarska K, Dydecka A, Felczykowska A, Topka G, Węgrzyn A & Węgrzyn G (2015). A small, microRNA-size, ribonucleic acid regulating gene expression and development of Shiga toxin-converting bacteriophage Φ24B. *Sci Rep* 5, 10080.
- Nolde MJ, Saka N, Reinert KL & Slack FJ (2007). The *Caenorhabditis elegans* pumilio homolog, *puf-9*, is required for the 3'UTR-mediated repression of the *let-7* microRNA target gene, *hbl-1*. *Dev Biol* 305, 551–563.

REFERENCES

- O'Connor L, Strasser A, O'Reilly LA, Hausmann G, Adams JM, Cory S & Huang DC (1998). Bim: a novel member of the Bcl-2 family that promotes apoptosis. *EMBO J* 17, 384–395.
- Oda E, Ohki R, Murasawa H, Nemoto J, Shibue T, Yamashita T, Tokino T, Taniguchi T & Tanaka N (2000). Noxa, a BH3-only member of the Bcl-2 family and candidate mediator of p53-induced apoptosis. *Science* 288, 1053–1058.
- Olsen PH & Ambros V (1999). The *lin-4* regulatory RNA controls developmental timing in *Caenorhabditis elegans* by blocking LIN-14 protein synthesis after the initiation of translation. *Dev Biol* 216, 671–680.
- Opperman L, Hook B, DeFino M, Bernstein DS & Wickens M (2005). A single spacer nucleotide determines the specificities of two mRNA regulatory proteins. *Nat Struct Mol Biol* 12, 945–951.
- Palozola KC, Donahue G, Liu H, Grant GR, Becker JS, Cote A, Yu H, Raj A & Zaret KS (2017). Mitotic transcription and waves of gene reactivation during mitotic exit. *Science* 358, 119–122.
- Pasquinelli AE, Reinhart BJ, Slack F, Martindale MQ, Kuroda MI, Maller B, Hayward DC, Ball EE, Degnan B, Müller P, Spring J, Srinivasan A, Fishman M, Finnerty J, Corbo J, Levine M, Leahy P, Davidson E & Ruvkun G (2000). Conservation of the sequence and temporal expression of *let-7* heterochronic regulatory RNA. *Nature* 408, 86–89.
- Pernaute B, Spruce T, Smith KM, Sánchez-Nieto JM, Manzanares M, Cobb B & Rodríguez TA (2014). MicroRNAs control the apoptotic threshold in primed pluripotent stem cells through regulation of BIM. *Genes Dev* 28, 1873–1878.
- Piqué M, López JM, Foissac S, Guigó R & Méndez R (2008). A combinatorial code for CPE-mediated translational control. *Cell* 132, 434–448.
- Poria DK, Guha A, Nandi I & Ray PS (2015). RNA-binding protein HuR sequesters microRNA-21 to prevent translation repression of proinflammatory tumor suppressor gene programmed cell death 4. *Oncogene* 35, 1703–1715.

- Potts MB, Wang DP & Cameron S (2009). Trithorax, Hox, and TALE-class homeodomain proteins ensure cell survival through repression of the BH3-only gene *egl-1*. *Dev Biol* 329, 374–385.
- Potts MB & Cameron S (2011). Cell lineage and cell death: *Caenorhabditis elegans* and cancer research. *Nat Rev Cancer* 11, 50–58.
- Prasad A, Porter DF, Kroll-Conner PL, Mohanty I, Ryan AR, Crittenden SL, Wickens M & Kimble J (2016). The PUF binding landscape in metazoan germ cells. *RNA* 22, 1026–1043.
- Preibisch S, Saalfeld S, Schindelin J & Tomancak P (2010). Software for bead-based registration of selective plane illumination microscopy data. *Nat Meth* 7, 418–419.
- Pushpa K, Kumar GA & Subramaniam K (2013). PUF-8 and TCER-1 are essential for normal levels of multiple mRNAs in the *C. elegans* germline. *Development* 140, 1312–1320.
- Puthalakath H, Huang DC, O'Reilly LA, King SM & Strasser A (1999). The proapoptotic activity of the Bcl-2 family member Bim is regulated by interaction with the dynein motor complex. *Mol Cell* 3, 287–296.
- Puthalakath H, Villunger A, O'Reilly LA, Beaumont JG, Coultas L, Cheney RE, Huang DC & Strasser A (2001). Bmf: a proapoptotic BH3-only protein regulated by interaction with the myosin V actin motor complex, activated by anoikis. *Science* 293, 1829–1832.
- Puthalakath H, O'Reilly LA, Gunn P, Lee L, Kelly PN, Huntington ND, Hughes PD, Michalak EM, McKimm-Breschkin J, Motoyama N, Gotoh T, Akira S, Bouillet P & Strasser A (2007). ER stress triggers apoptosis by activating BH3-only protein Bim. *Cell* 129, 1337–1349.
- Qi S, Pang Y, Hu Q, Liu Q, Li H, Zhou Y, He T, Liang Q, Liu Y, Yuan X, Luo G, Li H, Wang J, Yan N & Shi Y (2010). Crystal structure of the *Caenorhabditis elegans* apoptosome reveals an octameric assembly of CED-4. *Cell* 141, 446–457.
- Qian L, Van Laake LW, Huang Y, Liu S, Wendland MF & Srivastava D (2011). miR-24 inhibits apoptosis and represses Bim in mouse cardiomyocytes. *J Exp Med* 208, 549–560.

REFERENCES

- Quenault T, Lithgow T & Traven A (2011). PUF proteins: repression, activation and mRNA localization. *Trends Cell Biol* 21, 104–112.
- Raisin S, Pantalacci S, Breittmayer J-P & Léopold P (2003). A new genetic locus controlling growth and proliferation in *Drosophila melanogaster*. *Genetics* 164, 1015–1025.
- Raj A, van den Bogaard P, Rifkin SA, van Oudenaarden A & Tyagi S (2008). Imaging individual mRNA molecules using multiple singly labeled probes. *Nat Meth* 5, 877–879.
- Raj A & Tyagi S (2010). Detection of individual endogenous RNA transcripts in situ using multiple singly labeled probes. *Meth Enzymol* 472, 365–386.
- Ray D et al. (2013). A compendium of RNA-binding motifs for decoding gene regulation. *Nature* 499, 172–177.
- Rehwinkel J, Behm-Ansmant I, Gatfield D & Izaurralde E (2005). A crucial role for GW182 and the DCP1:DCP2 decapping complex in miRNA-mediated gene silencing. *RNA* 11, 1640–1647.
- Rinck A, Preusse M, Lagerbauer B, Lickert H, Engelhardt S & Theis FJ (2013). The human transcriptome is enriched for miRNA-binding sites located in cooperativity-permitting distance. *RNA Biol* 10, 1125–1135.
- Robertson AMG & Thomson JN (1982). Morphology of programmed cell death in the ventral nerve cord of *Caenorhabditis elegans* larvae. *Development* 67, 89–100.
- Rogell B, Fischer B, Rettel M, Krijgsveld J, Castello A & Hentze MW (2017). Specific RNP capture with antisense LNA/DNA mixmers. *RNA* 23, 1290–1302.
- Ross AJ, Li M, Yu B, Gao MX & Derry WB (2011). The EEL-1 ubiquitin ligase promotes DNA damage-induced germ cell apoptosis in *C. elegans*. *Cell Death Differ* 18, 1140–1149.
- Sabirzhanov B, Zhao Z, Stoica BA, Loane DJ, Wu J, Borroto C, Dorsey SG & Faden AI (2014). Downregulation of miR-23a and miR-27a following experimental traumatic brain injury induces neuronal cell death through activation of proapoptotic Bcl-2 proteins. *J Neurosci* 34, 10055–10071.

- Sætrom P, Heale BSE, Snøve O, Aagaard L, Alluin J & Rossi JJ (2007). Distance constraints between microRNA target sites dictate efficacy and cooperativity. *Nucleic Acids Res* 35, 2333–2342.
- Salmena L, Poliseno L, Tay Y, Kats L & Pandolfi PP (2011). A ceRNA hypothesis: the Rosetta Stone of a hidden RNA language? *Cell* 146, 353–358.
- Schaefer B, Sun W, Li Y-S, Fang L & Chen W (2018). The evolution of posttranscriptional regulation. *WIREs RNA* 9, e1485.
- Schindelin J, Arganda-Carreras I, Frise E, Kaynig V, Longair M, Pietzsch T, Preibisch S, Rueden C, Saalfeld S, Schmid B, Tinevez J-Y, White DJ, Hartenstein V, Eliceiri K, Tomancak P & Cardona A (2012). Fiji: an open-source platform for biological-image analysis. *Nat Meth* 9, 676–682.
- Schnabel R, Hutter H, Moerman D & Schnabel H (1997). Assessing normal embryogenesis in *Caenorhabditis elegans* using a 4D microscope: variability of development and regional specification. *Dev Biol* 184, 234–265.
- Schnabel R, Bischoff M, Hintze A, Schulz A-K, Hejnlol A, Meinhardt H & Hutter H (2006). Global cell sorting in the *C. elegans* embryo defines a new mechanism for pattern formation. *Dev Biol* 294, 418–431.
- Schoenberg DR & Maquat LE (2012). Regulation of cytoplasmic mRNA decay. *Nat Rev Genet* 13, 246–259.
- Sevrioukov EA, Burr J, Huang EW, Assi HH, Monserrate JP, Purves DC, Wu JN, Song EJ & Brachmann CB (2007). *Drosophila* Bcl-2 proteins participate in stress-induced apoptosis, but are not required for normal development. *Genesis* 45, 184–193.
- Shaham S & Horvitz HR (1996a). Developing *Caenorhabditis elegans* neurons may contain both cell-death protective and killer activities. *Genes Dev* 10, 578–591.
- Shaham S & Horvitz HR (1996b). An alternatively spliced *C. elegans ced-4* RNA encodes a novel cell death inhibitor. *Cell* 86, 201–208.
- Shaham S, Reddien PW, Davies B & Horvitz HR (1999). Mutational analysis of the *Caenorhabditis elegans* cell-death gene *ced-3*. *Genetics* 153, 1655–1671.

REFERENCES

- Shaw WR, Armisen J, Lehrbach NJ & Miska EA (2010). The conserved miR-51 microRNA family is redundantly required for embryonic development and pharynx attachment in *Caenorhabditis elegans*. *Genetics* 185, 897–905.
- Sherrard R, Luehr S, Holzkamp H, McJunkin K, Memar N & Conradt B (2017). miRNAs cooperate in apoptosis regulation during *C. elegans* development. *Genes Dev* 31, 209–222.
- Siepel A, Bejerano G, Pedersen JS, Hinrichs AS, Hou M, Rosenbloom K, Clawson H, Spieth J, Hillier LW, Richards S, Weinstock GM, Wilson RK, Gibbs RA, Kent WJ, Miller W & Haussler D (2005). Evolutionarily conserved elements in vertebrate, insect, worm, and yeast genomes. *Genome Res* 15, 1034–1050.
- Singh G, Pratt G, Yeo GW & Moore MJ (2015). The clothes make the mRNA: past and present trends in mRNP fashion. *Annu Rev Biochem* 84, 325–354.
- Sionov RV, Vlahopoulos SA & Granot Z (2015). Regulation of Bim in Health and Disease. *Oncotarget* 6, 23058–23134.
- Souers AJ et al. (2013). ABT-199, a potent and selective BCL-2 inhibitor, achieves antitumor activity while sparing platelets. *Nat Med* 19, 202–208.
- Spector MS, Desnoyers S, Hoepfner DJ & Hengartner MO (1997). Interaction between the *C. elegans* cell-death regulators CED-9 and CED-4. *Nature* 385, 653–656.
- Stanfield GM & Horvitz HR (2000). The *ced-8* gene controls the timing of programmed cell deaths in *C. elegans*. *Mol Cell* 5, 423–433.
- Steller H. (2008). Regulation of apoptosis in *Drosophila*. *Cell Death Differ* 15: 1132–1138.
- Sternburg EL, Estep JA, Nguyen DK, Li Y & Karginov FV (2018). Antagonistic and cooperative AGO2-PUM interactions in regulating mRNAs. *Sci Rep* 8, 15316.
- Stoeckius M, Maaskola J, Colombo T, Rahn H-P, Friedländer MR, Li N, Chen W, Piano F & Rajewsky N (2009). Large-scale sorting of *C. elegans* embryos reveals the dynamics of small RNA expression. *Nat Meth* 6, 745–751.
- Stumpf CR, Kimble J & Wickens M (2008). A *Caenorhabditis elegans* PUF protein family with distinct RNA binding specificity. *RNA* 14, 1550–1557.

- Stutz A, Conne B, Huarte J, Gubler P, Völkel V, Flandin P & Vassalli JD (1998). Masking, unmasking, and regulated polyadenylation cooperate in the translational control of a dormant mRNA in mouse oocytes. *Genes Dev* 12, 2535–2548.
- Su Y, Wu H, Pavlosky A, Zou L-L, Deng X, Zhang Z-X & Jevnikar AM (2016). Regulatory non-coding RNA: new instruments in the orchestration of cell death. *Cell Death Dis* 7, e2333–e2333.
- Subasic D, Brümmer A, Wu Y, Pinto SM, Imig J, Keller M, Jovanovic M, Lightfoot HL, Nasso S, Goetze S, Brunner E, Hall J, Aebersold R, Zavolan M & Hengartner MO (2015). Cooperative target mRNA destabilization and translation inhibition by miR-58 microRNA family in *C. elegans*. *Genome Res* 25, 1680–1691.
- Subasic D, Stoeger T, Eisenring S, Matia-González AM, Imig J, Zheng X, Xiong L, Gisler P, Eberhard R, Holtackers R, Gerber AP, Pelkmans L & Hengartner MO (2016). Post-transcriptional control of executioner caspases by RNA-binding proteins. *Genes Dev* 30, 2213–2225.
- Subramaniam K & Seydoux G (2003). Dedifferentiation of primary spermatocytes into germ cell tumors in *C. elegans* lacking the pumilio-like protein PUF-8. *Curr Biol* 13, 134–139.
- Subtelny AO, Eichhorn SW, Chen GR, Sive H & Bartel DP (2014). Poly(A)-tail profiling reveals an embryonic switch in translational control. *Nature* 508, 66–71.
- Sugimoto A, Kusano A, Hozak RR, Derry WB, Zhu J & Rothman JH (2001). Many genomic regions are required for normal embryonic programmed cell death in *Caenorhabditis elegans*. *Genetics* 158, 237–252.
- Suh N, Crittenden SL, Goldstrohm A, Hook B, Thompson B, Wickens M & Kimble J (2009). FBF and its dual control of *gld-1* expression in the *Caenorhabditis elegans* germline. *Genetics* 181, 1249–1260.
- Sulston JE & Horvitz HR (1977). Post-embryonic cell lineages of the nematode, *Caenorhabditis elegans*. *Dev Biol* 56, 110–156.
- Sulston JE, Schierenberg E, White JG & Thomson JN (1983). The embryonic cell lineage of the nematode *Caenorhabditis elegans*. *Dev Biol* 100, 64–119.

REFERENCES

- Suzuki J, Denning DP, Imanishi E, Horvitz HR & Nagata S (2013). Xk-related protein 8 and CED-8 promote phosphatidylserine exposure in apoptotic cells. *Science* 341, 403–406.
- Taliaferro JM, Lambert NJ, Sudmant PH, Dominguez D, Merkin JJ, Alexis MS, Bazile C & Burge CB (2016). RNA sequence context effects measured in vitro predict in vivo protein binding and regulation. *Mol Cell* 64, 294–306.
- Tan FJ, Fire AZ & Hill RB (2007). Regulation of apoptosis by *C. elegans* CED-9 in the absence of the C-terminal transmembrane domain. *Cell Death Differ* 14, 1925–1935.
- Tanner EA, Blute TA, Brachmann CB & McCall K (2011). Bcl-2 proteins and autophagy regulate mitochondrial dynamics during programmed cell death in the *Drosophila* ovary. *Development* 138, 327–338.
- Taylor RC, Brumatti G, Ito S, Hengartner MO, Derry WB & Martin SJ (2007). Establishing a blueprint for CED-3-dependent killing through identification of multiple substrates for this protease. *J Biol Chem* 282, 15011–15021.
- Taylor RC, Cullen SP & Martin SJ (2008). Apoptosis: controlled demolition at the cellular level. *Nat Rev Mol Cell Biol* 9, 231–241.
- Thellmann M, Hatzold J & Conradt B (2003). The Snail-like CES-1 protein of *C. elegans* can block the expression of the BH3-only cell-death activator gene *egl-1* by antagonizing the function of bHLH proteins. *Development* 130, 4057–4071.
- Thomson DW & Dinger ME (2016). Endogenous microRNA sponges: evidence and controversy. *Nat Rev Genet* 17, 272–283.
- Tominaga K, Srikantan S, Lee EK, Subaran SS, Martindale JL, Abdelmohsen K & Gorospe M (2011). Competitive regulation of nucleolin expression by HuR and miR-494. *Mol Cell Biol* 31, 4219–4231.
- Trent C, Tsuing N & Horvitz HR (1983). Egg-laying defective mutants of the nematode *Caenorhabditis elegans*. *Genetics* 104, 619–647.

- Tzur YB, Margalit A, Melamed-Book N & Gruenbaum Y (2006). Matefin/SUN-1 is a nuclear envelope receptor for CED-4 during *Caenorhabditis elegans* apoptosis. *Proc Natl Acad Sci USA* 103, 13397–13402.
- Ule J, Jensen K, Mele A & Darnell RB (2005). CLIP: a method for identifying protein-RNA interaction sites in living cells. *Methods* 37, 376–386.
- Ulm EA, Sleiman SF & Chamberlin HM (2011). Developmental functions for the *Caenorhabditis elegans* Sp protein SPTF-3. *Mech Dev* 128, 428–441.
- Vaidyanathan PP, AlSadhan I, Merriman DK, Al-Hashimi HM & Herschlag D (2017). Pseudouridine and N⁶-methyladenosine modifications weaken PUF protein/RNA interactions. *RNA* 23, 611–618.
- Vaux DL, Cory S & Adams JM (1988). *Bcl-2* gene promotes haemopoietic cell survival and cooperates with *c-myc* to immortalize pre-B cells. *Nature* 335, 440–442.
- Vaux DL, Weissman IL & Kim SK (1992). Prevention of programmed cell death in *Caenorhabditis elegans* by human *bcl-2*. *Science* 258, 1955–1957.
- Ventura A, Young AG, Winslow MM, Lintault L, Meissner A, Erkeland SJ, Newman J, Bronson RT, Crowley D, Stone JR, Jaenisch R, Sharp PA & Jacks T (2008). Targeted deletion reveals essential and overlapping functions of the miR-17~92 family of miRNA clusters. *Cell* 132, 875–886.
- Villunger A, Michalak EM, Coultas L, Müllauer F, Böck G, Ausserlechner MJ, Adams JM & Strasser A (2003). p53- and drug-induced apoptotic responses mediated by BH3-only proteins puma and noxa. *Science* 302, 1036–1038.
- Walser CB, Battu G, Hoier EF & Hajnal A (2006). Distinct roles of the Pumilio and FBF translational repressors during *C. elegans* vulval development. *Development* 133, 3461–3471.
- Wang J, Chitturi J, Ge Q, Laskova V, Wang W, Li X, Ding M, Zhen M & Huang X (2015). The *C. elegans* COE transcription factor UNC-3 activates lineage-specific apoptosis and affects neurite growth in the RID lineage. *Development* 142, 1447–1457.

REFERENCES

- Wang M, Ogé L, Perez-Garcia M-D, Hamama L & Sakr S (2018). The PUF protein family: overview on PUF RNA targets, biological functions, and post transcriptional regulation. *Int J Mol Sci* 19, 410.
- Wang X, Zamore PD & Hall TM (2001). Crystal structure of a Pumilio homology domain. *Mol Cell* 7, 855–865.
- Wang X, Lu Z, Gomez A, Hon GC, Yue Y, Han D, Fu Y, Parisien M, Dai Q, Jia G, Ren B, Pan T & He C (2014). N6-methyladenosine-dependent regulation of messenger RNA stability. *Nature* 505, 117–120.
- Wang X, Zhao BS, Roundtree IA, Lu Z, Han D, Ma H, Weng X, Chen K, Shi H & He C (2015). N(6)-methyladenosine modulates messenger RNA translation efficiency. *Cell* 161, 1388–1399.
- Wei H, Yan B, Gagneur J & Conradt B (2017). *Caenorhabditis elegans* CES-1 Snail represses *pig-1* MELK expression to control asymmetric cell division. *Genetics* 206, 2069–2084.
- Weidmann CA, Qiu C, Arvola RM, Lou T-F, Killingsworth J, Campbell ZT, Tanaka Hall TM & Goldstrohm AC (2016). *Drosophila* Nanos acts as a molecular clamp that modulates the RNA-binding and repression activities of Pumilio. *eLife* 5, 1948.
- Wickham L, Duchaine T, Luo M, Nabi IR & DesGroseillers L (1999). Mammalian staufen is a double-stranded-RNA- and tubulin-binding protein which localizes to the rough endoplasmic reticulum. *Mol Cell Biol* 19, 2220–2230.
- Wightman B, Ha I & Ruvkun G (1993). Posttranscriptional regulation of the heterochronic gene *lin-14* by *lin-4* mediates temporal pattern formation in *C. elegans*. *Cell* 75, 855–862.
- Winn J, Carter M, Avery L & Cameron S (2011). Hox and a newly identified E2F co-repress cell death in *Caenorhabditis elegans*. *Genetics* 188, 897–905.
- Woo J-S, Jung J-S, Ha N-C, Shin J, Kim K-H, Lee W & Oh B-H (2003). Unique structural features of a BCL-2 family protein CED-9 and biophysical characterization of CED-9/EGL-1 interactions. *Cell Death Differ* 10, 1310–1319.

- Wu D, Wallen HD & Núñez G (1997). Interaction and regulation of subcellular localization of CED-4 by CED-9. *Science* 275, 1126–1129.
- Wu E, Thivierge C, Flamand M, Mathonnet G, Vashisht AA, Wohlschlegel J, Fabian MR, Sonenberg N & Duchaine TF (2010). Pervasive and cooperative deadenylation of 3'UTRs by embryonic microRNA families. *Mol Cell* 40, 558–570.
- Wu L, Fan J & Belasco JG (2006). MicroRNAs direct rapid deadenylation of mRNA. *Proc Natl Acad Sci USA* 103, 4034–4039.
- Xiao W et al. (2016). Nuclear m(6)A Reader YTHDC1 Regulates mRNA Splicing. *Mol Cell* 61, 507–519.
- Xue D, Shaham S & Horvitz HR (1996). The *Caenorhabditis elegans* cell-death protein CED-3 is a cysteine protease with substrate specificities similar to those of the human CPP32 protease. *Genes Dev* 10, 1073–1083.
- Yan N, Gu L, Kokel D, Chai J, Li W, Han A, Chen L, Xue D & Shi Y (2004). Structural, biochemical, and functional analyses of CED-9 recognition by the proapoptotic proteins EGL-1 and CED-4. *Mol Cell* 15, 999–1006.
- Yan N, Chai J, Lee ES, Gu L, Liu Q, He J, Wu J-W, Kokel D, Li H, Hao Q, Xue D & Shi Y (2005). Structure of the CED-4-CED-9 complex provides insights into programmed cell death in *Caenorhabditis elegans*. *Nature* 437, 831–837.
- Yang X, Chang HY & Baltimore D (1998). Essential role of CED-4 oligomerization in CED-3 activation and apoptosis. *Science* 281, 1355–1357.
- Yoon J-H, Srikantan S & Gorospe M (2012). MS2-TRAP (MS2-tagged RNA affinity purification): tagging RNA to identify associated miRNAs. *Methods* 58, 81–87.
- Yoon J-H & Gorospe M (2016). Identification of mRNA-Interacting Factors by MS2-TRAP (MS2-Tagged RNA Affinity Purification). *Methods Mol Biol* 1421, 15–22.
- Youle RJ & Strasser A (2008). The BCL-2 protein family: opposing activities that mediate cell death. *Nat Rev Mol Cell Biol* 9, 47–59.
- Yuan J & Horvitz HR (1992). The *Caenorhabditis elegans* cell death gene *ced-4* encodes a novel protein and is expressed during the period of extensive programmed cell death. *Development* 116, 309–320.

REFERENCES

- Yuan J, Shaham S, Ledoux S, Ellis HM & Horvitz HR (1993). The *C. elegans* cell death gene *ced-3* encodes a protein similar to mammalian interleukin-1 β -converting enzyme. *Cell* 75, 641–652.
- Zamore PD, Williamson JR & Lehmann R (1997). The Pumilio protein binds RNA through a conserved domain that defines a new class of RNA-binding proteins. *RNA* 3, 1421–1433.
- Zha J, Harada H, Yang E, Jockel J & Korsmeyer SJ (1996). Serine phosphorylation of death agonist BAD in response to survival factor results in binding to 14-3-3 not BCL-X(L). *Cell* 87, 619–628.
- Zhang B, Gallegos M, Puoti A, Durkin E, Fields S, Kimble J & Wickens MP (1997). A conserved RNA-binding protein that regulates sexual fates in the *C. elegans* hermaphrodite germ line. *Nature* 390, 477–484.
- Zhang M, Chen D, Xia J, Han W, Cui X, Neuenkirchen N, Hermes G, Sestan N & Lin H (2017). Post-transcriptional regulation of mouse neurogenesis by Pumilio proteins. *Genes Dev* 31, 1–16.
- Zhang Y, Schiff D, Park D & Abounader R (2014). MicroRNA-608 and microRNA-34a regulate chordoma malignancy by targeting EGFR, Bcl-xL and MET. *PLoS ONE* 9, e91546.
- Zhao BS, Roundtree IA & He C (2017). Post-transcriptional gene regulation by mRNA modifications. *Nat Rev Mol Cell Biol* 18, 31–42.
- Zhong Q, Gao W, Du F & Wang X (2005). Mule/ARF-BP1, a BH3-only E3 ubiquitin ligase, catalyzes the polyubiquitination of Mcl-1 and regulates apoptosis. *Cell* 121, 1085–1095.
- Zhu W, Shan X, Wang T, Shu Y & Liu P (2010). miR-181b modulates multidrug resistance by targeting BCL2 in human cancer cell lines. *Int J Cancer* 127, 2520–2529.
- Zmasek CM & Godzik A (2013). Evolution of the animal apoptosis network. *Cold Spring Harb Perspect Biol* 5, a008649–a008649.

CURRICULUM VITAE

RYAN SHERRARD

LMU Munich, Biozentrum
Großhaderner Str. 2
81252 Planegg-Martinsried, Germany

sherrard@bio.lmu.de

Education

- Ph.D. Candidate, Biology 2013–2018
Ludwig-Maximilians-University, Munich, Germany
International Max Planck Research School for Molecular Life Sciences, Martinsried, Germany
- M.Sc., Biochemistry 2010–2013
Ludwig-Maximilians-University, Munich, Germany
- B.Sc. (Hons), Biochemistry 2004–2008
Mount Allison University, Sackville, Canada

Experience

- Ludwig-Maximilians-University, Munich, Germany 2012–2018
Graduate research with Prof. Dr. Barbara Conradt
 - Studied transcriptional and post-transcriptional regulation of genes involved in programmed cell death in the nematode *Caenorhabditis elegans*.
 - Performed cell lineaging and cell-fate determination during embryogenesis.
 - Quantified specific transcripts in single cells and whole animals by RNA FISH.
 - Co-produced an open online course for Coursera entitled “Programmed Cell Death”.
- EMP Genetech, Ingolstadt, Germany 2011
Research assistant with Dr. Franz Welser
 - Produced and purified recombinant proteins from human cells for sale to clients.
 - Established a large-scale bioreactor for continuous cell cultivation.
- University of New Brunswick, Saint John, Canada 2010
Research assistant with Prof. Dr. Chris Martyniuk
 - Studied molecular biomarkers of toxicity in salmonids due to aquatic pollutants.
 - Monitored changes in gene expression using quantitative PCR.
- Mount Allison University, Sackville, Canada 2007–2008
Undergraduate research with Prof. Dr. Doug Campbell
 - Studied the ecophysiology of phytoplankton upon changes in light irradiance.
 - Characterized molecular dynamics of photosystem II upon photoinhibition.

Publications

Sherrard R, Luehr S, Holzkamp H, McJunkin K, Memar N & Conradt B (2017). miRNAs cooperate in apoptosis regulation during *C. elegans* development. *Genes Dev* 31, 209–222.

Marlatt VL, **Sherrard R**, Kennedy CJ, Elphick JR & Martyniuk CJ (2016). Application of molecular endpoints in early life stage salmonid environmental biomonitoring. *Aquat Toxicol* 173, 178–191.

Six C, **Sherrard R**, Lionard M, Roy S & Campbell DA (2009). Photosystem II and pigment dynamics among ecotypes of the green alga *Ostreococcus*. *Plant Physiol* 151, 379–390.

Fellowships

Postgraduate Scholarship - Doctoral (\$63,000 CAD over 3 years) <i>Natural Sciences and Engineering Research Council of Canada (NSERC)</i>	2014–2017
Undergraduate Student Research Award (\$4,500 CAD over 16 weeks) <i>NSERC</i>	2007

Conferences and Workshops

RNA Transport Meeting <i>Düsseldorf, Germany</i>	2018
EMBO Conference: RNA Localization and Local Translation (Poster presentation) <i>Barga, Italy</i>	2017
21st International <i>C. elegans</i> Conference (Oral presentation) <i>Los Angeles, USA</i>	2017
EMBL Symposium: The Complex Life of mRNA (Poster presentation) <i>Heidelberg, Germany</i>	2016
International Meeting of the German Society for Cell Biology <i>Martinsried, Germany</i>	2016
EMBL Master Course: Bioimage Data Analysis <i>Heidelberg, Germany</i>	2015